

Structural, EPR and Antimicrobial Studies on Some Transition Metal Complexes of Thiosemicarbazones

**Thesis submitted to the Cochin University of Science and
Technology in partial fulfilment of the requirement for the degree of
Doctor of Philosophy in Chemistry**

by

Sreekanth A.

**Department of Applied chemistry
Cochin University of Science and Technology
Kochi- 682 022**

October 2003

G 8634



To my Appa, Amma and Binu

On Thy lotus feet

Lets all sing in praise of the lord who measured the universe, with love and affection we bathed the lord in pure water, blessed to have rain thrice every month, our sins washed out; well grown paddy bore the finest grain; fishes jump out; while honey bee slept on lotus flower:


Andaal: Thiruppavai-2.30

Department of Applied Chemistry
Cochin University of Science and Technology
Kochi 6820 22, India

Dr. M. R. Prathapachandra Kurup
Professor of Inorganic Chemistry

CERTIFICATE

Certified that the present work entitled "Structural, EPR and Antimicrobial Studies on Some Transition Metal Complexes of Thiosemicarbazones" submitted by Mr. A. Sreekanth is an authentic record of the research work carried out by him under my supervision in the Department of Applied Chemistry in partial fulfillment of the requirements for the Degree of Doctor of Philosophy of Cochin University of Science and Technology, and has not been included in any other thesis or submitted previously for the award of any degree.


M. R. Prathapachandra Kurup
(Supervising Guide)

Kochi-22
8th October 2003

DECLARATION

2

I hereby declare that the present work entitled "Structural, EPR and Antimicrobial Studies on Some Transition Metal Complexes of Thiosemicarbazones" is based on the original work done by me under the guidance of Dr. M. R. Prathapachandra Kurup, Professor, Department of Applied Chemistry, Cochin University of Science and Technology and has not been included in any other Thesis or submitted previously for the award of any degree.



Sreekanth. A

Kochi-22

8th October 2003

Acknowledgements

It is my immense pleasure and a great privilege to express my sincere gratitude and obligation to Dr. M. R. Prathapachandra Kurup, Professor of Inorganic Chemistry, Department of Applied Chemistry for his valuable guidance and endless support throughout my research endeavour.

My sincere thanks are due to Dr. K. K. Mohammed Yusuff, Professor of Catalysis, Dr. K. Girish Kumar, Dr. K. Sreekumar and Dr. P. A. Unnikrishnan, Department of Applied Chemistry for their encouragement through out my course of work. I am extremely thankful for the support extended by Dr. K. P. Rajappan Nair, Dean, Faculty of Sciences, CUSAT also.

I acknowledge Dr. P. Mathur, National Single Crystal X-Ray Diffraction Facility, Indian Institute of Technology, Bombay, Dr. Hoong Kun-Fun, School of Physics, Universiti Sains Malaysia, Malaysia, and Dr. M. Nethaji, Principal Research Scientist, Indian Institute of Science, Bangalore, for Single Crystal X-Ray diffraction studies. Acknowledgements are also due to the services provided by the Regional Sophisticated Instrumentation Centres, at Central Drug Research Institute, Lucknow, IIT-Bombay and Sophisticated Instrumentation Facility, IISc, Bangalore. I am thankful to Dr. Ajay Gupta and Mr. Amith Sariya, Inter University Consortium, Indore, for helping me in ^{57}Fe Mössbauer Spectral experiments. On a personal basis, I am grateful to Dr. M. V. Rajashekar, Professor, School of Chemistry, University of Hyderabad, Dr. S. Sailaja, Dr. V. Rajakannan and Dr. Turpu Goverdhan Reddy for their helps. Special thanks are also due to Dr. Saritha Bhatt and Ms. Archana Kishore, Department of Biotechnology, CUSAT for helping me in antimicrobial studies. I am also thankful to Dr. Binoy Paul, International School of Photonics, CUSAT for helping me to record Electronic Spectral data.

I am grateful to my seniors Dr. Rohith P. John, Dr. S. Sivakumar and Mr. Varughese Philip for their boundless support, timely help and encouragement whenever I needed it most. I am thankful to my colleagues especially to Dr. Chandini R. Nayar, P. B. Sreeja and V. Suni who provided me with a conducive atmosphere during my stay here. I am thankful to Sanjay Gopinath, Daly Davis and T. Radhika for a nice companionship right from my early CUSAT days.

Sometimes deepest feelings are hardest to convey and for me it is the right time to thank my dearest friends P. K. Baby, K. A. Mani Ram, K. K. Sooraj, K. P. Iqbal, K. S. Harikrishnan, C. Harimohan, Abhinand Bhaskar, K. Jidesh Babu, R. Renjith, Jaison Kurian, S. Jayakumar, Dally Gopinath, Dinker Bhaskaran, B. Jayadev, M. Krishna Kumar, Jithu Jacob John, M. Navanith, B. Ajith, V. Devdas and many of the dearest Hostellers of Sanathana, for the times they have encouraged, tolerated and comforted me with their love and talks. Without our fights, jokes and vibrant camaraderie, my life at CUSAT would have been dull and incomplete.

I owe immensely to my dearest brother Binu P. Paul, for his symbiotic support; for keeping me in a lively mood. He has given me a hand of support, love and care in all my activities and in shaping my personality. He believed in me when I didn't believe in myself; He has selflessly supported me whenever and whatever I have decided to do. I am grateful to my grand parents late A. Krishna Iyyer, and S. Meenakshi Ammal for their special concern for me from my childhood. I owe much to my parents K. Anantharam and M. V. Janaky for their love, affection and support.

Sreekanth

Table of Contents

	Foreword	1
	Chapter 1	3
1	Thiosemicarbazones and their metal complexes- A brief survey	3
1.1	Bonding and stereochemistry	4
1.2	Objective and scope of the work	6
1.3	Physical methods	6
13.1.	Elemental analysis and magnetic susceptibility	6
1.3.2	NMR spectra	7
1.3.3	Electronic spectra	7
1.3.4	IR Spectra	7
1.3.5	EPR Spectra	7
1.3.6	Mössbauer Spectra	8
1.3.7	X-Ray Crystallography	8
	Chapter 2	9
2	Synthesis and Studies on Thiosemicarbazone Ligands	9
2.1	Experimental	10
2.1.1	General	10
2.1.2	Carboxymethyl N-methyl N-phenyldithiocarbamate	10
2.1.3	4-Methyl-4-phenyl-3-thiosemicarbazide (1a)	10
2.1.4	Pyrrolidine-1-thiocarboxylic acid hydrazide (1b)	11
2.1.5	2-Benzoylpyridine N(4), N(4)-(butane-1, 4-diyl) thiosemicarbazone	11
2.1.6	2-Acetylpyridine N(4), N(4)-(butane-1, 4-diyl) thiosemicarbazone	12
2.1.7	Di-2-pyridyl ketone thiosemicarbazone	12
2.2	Results and discussions	13
2.2.1	Synthesis	13
2.2.2	Structure of HBpypTsc	15
2.2.3	Structure of HPranThas	18
2.2.4	Structure of HDpkTsc	20
2.2.5	NMR spectra of HBpypTsc	22
2.2.6	Electronic spectra	24
2.2.7	IR spectra	25
2.3	Antimicrobial studies	26
	Chapter 3	29
3	Synthesis and studies on copper(II) complexes	29
3.1	Experimental	30
3.1.1	CuBpypTscN ₃ (1)	30
3.1.2	Cu ₂ (BpypTsc) ₂ Cl ₂ (2) and CuBpypTscCl (10)	30
3.1.3	CuBpypTscNO ₃ (3)	30
3.1.4	CuBpypTscNCS (4)	30
3.1.5	CuBpypTscClO ₄ (5)	31
3.1.6	CuBpypTscBr (6)	31
3.1.7	CuBpypTscSH (7) and Cu ₂ (BpypTsc) ₂ S ₂ (9)	31
3.1.8	CuBpypTscCN (8)	31
3.2	Results and discussion	32
3.2.1.	Synthesis	32
3.2.2	Electronic spectra	33

3.2.3	Infrared spectra	35
3.2.4	Electron paramagnetic resonance spectra	39
3.2.5	Molecular and crystal structure of compound 2	47
3.2.6	Molecular and crystal structure of compound 6	51
3.2.7	Molecular and crystal structure of compound 7	54
3.2.8	Molecular and crystal structure of compound 9	58
3.2.9	Molecular and crystal structure of compound 10	62
3.3	Antimicrobial studies of the complexes	64
	Chapter 4	66
4	Synthesis and studies of iron(III) complexes	66
4.1	Experimental	66
4.1.1	General	66
4.1.2	[Fe(BpypTsc) ₂](ClO ₄) (11)	67
4.1.3	[Fe(PranThas) ₂](FeCl ₄) (12)	67
4.1.4	[Fe(BpypTsc) ₂](NO ₃) (13)	67
4.1.5	[Fe(BpypTsc) ₂](FeCl ₄) (14)	67
4.2	Results and discussions	68
4.2.1	Syntheses	68
4.2.2	Molecular and crystal structure of compound 12	69
4.2.3	Molecular and crystal structure of compound 14	72
4.2.4	IR spectra	75
4.2.5	Electronic spectra	77
4.2.6	Electron paramagnetic resonance spectra	79
4.2.7	Mössbauer spectra	82
4.3	Antimicrobial studies	85
	Chapter 5	86
5	Synthesis and studies of manganese(II) complexes	86
5.1	Experimental	86
5.1.1	General	86
5.1.2	Mn(BpypTsc) ₂ (15)	86
5.1.3	Mn(DpkTsc) ₂ (16)	86
5.2	Results and discussions	87
5.2.1	Syntheses	87
5.2.2	Electronic spectra	87
5.2.3	IR spectra	88
5.2.4	Electron paramagnetic resonance spectra	89
5.2.5	Molecular and crystal structure of compound 15	90
	Chapter 6	93
6	Synthesis and studies of a gold complex	93
6.1	Experimental	93
6.1.1	General	93
6.1.2	[AuBpypTscCl]AuCl ₂ (17)	93
6.2	Results and discussions	94
6.2.1	Synthesis	94
6.2.2	IR spectra	95
6.2.3	Molecular and crystal structure of compound 17	97

Chapter 7	100
7 Synthesis and studies of vanadium complexes	100
7.1 Experimental	100
7.1.1 General	100
7.1.2 Synthesis of compound 18 and 19	100
7.2 Results and discussions	101
7.2.1 Synthesis	101
7.2.2 Electronic spectra	101
7.2.3 IR spectra	102
7.2.4 Electron paramagnetic resonance spectra	103
7.2.5 Molecular and crystal structure of compound 19	104
Summary and conclusion	107
References	110
Publications of the candidate	
Bio data of the candidate	

Foreword

In the past decade, the crystal design and engineering of multidimensional arrays and networks containing transition metal complexes as nodes have achieved considerable progress. The increasing interest in this field, which involves both synthetic and theoretical chemists, physicists, crystallographers and materials scientists, is justified by the potential utility of these compounds as zeolite-like materials, catalysts or molecular electronics devices. Although numerous beautiful compounds illustrate reliable predictions of the solid-state architectures, many other interesting structures could not be predicted. However, their retrospective analysis provides the necessary information in the attempt to design intentionally inorganic or organic/inorganic hybrid materials with specific functions and properties. More recently researchers have started thinking to the extent of introducing and investigating the concept of aromaticity in the metal containing chelate rings. In recent years there is a resurgence of interest in this field probably due to the advances in synthesis, spectroscopy, crystallography and theory. It is often quoted that the concept of metalloaromaticity may play an important role in understanding organometallic mediated reactions. Ligand design is also an important area which is being developed. This topic spans the whole field, as specific ligand systems are required to “tune” the metal complex to the required function. Ligand design is important in the development of biomimics, selective metal extractants, catalysts, metal-based drugs and new materials. New ligand systems such as the cryptands and the cyclic polyethers have had a wide impact on chemistry in general. Much of modern synthetic organic chemistry depends on the use of new coordination compounds and organometallic derivatives as specific reagents.

The importance of transition metal complexes has been wide varied as homogeneous catalysts in industry, reagents in the spectroscopic determination of trace elements, and as important drugs. Among a number of transition metal complexes synthesized since the pioneering works of Werner, most of them were aimed at a biological activity which they suppose to exhibit. Later interests in this field also turned in to crystallographer’s or photochemist’s hand so as to engineer

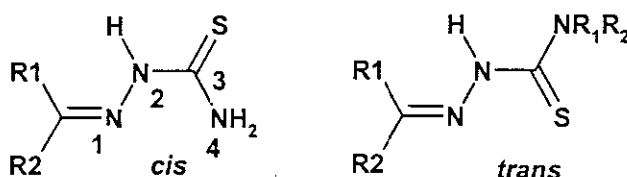
these molecules with photonic applications or with short lived memories applicable in molecular electronics. But the biological implications of these metal complexes continued to be of interest because of the remarkable and often unexpected results in that area of research. And after decades of research people have arrived at the structure-to-activity correlation in these compounds. Among a large variety of compounds metal containing thiosemicarbazones have gained so much of interest because of their unique gamut of properties. They were known to possess antiviral, antifungal, antitumor and enzyme mimetic properties which are inimitable due to their versatile chelating behavior. The work embodied in this thesis was carried out by the author in the Department of Applied Chemistry during 2001-2003. This work stems from our interests in the biological activity as well as the structure of the metal complexes of the metal complexes of thiosemicarbazones. The incipient aim of this investigation is to probe the spectroscopic, structural and antimicrobial studies of some selected transition metal complexes of some thiosemicarbazones. We have encountered with a variety of unexpected structures during our pursuit and it was rather interesting to see the thiosemicarbazones coordinating as well as reacting with the metal ions to make little surprises in the reaction flask. The thesis has been divided in to seven chapters carrying a detailed account of our attempts to tune the ligands to react with copper, iron, manganese, gold and vanadium ions. First chapter is a small review of the recent trends observed in thiosemicarbazone's research. Second chapter deals with the synthesis of the thiosemicarbazone ligands and their structural and spectral characterization. Antimicrobial studies of the ligands and their synthetic precursors were carried out to garnish our observations in the metal complexes. Chapter 3 deals with an array of copper complexes which really showed its power of reaction with the ligands. A number of structures were revealed whose microbial inhibitory activities are also discussed. Chapter 4 accounts the structure of iron(III) complexes along with their microbial studies. Chapters 5-7 discusses an attempt to understand the structure and spectroscopy of manganese, gold and vanadium complexes, which are rare in these types of complexes and are least studied. Throughout the work we have attempted to correlate between the observed spectroscopic, crystallographic, self-assembling and biological activities to the best of our knowledge.

Chapter 1

Thiosemicarbazones and their metal complexes

– A brief survey

Metal complexes of thiosemicarbazones (TSCs) have been extensively studied and have been subject of several reviews¹⁻⁴. These compounds exhibit a plethora of biological activities either as an organic compound or in the coordinated form. Often the metal complexes exhibit remarkable activity than the ligands. According to the IUPAC recommendations for the nomenclature of organic compounds, derivatives of thiosemicarbazides⁵ of the types $R^1R^2C=N-NH-CS-NR^3R^4$ which are usually obtained by the condensation of thiosemicarbazides with suitable aldehydes or ketones may be named by adding the class name thiosemicarbazone after the name of condensed aldehyde or ketone. Research in coordination chemistry⁶, analytical applications⁷ and biological activities⁸ has augmented progressively for past five decades. The structure of the $C=N-NH-CS-N$ back bone of the TSC is usually almost planar, with the sulfur atom *trans* to azomethine nitrogen. Scheme 1.1 shows the *cis-trans* isomers with their numbering scheme. Few compounds are exceptions to this rule existing in *cis* form. Although there are several electronic and steric factors that may contribute to the adoption of this arrangement, the most important factor is probably that the *trans* arrangement places the amine and azomethine nitrogen atoms in relative positions suitable for intramolecular hydrogen bonding⁹. In fact the complete substitution of amine crystallize with S atom *cis* with azomethine nitrogen giving Z- configuration.



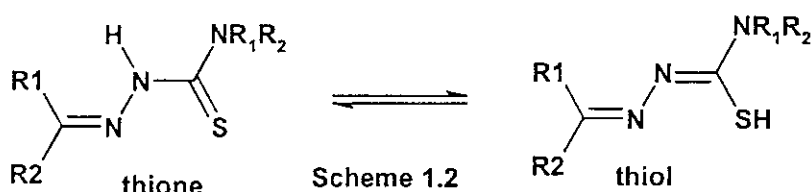
Scheme 1.1

In Scheme 1.1, conventional single and double bonds are represented. However as was pointed out by Palenik *et al*¹⁰, on the basis of their pioneering work in the field, TSCs are extensively delocalized systems, especially when aromatic radicals are bound to the azomethine carbon atom. Usually chelation takes place by deprotonation of the TSC's hydrazinic –NH group, and anions are usually found in Z-form. The coordination possibilities deriving from the many potential donor atoms in TSC back bone is increased if substituents R1 or R2 includes additional donor atoms.

This chapter attempts to review the structural aspects including bonding and stereochemistry along with the biological aspects of the TSCs and their transition metal complexes. The objective and scope of the work embodied in this thesis is also discussed along with the physical methods used for the analysis of the ligands and metal complexes.

1.1. Bonding and stereochemistry

The stereochemistries adopted by TSCs while interacting with transition metal ions, depend essentially upon the presence of an additional coordination centre in the ligand moiety and the charge on the ligand, which in turn is influenced by the thione \leftrightarrow thiol equilibrium. It has been shown that the arrangement of non-hydrogen atoms in the thiosemicarbazides molecule is nearly planar and the sulfur atom and hydrazinic ²NH₂ group are *trans* with respect to the C=N bond¹¹. When forming complexes in this configuration bonding occurs via sulfur atoms as monodentate ligand. However in most of the cases TSCs coordinate as bidentate ligands via azomethine nitrogen and thione/thiolato sulfur. Besides the denticity variation, consideration of the charge distribution is complicated in all thiosemicarbazones due to the existence of thione \leftrightarrow thiol tautomers (Scheme 1.2). Although the thione form predominates in the solid state, solutions of thiosemicarbazones show mixture of both tautomers.



TSCs are known to react with almost all metal ions, and the most well studied TSCs are those made from 2-acetylpyridine. 2-Acetylpyridine thiosemicarbazones are the first thiosemicarbazones in which antimalarial activity was detected¹². The highest activity is reported when the N(4) position is either disubstituted or is part of a ring system. A wide spectrum of work was attributed to this field in past five decades due to the extensive biological activity shown by these TSCs and their metal complexes of copper¹³, manganese¹⁴, iron¹⁵, zinc¹⁶ and nickel¹⁷ complexes. TSCs are known to mimic ribonucleotide reductase inhibiting DNA synthesis¹⁸. A large number of heterocyclic thiosemicarbazones are known to inhibit Mycobacterium tubercle¹⁹. Particular attentions were given to the antineoplastic activity displayed both *in vitro* and *in vivo* by α -(N)-heterocyclic carbaldehyde thiosemicarbazones²⁰. Besides these they are also known to selectively inhibit Herpes Simplex Virus (HSV)²¹. In recent years there is a resurgence of interest in these compounds as photonic materials with the advancement of lasers and crystallographic techniques. A large number of transition metal complexes are known to self assemble in the crystal lattice making them interesting materials in non linear optics.

There are some recent reports on the large second harmonic generation efficiency of zinc complexes of thiosemicarbazones²² which makes them interesting molecules which shows excellent transparency trade-off in the optical non-linearity. Recently palladium(II) complexes of thiosemicarbazones are known to catalyze homogeneous hydrogenation under normal temperature and atmospheric pressure²³. A recent report by Casas *et al.*²⁴ accounts an interesting metal induced cyclization of thiosemicarbazones derived from α -ketoamides and α -keto esters. Many peoples were able to arrive at interesting transformations and stereochemistries by making use of the chelation of TSCs with metals such as ruthenium²⁵ and platinum in which reductive cleavage²⁶ of the hydrazinic N-N bond is catalyzed by the metal centre giving rise to interesting structures. Transition metal complexes of bis(TSC) ligands are also of interest due to their interesting redox properties, and hypoxic selectivity thereby making them vehicles for the delivery of radio active isotopes to the tumor or leucocytes cells²⁷. Palladium and platinum complexes of a p-isopropyl benzaldehyde thiosemicarbazone have reported to posses cytotoxic properties since

they are able to circumvent *cis-DDP* resistance in transformed *ras* oncogenes (Pam 212-*ras*), in addition to killing these cells by apoptosis²⁸. The structures of Group 13 metal thiosemicarbazones, which have been reviewed²⁹ very recently are especially interesting since the metallic and organometallic ions of this group are able to use simultaneously all the potential donors of both E and Z-TSC chains.

1.2. Objective of this work

As discussed previously transition metal complexes of thiosemicarbazones possess a large spectrum of properties. The work embodied in this thesis mainly aims at weaving a network about their interesting spectroscopic, crystallographic and antimicrobial properties. The present study mainly aims at,

- Synthesizing a plethora of TSCs complexes with transition metal ions with interesting structural features.
- To understand the spectroscopy of these structures.
- To understand the exact structure and stereochemistry adopted by these compounds through single crystal X-ray diffraction.
- To understand the self assembling aspects by looking at the intermolecular interaction parameters in the crystal lattice.
- To study the biological activities of the complexes and the ligands.
- To arrive at a structure to activity correlation.

1.3. Physical methods

1.3.1. Elemental analyses and magnetic susceptibility measurements

CHN analyses were performed on a Heracus elemental analyzer at Central Drug Research Institute, Lucknow. Room temperature magnetic susceptibility measurements in the polycrystalline state were carried out in a Guoy balance using cobalt mercuric thiocyanate as a reference standard at 298 K. Molar conductance measurements of complexes were carried out in DMF solvent at 28 ± 2 °C on a Century CC-601 digital conductivity meter with dip type cell and platinum electrode. Approximately 10^{-3} M solutions were used for these studies.

1.3.2. NMR spectra

^1H and ^{13}C NMR spectra were obtained in a Bruker DRX 500 instrument using CDCl_3 as the solvent and TMS as the internal reference at Sophisticated Instruments Facility, Indian Institute of Science, Bangalore, India. The tentative structures were assigned on the basis of different NMR experiments, based on the couplings and connectivities of the signals observed. The ^1H resonances were assigned on the basis of chemical shifts, assignments of the acidic hydrogens were made by comparison with the spectra recorded on deuterium exchange. The carbon types were determined by ^{13}C - Spin Echo Fourier Transform (SEFT) experiments.

1.3.3. Electronic spectra

Electronic spectra were recorded in the room temperature polycrystalline state in magnesium oxide matrix in Ocean Optics SD 200 fiber optic spectrophotometer in the 250-1000 nm range. UV-Vis-NIR spectra in solution was recorded in the 1200-200 nm range on a JASCO UV-Vis-NIR Spectrophotometer in CHCl_3 solution at the International School of Photonics, CUSAT, Kochi, Kerala.

1.3.4. IR spectra

Infrared spectra were recorded on a Shimadzu DR 8001 series FT-IR instrument as KBr pellets in the range $400\text{-}4000\text{ cm}^{-1}$ at CDRI, Lucknow and far IR spectra was recorded in the range $50\text{-}500\text{ cm}^{-1}$ on a NICOLET MAGNA 550 FT-IR spectrometer using polyethylene pellets at RSIC, IIT- Bombay, India.

1.3.5. EPR spectra

EPR spectra were recorded on a Varian E-112 X-band EPR Spectrometer using tetracyanoethylene (TCNE) as a standard at RSIC, IIT, Bombay, India. The EPR spectra of polycrystalline sample at 298 K, solution at 298 K and 77 K were recorded in the X band, using the 100-kHz field modulation; g factors were quoted relative to the standard marker TCNE ($g = 2.00277$).

1.3.6. Mössbauer Spectra

^{57}Fe Mössbauer Spectra were recorded on a constant-acceleration spectrometer with a multi channel analyzer using a ^{57}Co in a Rhodium matrix at Inter University Consortium, Indore, India. Low temperatures up to 20 K were obtained using 22C/350C cryodyne refrigerator, circulating liquid helium through the system.

1.3.7. X-Ray Crystallography

Single crystal X-ray crystallographic analysis of the compounds HBpypTsc, **2**, **6**, **7** and **14** were carried out at room temperature (293 K) on an Nonius MACH3 diffractometer equipped with graphite-monochromated $\text{MoK}\alpha$ ($\lambda = 0.71073 \text{ \AA}$) radiation at National Single Crystal X-Ray Diffraction Facility, Indian Institute of Technology, Mumbai, India. Data for compounds HPranThas, **9**, **12**, **15**, **18** and **19** were collected using a Siemens SMART CCD area-detector diffractometer at School of Physics, Universiti Sains Malaysia, Hong Kong, and that of compound **10** was analyzed by using a Siemens SMART CCD area-detector diffractometer at the Department of Inorganic and Physical Chemistry, Indian Institute of Science, Bangalore, India. The intensity data were collected by ω -scan mode for hkl. Empirical absorption corrections were employed by using ψ -scan technique. The trial structure was obtained by direct methods using SHELXL-97³⁰ and refined by full-matrix least squares on F^2 (SHELXS-97)³¹. The non-hydrogen atoms were refined with anisotropic thermal parameters. All hydrogen atoms were geometrically fixed and allowed to refine using a riding model. Graphics quality Plots were made by using the packages ORTEP³² and PLATON³³. Intermolecular interaction parameters were calculated by using the full geometry calculations and analysis of short ring interactions in PLATON.

Chapter 2

Synthesis and Studies on Thiosemicarbazone Ligands

The importance of thiosemicarbazones as bioactive agents has already been discussed in last chapter. Three thiosemicarbazones viz. 2-benzoylpyridine *N*(4), *N*(4)-(butane-1, 4-diyl) thiosemicarbazone (HBpypTsc), 2-acetylpyridine *N*(4), *N*(4)-(butane-1, 4-diyl) thiosemicarbazone (HPranThas) and di-2-pyridylketone thiosemicarbazone (HDpkTsc) were synthesized by adopting and modifying a reported procedure³⁴. HBpypTsc and HPranThas have an *N*(4) substitution as part of a pyrrolidine ring system where HDpkTsc is *N*(4) unsubstituted. Figure 2.1 presents the structural formulae of the ligands under study. The newly synthesized HBpypTsc is chosen as the principal ligand for majority of the investigations. While HPranThas and HDpkTsc were reinvestigated for their crystal structures. Details about the preparation of the compounds, their spectral crystallographic properties of HBpypTsc, HDpkTsc and HPranThas are discussed in the chapter. Antimicrobial activities of the compound HBpypTsc with its synthetic precursors are also discussed.

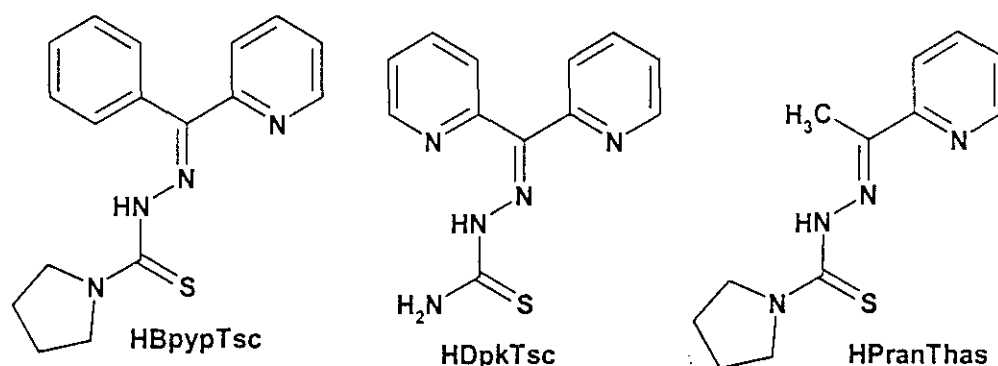


Figure. 2.1 Structural formulae of thiosemicarbazones.

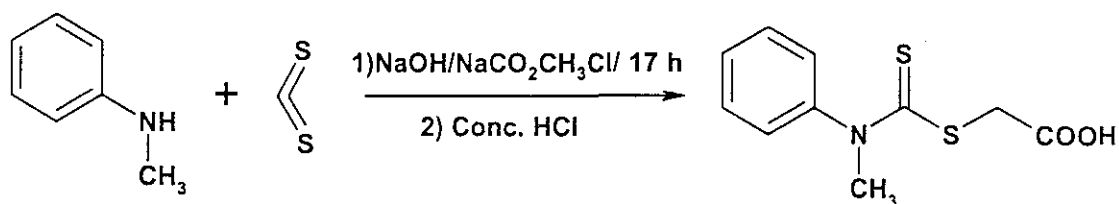
2.1. Experimental

2.1.1 General

2-Acetylpyridine (Fluka), 2-benzoylpyridine (Lancaster), di-2-pyridylketone (Fluka), pyrrolidine (SRL), N-methyl aniline (Merck), thiosemicarbazide (SRL), carbon disulfide (Merck), hydrazine hydrate (99 %, SRL) were used as received. All solvents were purified by distillation and kept under inert atmosphere. Methanol was dried over fused calcium chloride in the presence of magnesium isopropoxide. Acetonitrile was dried over activated alumina and distilled.

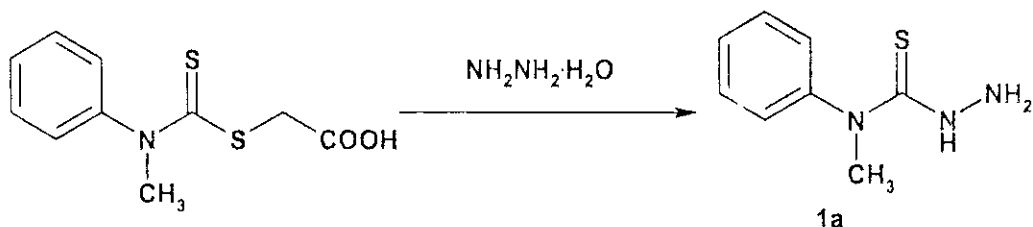
2.1.2. Carboxymethyl N-methyl N-phenyldithiocarbamate

A mixture consisting of 12.0 mL (15.2 g, 0.2 mol) of CS₂ and 21.6 mL N-methyl aniline was treated with a solution of 8.4 g (0.21 mol) of NaOH in 250 mL water. After stirring at room temperature for 4 h, the organic layer had disappeared. At this point, the straw colored solution was treated with 23.2 g (0.20 mol) of sodium chloroacetate and allowed to stand overnight for 17 h. The solution was acidified with 25 mL of conc HCl and the solid which separated was collected and dried. This afforded 39.7 g of pale buff colored carboxymethyl N-methyl N-phenyldithiocarbamate. mp 197-198 °C



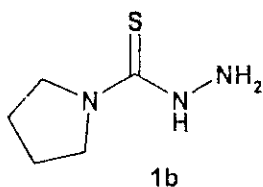
2.1.3. 4-Methyl-4-phenyl-3thiosemicarbazide (1a)

A solution of carboxymethyl N-methyl N-phenyldithiocarbamate in 20 mL 99 hydrazine hydrate and 10 mL of water was heated on the rings of a steam bath. After 3 min crystals begin to separate. Heating was continued for 22 min. The crystals were collected by filtration, washed well with water and dried under a heat lamp. The crude product was recrystallized from a mixture of 50 mL ethanol and 25 mL of water. This gave 10.8 g of stout colorless rods of 4-Methyl-4-phenyl-3thiosemicarbazide (**1a**). mp 124-125°C



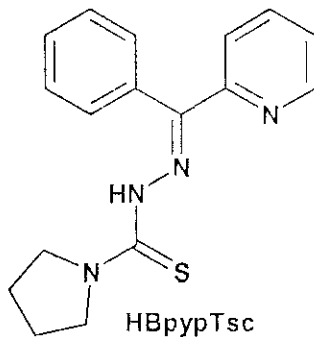
2.1.4. Pyrrolidine-1-thiocarboxylic acid hydrazide (1b)

A solution of 1.0 g of **1a** in 5 mL of acetonitrile was treated with 395 mg of pyrrolidine and the solution was heated under reflux for 15 min. The solution was chilled and the microporous off white crystals separated were collected and washed with acetonitrile. This afforded 570 mg of **1b**. mp 174-175°C



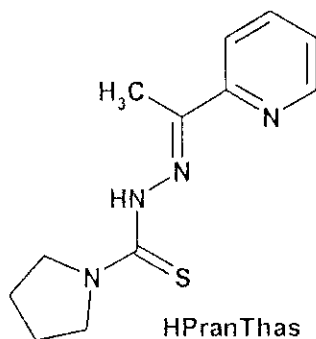
2.1.5. 2-Benzoylpyridine N(4), N(4)-(butane-1, 4-diyl) thiosemicarbazone

To a solution of **1b** (0.1 mol) and 2-benzoylpyridine (0.1 mol) in 20 mL methanol, 2 drops of conc. acetic acid was added and the reaction mixture was heated under reflux for 5 h. the progress of the reaction was monitored by TLC. The reaction mixture was kept for 3 days where the deep yellow colored crystals of HBpypTsc began to separate in a decent yield. X-Ray quality single crystals of the compound were grown from a solution of the compound HBpypTsc in chloroform layered with methanol in 5 days. mp. 185-186 °C. Anal Found (Calcd)%: C,65.75 (65.78); H, 5.85 (5.84); N, 18.05 (18.05). IR (cm⁻¹): ν(C=N), 1630 s; ν(N=N), 1118 s ; νδ(C=S), 1342s, 842m; ν(NH), 3448 m; ρ ip/op, 649 m, 455 w. ¹H-NMR δ (ppm): NH, 14.3, singlet 1H; 8.73, doublet, aromatic, 1H, J= 7.5 Hz; 8.5, aromatic, doublet, 1H; 7.1-7.8, aromatic, multiplet, 7H, 3.8, aliphatic, multiplet, 4H, 1.9, aliphatic, multiplet, 4H.



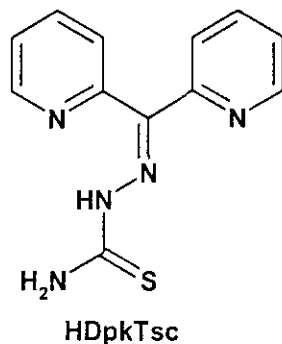
2.1.6. 2-Acetylpyridine *N*(4), *N*(4)-(butane-1, 4-diyl) thiosemicarbazone

To a solution of **1b** (0.1 mol) and 2-acetylpyridine (0.1 mol) in 20 mL methanol, 2 drops of conc. acetic acid was added and the reaction mixture was heated under reflux for 4 h. The reaction mixture was kept overnight where the pale yellow colored crystals of HPranThas began to separate in a decent yield. X-Ray quality single crystals of the compound were grown from a solution of the compound HPranThas in methanol in 4 days. mp. 148-149°C. Anal Found(Calcd)%: C, 58.00(58.03); H, 6.45(6.49); N, 22.54 (22.56).



2.1.7. Di-2-pyridyl ketone thiosemicarbazone

To a solution of thiosemicarbazide (0.1 mol) and di-2-pyridyl ketone (0.1 mol) in 20 mL methanol, 2 drops of conc. acetic acid was added and the reaction mixture was heated under reflux for 3 h. the progress of the reaction was monitored by TLC. The reaction mixture was kept overnight where off-white colored crystals of HDpkTsc began to separate in a decent yield. mp. 180-181°C. Anal Found (Calcd)%: C, 56.00 (56.01); H, 4.32 (4.31); N, 27.52 (27.22).



2.2. Results and discussions

2.2.1. Syntheses

Figure 2.2 shows the energy minimized structures¹ of the compounds HDpkTsc and HBpypTsc under study showing planarity in the thiosemicarbazide skeleton while the ketonic residue is slightly tilted from the plane into a propeller like structure.

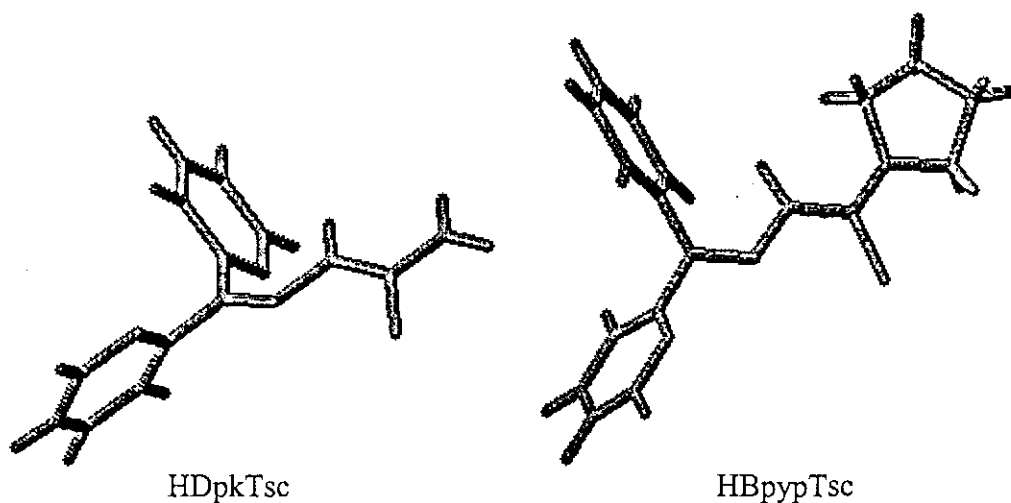
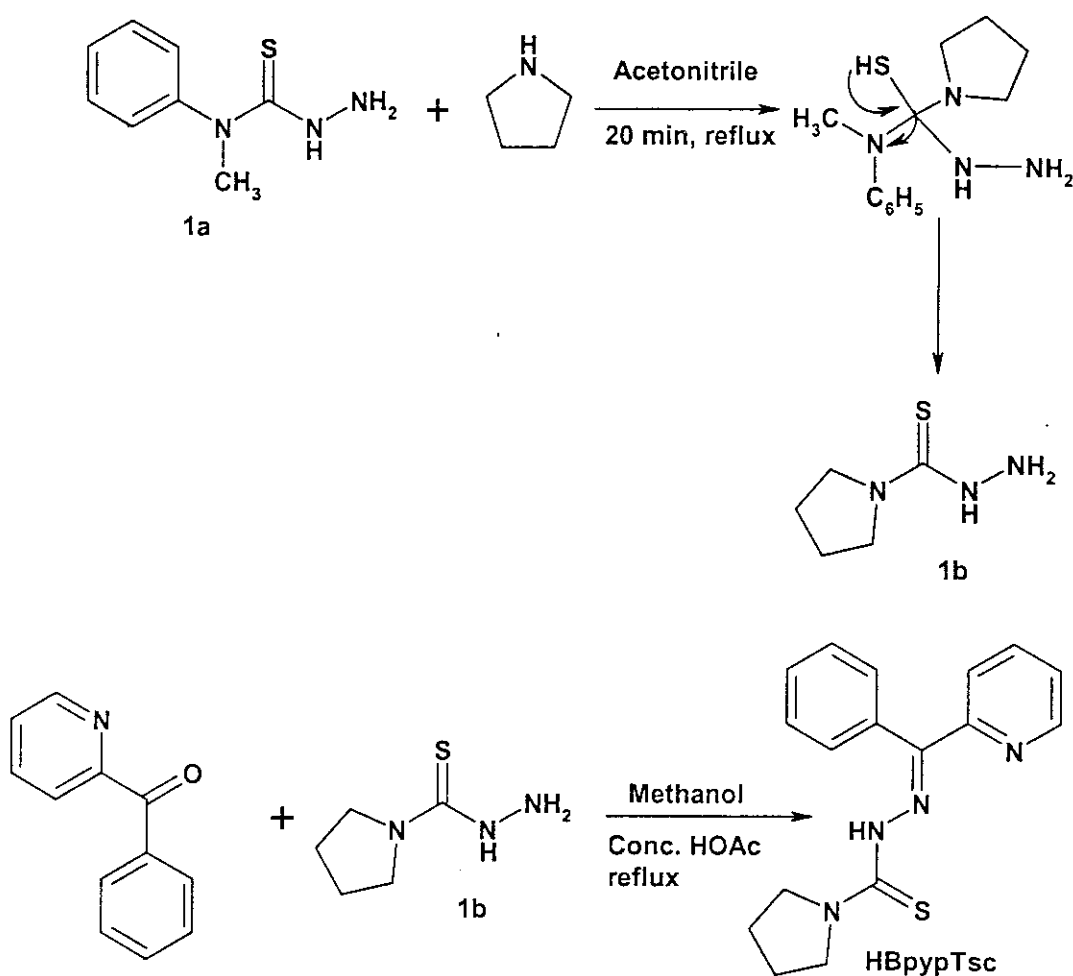


Figure 2.2. Energy minimized diagram of the thiosemicarbazones

Carboxymethyl-N-methyl-N-phenyl dithiocarbamate is formed by the reaction between carbondisulfide, N-methylaniline, sodium hydroxide and sodium monochloroacetate. After stirring for 17 h the resultant solution is acidified with conc. HCl to give the product. This product is reacted with hydrazine hydrate to get

1. Energy minimized structures were drawn by ACD labs Chem sketch v 5.08 and 3D viewer free ware program from Advanced Chemistry Developments Inc. USA

1a. The Synthesis of thiosemicarbazones from **1a** involves two steps such as transamination followed by a condensation with corresponding aldehyde or ketone. Transamination involves replacement of the N-methyl N-phenyl group from **1a** by a secondary amine present in the solution following a standard addition elimination reaction. Nucleophilic addition of an amine to the thiocarbonyl group of **1a** produces a tetrahedral intermediate. Elimination of N-methylaniline from this intermediate reforms the thiocarbonyl group and yields the N(4) substituted thiosemicarbazide **1b** (scheme 1). The condensation process is a direct reaction of **1b** with the carbonyl compound to yield the thiosemicarbazone moiety.



Scheme 1

2.2.2. Structure of HBpypTsc

The compound HBpypTsc crystallizes into an orthorhombic lattice with P212121 space group symmetry. The experimental details and crystallographic refinement parameters are presented in Table 2.1. Figure 2.3 shows the molecular structure of the compound and Figure 2.4 shows the molecular packing to the compound in a unit cell. The structure reveals the fact the two aromatic rings are slightly tilted from the plane of the ring existing in a propeller like fashion. The molecule exists in Z conformation around the N2-N3 bond. The structure reveals quasicoplanarity in the plain of the thiosemicarbazone but both the aromatic rings are bifurcated. The molecular structure reveals that the compound exists in thione form. Table 2.2 illustrates the selected bond lengths and angles.

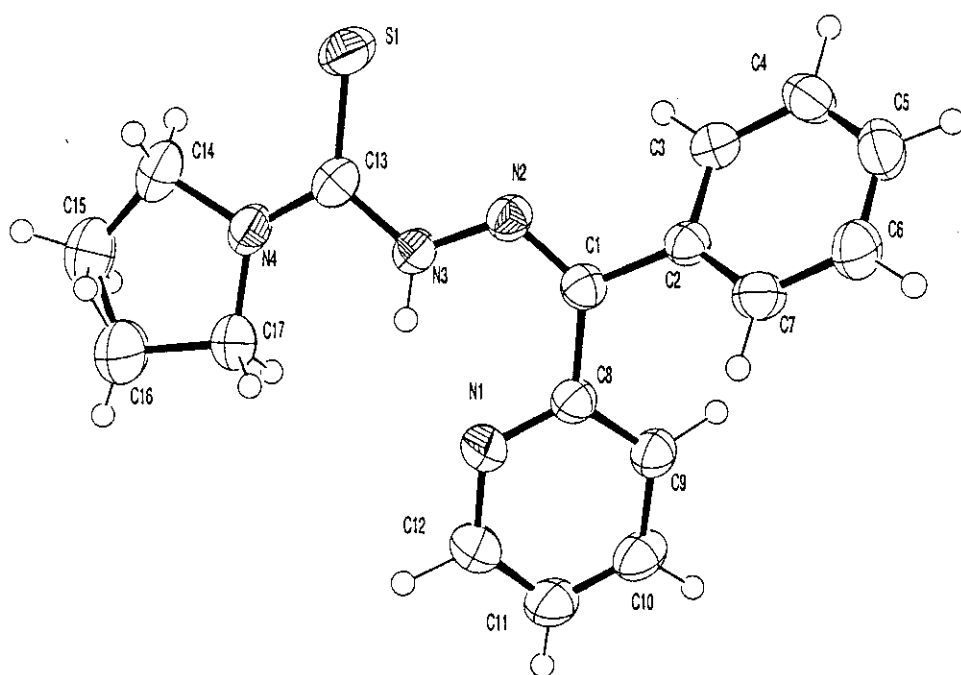


Figure 2.3. ORTEP diagram of the compound HBpypTsc in 54% probability. All hydrogen atoms are shown as small spheres of arbitrary radii.

The compound has two double bonds in the thiosemicarbazones moiety viz. C1-N2 1.295 Å and C13-S1 1.681 Å which are consistent with the previously reported cases. The planarity in the thiosemicarbazone is revealed by a smaller dihedral angle of the N2-N3-C13-S1 (0.9°) skeleton. Considerable amount of the ring bifurcation from the plane of the thiosemicarbazone is indicated by the dihedral angles C1-N2-N3-C13 (-176.9°) and C8-C1-C2-C7 (-44.7 °). The S and pyridyl N1

atoms are in E configuration with respect to C1-N2 bond. The five membered pentamethyleneimine ring is not planar and tends towards an envelope conformation³⁵. The smaller dihedral angles between the pyridyl ring and the phenyl ring of the 2-benzoylpyridine moiety and thiosemicarbazone moiety (C2-C1-C8-C9 (-28.2°), and N3-N2-C1-C8 (2.2°) is due to a resonance effect between the π systems. The packing of the compound is assisted by the 2-D network formed by the self assembly of the molecules is aided by the intramolecular hydrogen bonding and C-H..... π Interactions which arranges the molecule in to a zigzag manner in a unit cell. Pyridyl nitrogen N1 is intramolecularly hydrogen bonded to N3-H103 at 2.65 Å distance forming a six membered ring.

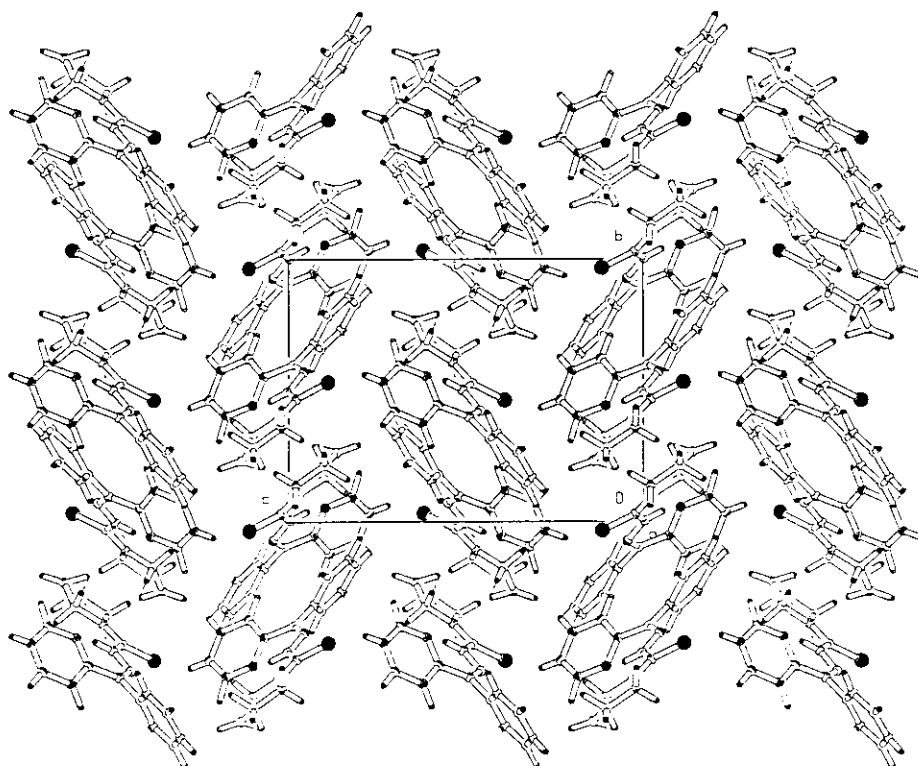


Figure 2.4. Packing of the compound HBpypTsc, viewed along b axis

Table 2.1 Crystal refinement parameters of the compound HBpypTsc

Empirical formula	C ₁₇ H ₁₈ N ₄ S
Formula weight	310.41
Temperature/ λ	293 K/ 0.7093 Å
Crystal system/space group	Orthorhombic, P212121
Unit cell dimensions	a= 9.9500, α = 90.000(17)° b= 10.7690, β = 90.000(15)° c= 14.898, γ = 90.000(8)°
Volume	1596.3(6) Å ³
Z, calculated density	4, 1.292 mgm ⁻³
Absorption coefficient	0.205 mm ⁻¹
F(000)	656
Crystal size	0.35×0.35×0.30 mm
Limiting indices	0 ≤ h ≤ 11, 0 ≤ k ≤ 12, 0 ≤ l ≤ 17
Reflection collected/unique	1526/1526 [R(int)= 0.000]
Max. and min. transmission	1.000 and 0.989
Data, restraints, parameters	1526/0/271
Goodness-of-fit on F ²	1.075
Final R indices [I>2σI]	R1 = 0.0387, wR2 = 0.1535
R indices all data	R1= 0.0895, wR2= 0.1726
Largest diff. peak and hole	0.174 and -0.224 eÅ ⁻³

Table 2.2. Selected bond lengths and angles of HBpypTsc

Bond lengths		Bond angles	
S(1)-C(13)	1.681(3)	C(1)-N(2)-N(3)	118.4(2)
N(1)-C(12)	1.341(4)	C(13)-N(3)-N(2)	121.1(2)
N(1)-C(8)	1.342(4)	N(1)-C(8)-C(9)	121.7(3)
N(2)-C(1)	1.295(4)	N(1)-C(8)-C(1)	117.5(2)
N(2)-N(3)	1.366(3)	N(1)-C(12)-C(11)	123.9(4)
N(3)-C(13)	1.360(4)	N(3)-C(13)-S(1)	124.0(2)
X-H...Cg	H.....Cg (Å)	X....Cg (Å)	∠X-H...Cg (°)
C12-H12...Cg(3) ^a	2.8518	3.6071	126.85
C16-H16...Cg(2) ^b	3.2937	4.1282	145.44
a= ½-x, 1-y, ½+z	Cg(2) = N1, C8, C9, C10, C11, C12		
b= 1-x, -½+y, ½-z	Cg(3) = C2, C3, C4, C5, C6, C7		
D-H...A	H.....A (Å)	D....A (Å)	∠D-H.....A °
N3-H103.....N1 ^c	1.94	2.659	136
C11-H11...N2 ^c	2.59	3.409	153
c = x, y, z			

2.2.3. Structure of HPranThas

The compound HPranThas crystallizes in to a monoclinic lattice with P21/c space group symmetry. The experimental details and crystallographic refinement parameters are presented in Table 2.3. Figure 2.5 shows the molecular structure of the compound and Figure 2.6 shows the molecular packing to the compound in a unit cell.

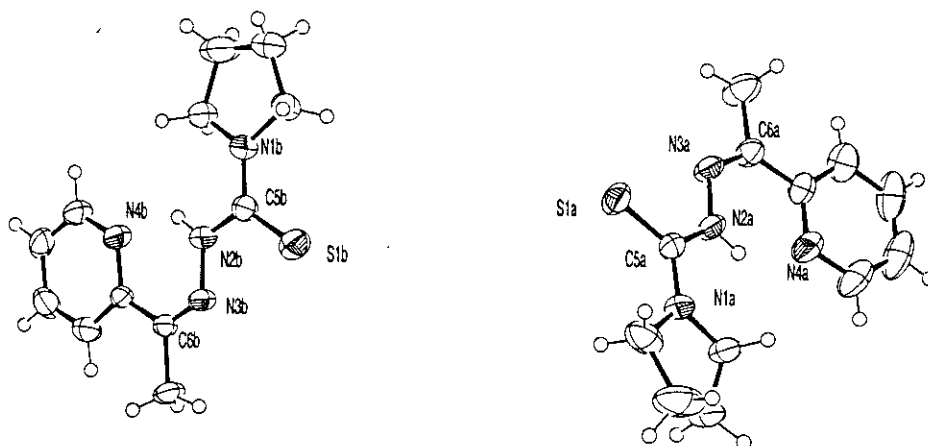


Figure 2.5. ORTEP diagram of the compound HPranThas drawn at 55% probability level. All hydrogen atoms are placed as small spheres of arbitrary radii.

The structure reveals quasi co-planarity with two crystallographically equivalent molecule in a unit cell. Table 2.4 presents the selected bond lengths and angles along with the H-bonding parameters. There are two crystallographically independent molecules A and B in the asymmetric unit of the compound HPranThas with bond lengths and angles which agree with each other and are within normal ranges.

Both molecules are related by a local pseudo-twofold rotation axis and exists in an E configuration about the C6-N3 and C5-N2 bonds relative to the N3-N2 bond. The S and hydrazine N3 atoms are in Z configuration with respect to C5-N2 bond. In both molecules the five membered pyrrolidine ring is not planar and tends towards an envelope conformation. In both molecules, the relative conformations of the pyridine ring and methyl group with respect to planar thiosemicarbazone are conditioned by the sp^2 hybridized carbon atom.

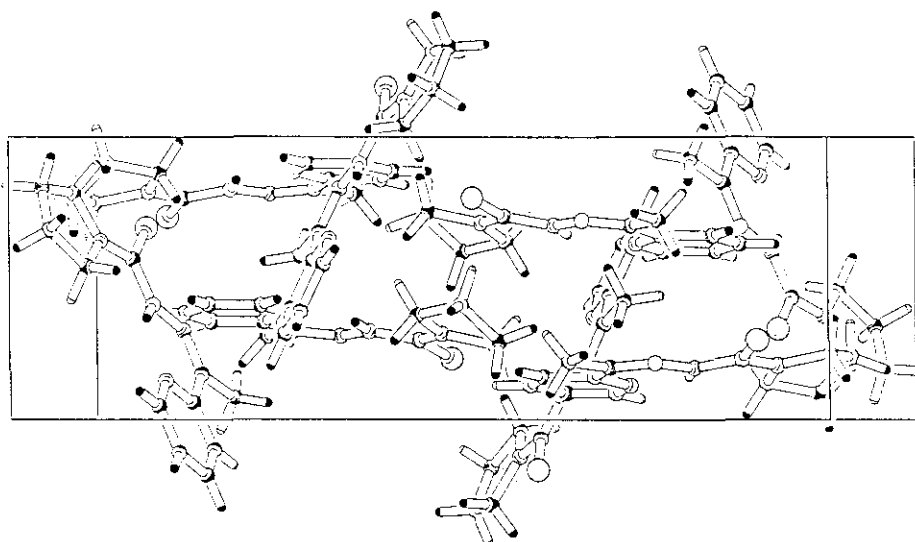


Figure 2.6. Packing of the compound *HPranThas* viewed along *c* axis.

Table 2.3 Crystal refinement parameters of the compound *HPranThas*

Empirical formula	$C_{12}H_{16}N_4S$
Formula weight	248.35
Temperature	293 K
Wavelength	0.71073 Å
Crystal system/space group	Monoclinic, P21/c
Unit cell dimensions	$a=15.627$ Å, $\alpha=90.000^\circ$ $b=22.115$ Å, $\beta=94.362^\circ$ $c=7.444$ Å, $\gamma=90.000^\circ$
Volume	2565.1 Å ³
Z, calculated density	8, 1.286 Mgm ⁻³
Absorption coefficient	0.237 mm ⁻¹
F(000)	1056
Crystal size	0.52×0.40×0.20 mm
Theta range for data collection	2.61 to 25.00°
Limiting indices	$-17 \leq h \leq 8$, $-24 \leq k \leq 22$, $-8 \leq l \leq 8$
Completeness to 2 θ	25.00, 92.8 %
Absorption correction	ψ -scan
Max. and min. transmission	0.9542 and 0.8869
Refinement method	Full-matrix linear least square on F^2
Data, restraints, parameters	4194/0/309
Goodness-of-fit on F^2	.112
Final R indices [$I > 2\sigma I$]	$R1 = 0.0861$, $wR2 = 0.2135$
R indices all data	$R1 = 0.1200$, $wR2 = 0.2373$
Largest diff. peak and hole	and 0.468 and -0.432 eÅ ⁻³

Table 2.4. Selected bond lengths and angles of HPranThas

Bond lengths		Bond angles	
S(1A)-C(5A)	1.692(4)	C(5A)-N(1A)-C(4A)	124.0
N(1A)-C(5A)	1.347(6)	C(5A)-N(2A)-N(3A)	121.4
N(2A)-C(5A)	1.349(6)	C(6A)-N(3A)-N(2A)	118.6
N(2A)-N(3A)	1.364(5)	C(2A)-C(3A)-C(4A)	105.3
N(3A)-C(6A)	1.293(6)	N(1A)-C(5A)-N(2A)	114.7
C(1A)-C(2A)	1.511(9)	N(2A)-C(5A)-S(1A)	124.0
X-H....Cg	H.....Cg(Å)	X....Cg(Å)	∠X-H...Cg(°)
C9-H9BA-Cg(4) ^a	2.8854	3.6978	146.67
A=x, 1/2 -y, 1/2 +z	Cg(4)=N4B,C7B,C8B, C9B, C10B, C11B		
D-H...A	H.....A(Å)	D....A(Å)	∠D-H.....A°
N2A-H2AC.....N4A	1.93	2.6184	136
N2B-H2Bc.....N4B	1.95	2.6249	135
C3B-H3BC.....S1A ^b	2.83	3.7531	160
B= 1+x, y, z			

2.2.4. Structure of HDpkTsc

The compound HDpkTsc crystallizes in to a monoclinic lattice with C2/c space group symmetry. The selected bond lengths and angles are presented in Table 2.5. Figure 2.7 shows the molecular structure of the compound and Figure 2.8 shows the molecular packing to the compound in a unit cell.

The molecule exists in an E configuration about the C2-N3 and C1-N2 bonds relative to the N3-N2 bond. The S and hydrazine N3 atoms are in Z configuration with respect to C1-N2 bond. The C1-S1 and C2-N3 bonds are typical of C=S double bond and C=N double bond character. The single bond character of N2-N3 bond and C1-N2 proves the existence of thione tautomer in the crystal lattice. The two pyridyl rings are skewed from the plane of the thiosemicarbazone moiety. Strong intermolecular H-Bonding interactions between the pyridyl nitrogen and NH₂ protons packs the molecule in a inverted face-to-face fashion which arranges in to molecular columns.

Table 2.5. Selected bond lengths and angles of the compound HDpkTsc

Bond lengths(Å)		Bond angles(°)	
C1-N1	1.321	N2-C1-S1	118.52
C1-N2	1.365	N3-C2-C7	128.11
C1-S1	1.681	N3-N2-C1	119.72
C2-N3	1.300	C2-N3-N2	120.02
S1-C1	1.681		

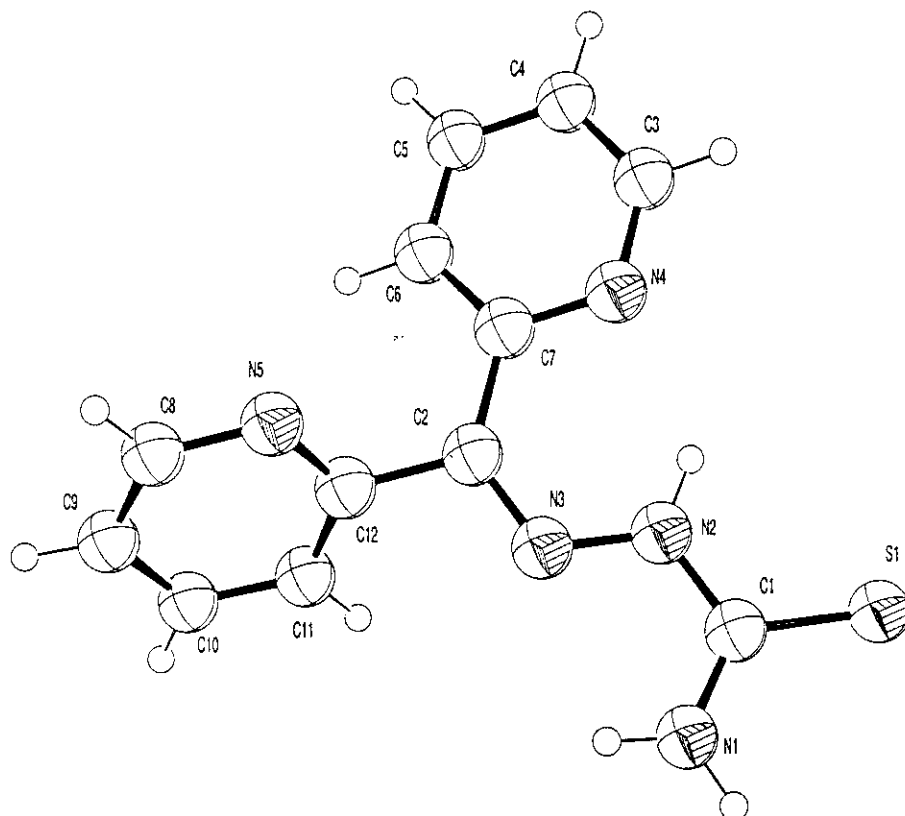


Figure 2.7. ORTEP diagram of the compound HDpkTsc. Displacement ellipsoids drawn in 55% probability level. Hydrogen atoms are shown as small spheres of arbitrary radii.

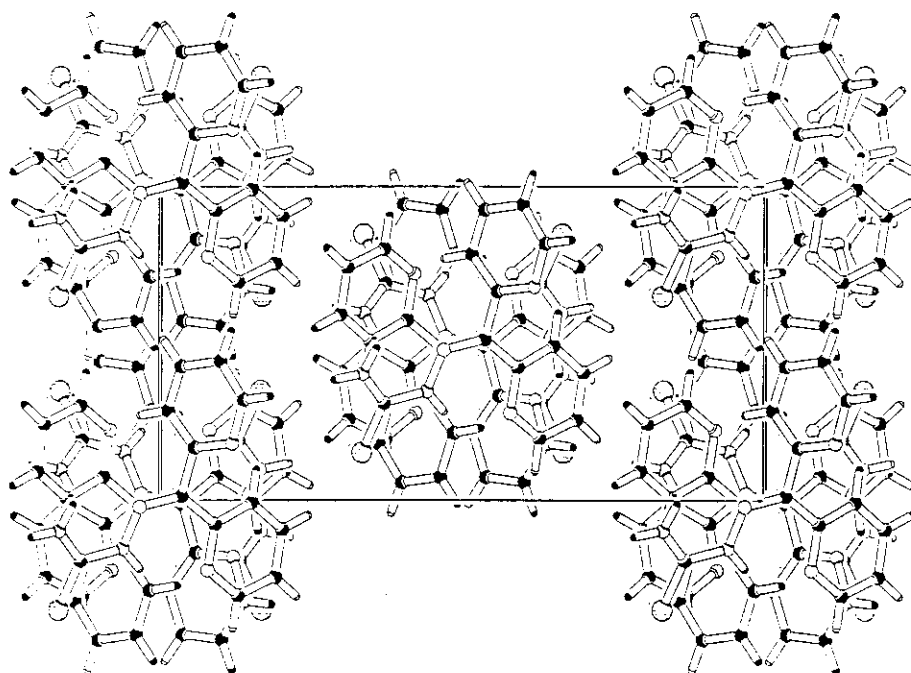


Figure 2.8. Packing of the compound view along c axis

2.2.5. NMR spectra of HBpypTsc

The tentative structure of the compound HBpypTsc was assigned on the basis of different NMR experiments, based on the couplings and connectivities of the signals observed. The ^1H resonances were assigned on the basis of chemical shifts, multiplicities and coupling constants from ^1H NMR experiments³⁶. The assignments of the NH and OH hydrogens were made by comparison with the spectra recorded on deuterium exchange.

In the ^1H NMR spectrum the signal for N(2)H is observed at $\delta = 14.35$ ppm which disappears on deuterium exchange is consistent with the *Z* configuration of the thiosemicarbazone moiety. The low frequency multiplets at $\delta = 3.8$ (4H) and 1.9 (4H) ppm was attributed to pyrrolidine ring protons C14 and C15 respectively which are chemically and magnetically equivalent with C17 and C16. Figure 2.9 shows a ^1H -NMR spectrum of the compound HBpypTsc. Aromatic protons of the pyridine and phenyl ring appear at $\delta = 8.73$, doublet, aromatic, 1H, $J = 7.5$ Hz; 8.5, aromatic, doublet, 1H and 7.1-7.8, aromatic, multiplet, 7H respectively.

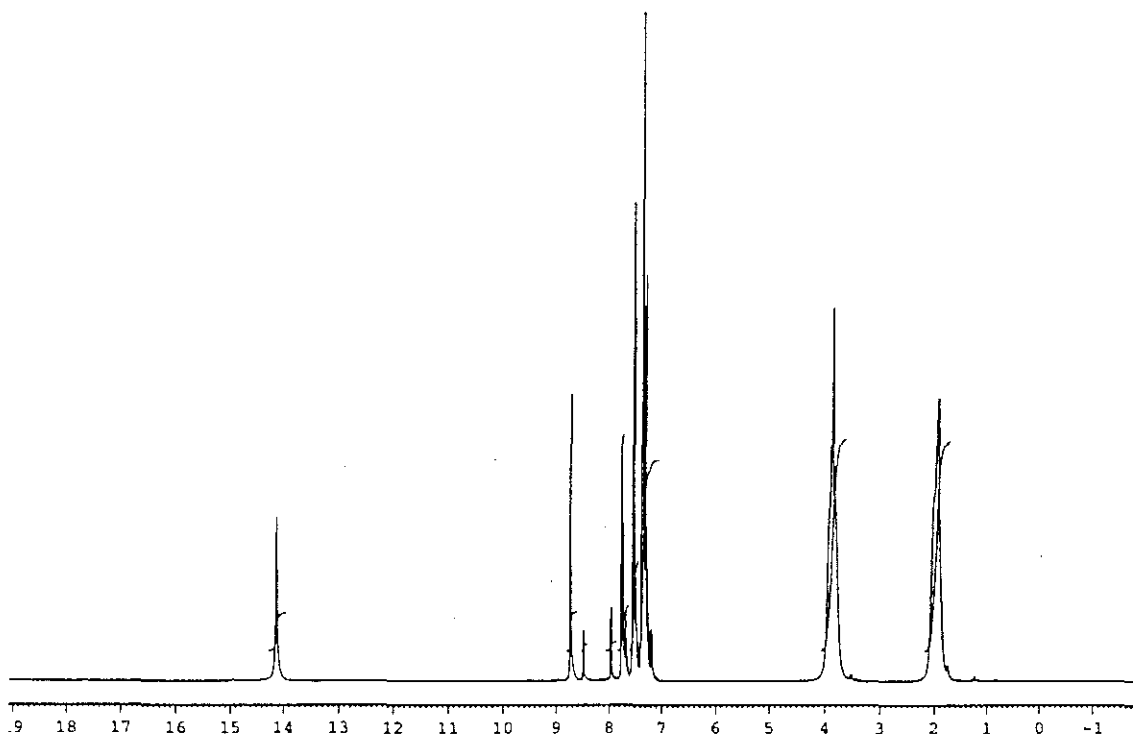


Figure 2.9. ^1H -NMR spectrum of the compound HBpypTsc

The carbon atoms were assigned on the basis of proton decoupled ^{13}C (Figure 2.10) and ^{13}C - Spin Echo Fourier Transform NMR (Figure 2.11) spectra. In the ^{13}C - SEFT NMR spectra quaternary carbons (C) and secondary (CH_2) carbons are shown as peaks pointing up and the downward peaks are CH carbons. Eighteen signals were observed in the ^{13}C NMR spectrum, which are assigned as follows. Signals at $\delta = 177.0$ and 177.6 ppm were attributed to $\text{C}(1)=\text{N}$ and $\text{C}(13)=\text{S}(1)$ of the thiosemicarbazone moiety. Aromatic carbons of the pyridine and phenyl ring of 2-benzoylpyridine moiety appear at $\delta = 121.5$ (C5), 123.8 (C4), 126.1 (C6), 128.4 (C10), 129.2 (C11), 129.6 (C3), 129.9 (C9), 137.3 (C7), 143.9 (C2), 148.0 (C9), 149.2 (C12), 152.8 (C8) respectively; where the peaks at $\delta = 53.4$, 50.4 , 26.6 , 24.3 were assigned to aliphatic carbons C14, C17, C15 and C16 respectively of the pyrrolidine ring.

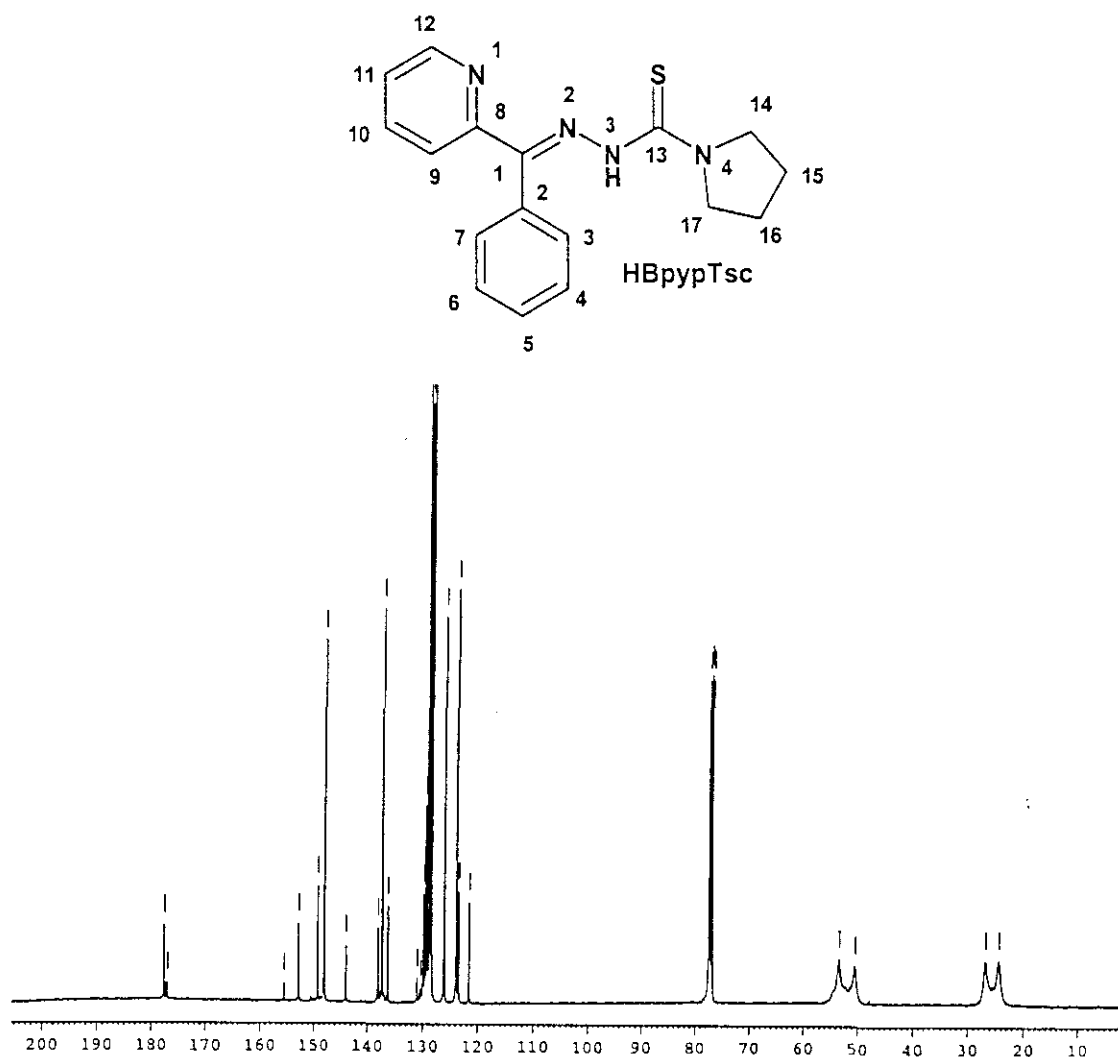


Figure 2. 10. ^{13}C NMR Spectrum of the compound HBpypTsc

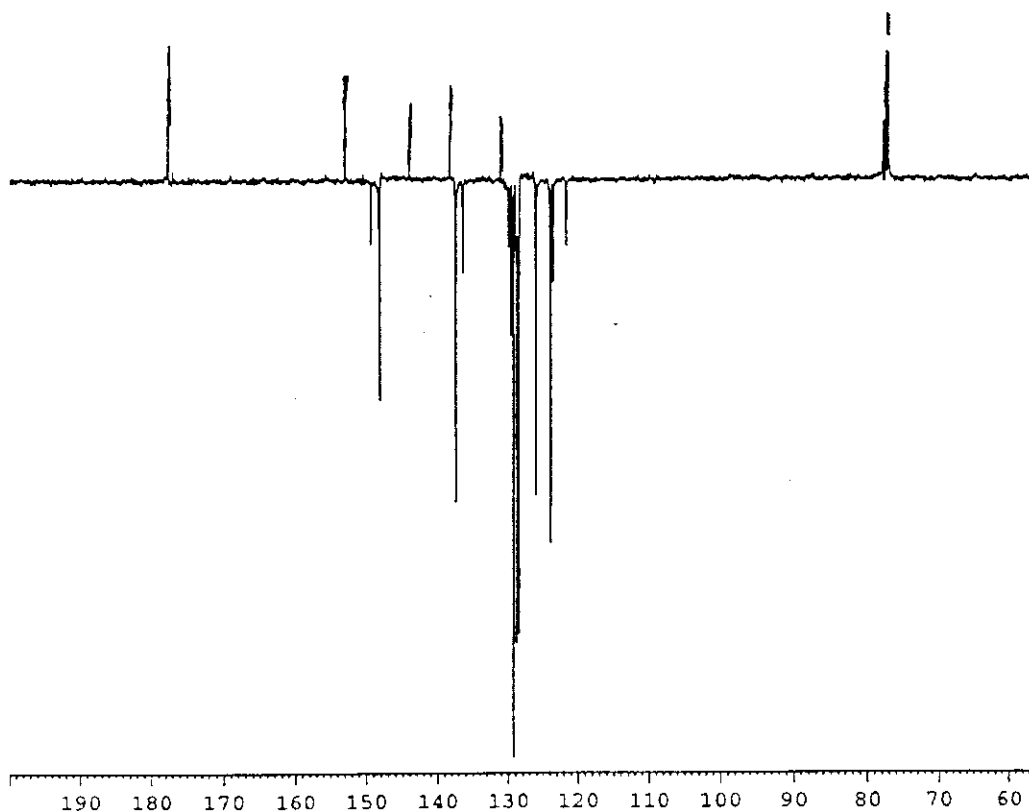


Figure 2.11. SEFT ^{13}C -NMR spectrum of the compound *HBpypTsc*

2.2.6. Electronic spectrum

The electronic spectrum of *HBpypTsc* and its complexes consisted of two broad bands in the regions 40300 and 29240 cm^{-1} . These bands were assigned to the $\pi\rightarrow\pi^*$ and $n\rightarrow\pi^*$ transitions of the thiosemicarbazone moiety. A second $n\rightarrow\pi^*$ band³⁷ corresponding to the thiocarbonyl group is found below at 29760 cm^{-1} . Figure 2.12 shows the electronic spectrum of the compound in chloroform. Similar values were observed in the diffused reflectance spectrum of the compound in MgO matrix. Compared to solid state spectrum, the solution spectral bands showed a bathochromic shift. This phenomena is common for the thiosemicarbazones assumed to be due to the delocalization caused by the enolization of the thiocarbonyl group in solution.

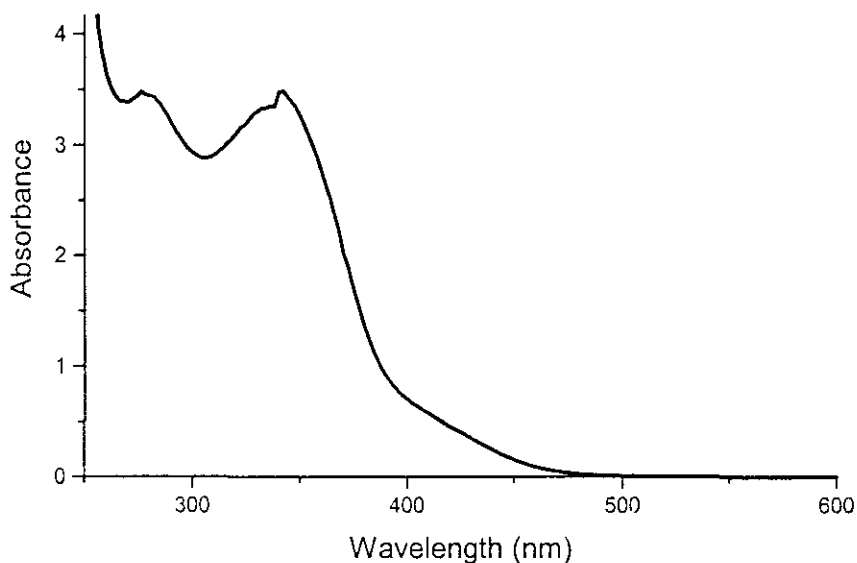


Figure 2.12. Electronic spectrum of the compound HBpypTsc in chloroform

2.2.7. IR spectrum

Figure 2.13 shows the IR spectrum of the compound HBpypTsc. In solid state the compound remains in the thione form indicated by a band at 1342cm^{-1} attributable to $\nu(\text{C}=\text{S})$, asymmetric bending frequency of the thiocarbonyl group is also observed at 842 cm^{-1} ($\delta \text{C}=\text{S}$). A broad absorption band at 3448 cm^{-1} is assigned to the N(3)H of the thiosemicarbazone. Azomethine stretching frequency is observed at 1630 cm^{-1} followed by a sharp band at 1118 cm^{-1} assignable to $\nu(\text{N}-\text{N})$ ³⁸. The region below 1300 cm^{-1} is rich in peaks assignable to a combination of the ring breathing and stretching frequencies of the heterocyclic ring and phenyl ring.

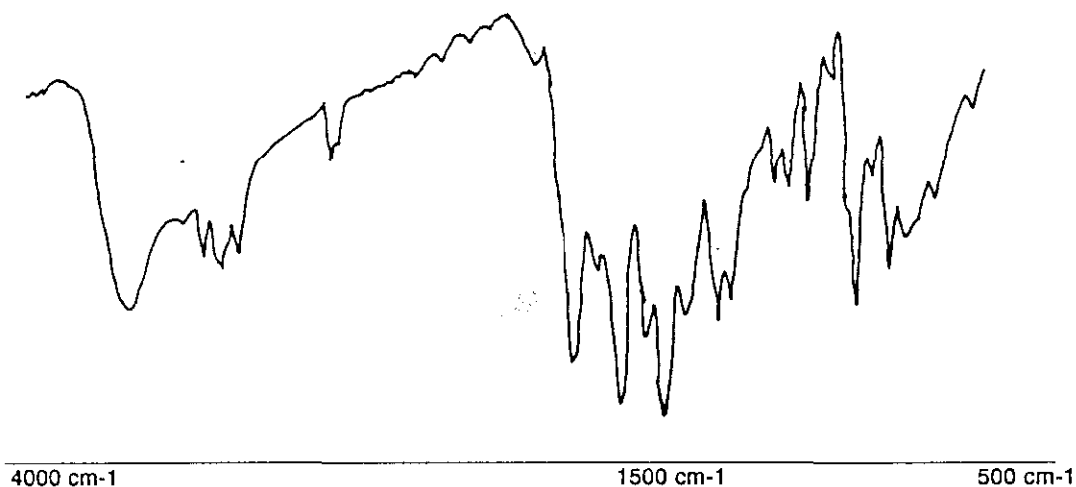


Figure 2.13. IR Spectrum of the compound HBpypTsc

2.3. Antimicrobial studies

Wide variety of chemicals called antimicrobial agents is available for controlling the growth of microbial organisms. Chemotherapeutic agents include antibiotics, disinfectants and antiseptics. For the last two decades a large number of studies in the area of transition metal complexes were dedicated to the antimicrobial activities of the thiosemicarbazones and their metal complexes³⁹. The real impetus towards developing the coordination chemistry of thiosemicarbazones has been provided by remarkable biological activities observed for these compounds which has since been shown to be related their metal complexing ability. Among a plethora of complexes and ligands which were screened for activity a majority of works deals with pyridine derivatives especially 2-acetylpyridine. Herein we present the microbial studies of the compounds **1a**, **1b**, 2-benzoylpyridine and HBpypTsc screened against a number of clinical pathogens.

The effectiveness of an antimicrobial agent in sensitivity testing is based on the area of zone of inhibition. When the test substances are introduced on to a lawn of bacterial culture by either disc diffusion or well method, and if the organism is sensitive there develops a zone of no growth around the disc. This is referred to as zone of inhibition⁴⁰. The diameter of the zone is measured to the nearest millimeter (mm). Test substance that produce a zone of inhibition of 7 mm or more are regarded as positive, i.e. having antimicrobial activity, while in those cases where the diameter is less than 9 mm, the microbe is resistant to the sample which is under test for activity.

Based on a stain test microbial organisms can be divided in to two types, Gram-positive and Gram-negative. The following five bacteria are used for our studies. 1) *Staphylococcus aureus*, 2) *Bacillus* sp (Gram positive); 3) *Escherichia coli*, 4) *Salmonella paratyphi*, 5) *Vibrio cholerae O1* (Gram negative)

The compounds were dissolved in DMF in to a 1% solution by molecular weight and then diluted with the same solvent so that the concentration per disc would be 0.5µg. Discs of 4 mm diameter were made from Whatman No-1 filter paper and autoclaved at 15 psi for 15 minutes under aseptic conditions. Test samples (5 µL) were dispensed on to the disc. The discs were dried at 30°C, and stored in sterile vials until further use. The medium used for growing the cultures was nutrient

agar, unless other wise specified. Disc diffusion method was employed for the study of the compounds.

2.3.1. Disc diffusion method.

When a filter paper disc is impregnated with a chemical is placed on agar, the chemical will diffuse from the filter paper to agar. The solubility of the chemical and its molecular size will determine the size of the area of chemical infiltration around the disc if it is susceptible to the chemical. A loopful of an overnight slant culture of the test organism was inoculated to 5 μ L of sterile physiological saline to make uniform suspension. This suspension culture was surface spread on nutrient agar plate by swabbing with a sterile cotton to get uniform lawn culture. The discs with test samples prepared as mentioned above, were placed on the swabbed surfaces of the plates using forceps. The plates were incubated at 37°C for 24 h and then checked for zones of inhibition around the discs. The zone diameters were measured and the each experiment was repeated five times for the consistency of the results. The organisms strains of *Staphylococcus aureus*, *Bacillus* sp, *Escherichia coli*, *Salmonella paratyphi* were kindly provided by the clinical laboratories of some local hospitals near Cochin, which were collected from the patients and pure isolated strain of *Vibrio cholerae* O1 was kindly provided by the National Institute of Cholerae and Enteric Diseases, Calcutta

The ligands HBpypTsc and HPranThas were screened along with its synthetic precursors. The results obtained after the screening of the compounds **1a**, **1b**, 2-benzoylpyridine, HBpypTsc and HPranThas are tabulated in Table 2.6.

Table 2.6. Microbial studies of the ligands

Compounds	1 [#]	2 [#]	3 [#]	4 [#]	5 [#]
HPranThas	+ 22 mm	+ 21 mm	-	-	+ 23 mm
1a	-	-	-	-	-
1b	-	-	-	-	-
2-benzoylpyridine					
HBpypTsc	+ 13 mm	+ 8 mm	-	-	+ 13 mm

1) *Staphylococcus aureus*, 2) *Bacillus* sp (Gram positive); 3) *Escherichia coli*, 4) *Salmonella paratyphi*, 5) *Vibrio cholerae* O1 (Gram negative)

The results were compared with previously studied results for HPranThas⁴¹, and we have found the compound HBpypTsc was of good activity against *Staphylococcus aureus*, *Bacillus* Sp and *Vibrio cholerae* O1. The results obtained

showed the superior activity of the 2-Acetylpyridine thiosemicarbazones among the heterocyclic thiosemicarbazones synthesized. Both compounds were inactive against *Escherichia Coil*, and *Salmonella paratyphi*. All the synthetic precursors were inactive against any of the organisms. This obtained activities points to an interesting observation that the formation of azomethine C=N by the condensation of the ketone/aldehyde and the hydrazinic -NH₂ of the thiosemicarbazides could be a key step in determining the microbial activity. Azomethine nitrogen which is the most basic centre in the thiosemicarbazone moiety contributes a key role, and could be an active centre in the whole molecule.

Chapter 3

Synthesis and studies of copper(II) complexes

Copper is one of the more abundant element (20th in the order of abundance), occurring at a concentration of about 100 g per ton of earth's crust. It is the third most abundant biometal in living systems responsible for a number of redox reactions occur in a living organism. The copper(II) state is significantly more common and is extensively involved as an intermediate oxidation state in mechanistic studies especially those involving amino acid species. Its major role in biological systems is to trigger the reduction of oxygen to the substrate as blue copper proteins, as a peroxide ion scavenger in superoxide dismutase, etc. Investigations in coordination chemistry of copper(II) continue to be of interest in developing models for copper proteins and in understanding factors, which give rise to seemingly infinite variety of distortions from regular stereochemistry observed in copper(II) complexes. Generally copper(II) forms square planar complexes or octahedral complexes with weakening of axial bonds. Occasionally square pyramidal and trigonal bipyramidal species also form in which one ligand is weaker at the axial position. Electrons paramagnetic resonance spectroscopy is one of the most suitable techniques for studying the changes in molecular structure of the paramagnetic complexes. Recently there has been considerable interest in the coordination chemistry of copper(II) complexes mainly due to their interesting physico-chemical and biological properties. Thiosemicarbazones react as chelating agents with copper(II) ion by bonding through thioketo sulfur and hydrazine nitrogen atoms. Therefore these type of compounds can coordinate *in vivo* to metal ion. Because of such coordination, the thiosemicarbazone moiety undergoes a sterical reorientation that could favor its biological activity. This chapter attempts to explore the structural, spectral and antimicrobial properties of copper(II) complexes of 2-benzoylpyridine N(4)-N(4)-(butane-1, 4-diyl) thiosemicarbazone (HBpypTsc) with coordinated gegenions. We expected the coordination of HBpypTsc via pyridyl nitrogen, azomethine nitrogen and thiolate sulfur as a monoanionic terdentate ligand.

3.1. Experimental

3.1.1. *CuBpypTscN₃* (1)

A solution of HBpypTsc (1 mmol) in 5 mL of chloroform was refluxed with a 5 mL solution of cupric acetate (1 mmol) in methanol for 5 minutes. To this was added a 5 mL methanolic solution of NaN₃ (1 mmol). The reaction was continued for 20 minutes. The resulting solution was cooled to get microcrystalline powders of the compound 1. The compound was filtered washed thoroughly with diethyl ether and dried over P₄O₁₀ *in vacuo*.

3.1.2. *Cu₂(BpypTsc)₂Cl₂* (2) and *CuBpypTscCl* (10)

A solution of HBpypTsc (1 mmol) in 5 mL of chloroform was refluxed with a 5 mL solution of cupric chloride (1 mmol) in methanol for 15 minutes. The resulting solution was cooled, and allowed to stand for 2 days to isolate single crystals of compound 10. The isolated product was dissolved in chloroform and layered with methanol. This was allowed to diffuse slowly for 8 days yielded the X-Ray quality single crystals of the compound 2. Both compounds were filtered, washed thoroughly with diethyl ether and dried over P₄O₁₀ *in vacuo*.

3.1.3. *CuBpypTscNO₃* (3)

A solution of HBpypTsc (1 mmol) in 5 mL of chloroform was refluxed with a 5 mL solution of cupric nitrate (1 mmol) in methanol for 30 minutes. The resulting solution was cooled to get microcrystalline powders of the compound 3. The compound was filtered washed thoroughly with diethyl ether and dried over P₄O₁₀ *in vacuo*.

3.1.4. *CuBpypTscNCS* (4)

A solution of HBpypTsc (1 mmol) in 5 mL of chloroform was refluxed with a 5 mL solution of cupric acetate (1 mmol) in methanol for 5 minutes. To this was added a 5 mL methanolic solution of KCNS (1 mmol). The reaction was continued for 20 minutes. The resulting solution was cooled to get microcrystalline powders of the compound 4. The compound was filtered washed thoroughly with diethyl ether and dried over P₄O₁₀ *in vacuo*.

3.1.5. *CuBpypTscClO₄* (5)

A solution of HBpypTsc (1 mmol) in 5 mL of chloroform was refluxed with a 5 mL solution of copper perchlorate (1 mmol) in methanol for 35 minutes. The resulting solution was cooled to get microcrystalline powders of the compound 5. The compound was filtered washed thoroughly with diethyl ether and dried over P₄O₁₀ *in vacuo*.

3.1.6. *CuBpypTscBr* (6)

A solution of HBpypTsc (1 mmol) in 5 mL of chloroform was refluxed with a 5 mL solution of cupric bromide (1 mmol) in methanol for 15 minutes. The resulting solution was cooled to get microcrystalline powders of the compound 6. The compound was filtered washed thoroughly with diethyl ether and dried over P₄O₁₀ *in vacuo*. X-Ray quality single crystals were grown from a solution of the compound in chloroform layered with methanol in 5 days.

3.1.7. *CuBpypTscSH* (7) and *Cu₂(BpypTsc)₂S₂* (9)

A solution of HBpypTsc (1 mmol) in 5 mL of chloroform was refluxed with a 5 mL solution of cupric sulfate (1 mmol) in methanol for 45 minutes. The resulting solution was cooled, and allowed to stand for 1 day to isolate single crystals of compound 9. The isolated product was dissolved in chloroform and layered with methanol. This was allowed to evaporate slowly for 12 days yielded the X-Ray quality single crystals of the compound 7. Both compounds were filtered, washed thoroughly with diethyl ether and dried over P₄O₁₀ *in vacuo*.

3.1.8. *CuBpypTscCN* (8)

A solution of HBpypTsc (1 mmol) in 5 mL of chloroform was refluxed with a 5 mL solution of copper acetate (1 mmol) in methanol for 5 minutes. To this was added a 5 mL methanolic solution of NaCN (1 mmol). The reaction was continued for 20 minutes. The resulting solution was cooled to get microcrystalline powders of the compound 8. The compound was filtered washed thoroughly with diethyl ether and dried over P₄O₁₀ *in vacuo*.

3.2. Results and discussion

3.2.1. Syntheses

All complexes were found to form readily from the reaction mixture of appropriate copper(II) salts and ligand HBpypTsc in hot methanol/chloroform. The compounds **1**, **4** and **8** were formed by the metathetical displacement of OAc⁻ anion by N₃/NCS/CN anions. The elemental analysis data (Table 3.1) suggests the formulation CuBpypTscX [X= N₃, Cl, NO₃, NCS, ClO₄, Br, SH and CN] which indicate that HBpypTsc is coordinated as a monoanionic terdentate ligand. Figure 3.1 shows an approximate structural formula of the copper complexes. All compounds were readily soluble in chloroform, dichloromethane, acetone and DMF. Magnetic susceptibility measurements were carried out at room temperature using Gouy balances which are in the range of 1.77-2.11 BM. These values indicate that all complexes are magnetically dilute and contains one unpaired electron as expected for a d⁹ copper(II) complexes⁴². These values are in the range of normal values of square planar copper(II) species. All complexes were non-conductors in CHCl₃ indicating the coordination of the anions to the metal center.

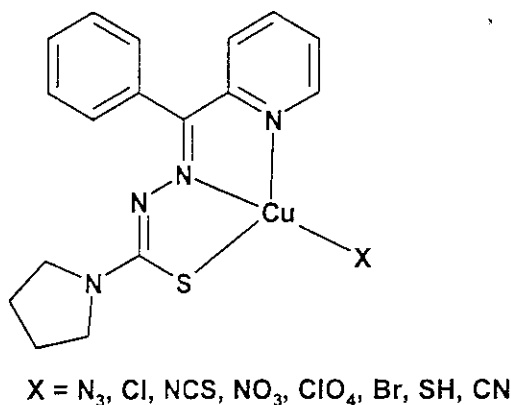


Figure 3.1 Structural formula of copper complexes

The compounds **2** and **10** were found to form from a single reaction medium which was found to crystallize into two different types of crystals. The single crystal isolated from the reaction medium yielded the compound CuBpypTscCl , (**10**) with terminally bonded chlorine, however the recrystallized product $\text{Cu}_2(\text{BpypTsc})_2\text{Cl}_2$ (**2**) was found to be chloro bridging. But both compounds gave a same analytical data. The formation of compound **7** and **9** were also unusual. The compound was synthesized by using CuSO_4 , but after synthesis the compound was obtained as single crystals from the reaction medium had an approximate composition $\text{Cu}_2(\text{BpypTsc})_2\text{S}_2$ (**9**) with disulfide bridging, but the recrystallized product from methanol/chloroform yielded a compound with the formula CuBpypTscSH (**7**). But the possibilities of formation of such an SH coordinated complex is described in a recent report by Anacona *et al.*⁴³, which suggests the formation of an mercapto (SH) coordinated tetrahedral Co(II) complex as a byproduct. To our knowledge this is a first structural report of a square planar copper(II) ion containing mercapto group.

Table 3.1. Colors and partial elemental analysis data of the complexes.

Compound	Formula	Color	Found (Calcd)%		
			C	H	N
CuBpypTscN_3 (1)	$\text{C}_{17}\text{H}_{17}\text{CuN}_7\text{S}$	Green	49.86 (49.20)	4.27 (4.13)	23.95 (23.63)
CuBpypTscCl (2)	$\text{C}_{34}\text{H}_{34}\text{Cl}_2\text{Cu}_2\text{N}_8\text{S}_2$	Dark green	50.36 (49.99)	4.32 (4.26)	13.80 (13.77)
CuBpypTscNO_3 (3)	$\text{C}_{17}\text{H}_{17}\text{CuN}_5\text{O}_3\text{S}$	Moss green	46.87 (46.94)	4.02 (3.94)	15.98 (16.10)
CuBpypTscNCS (4)	$\text{C}_{18}\text{H}_{17}\text{CuN}_5\text{S}_2$	Olive green	49.98 (50.16)	3.95 (3.98)	16.13 (16.25)
CuBpypTscClO_4 (5)	$\text{C}_{17}\text{H}_{17}\text{ClCuN}_4\text{O}_4\text{S}$	Dark green	43.10 (43.22)	3.55 (3.63)	11.10 (11.86)
CuBpypTscBr (6)	$\text{C}_{17}\text{H}_{17}\text{BrCuN}_4\text{S}$	Olive green	45.12 (45.09)	3.75 (3.78)	12.24 (12.37)
CuBpypTscSH (7)	$\text{C}_{17}\text{H}_{18}\text{CuN}_4\text{S}_2$	Dark green	50.24 (50.29)	4.38 (4.45)	13.20 (13.80)
CuBpypTscCN (8)	$\text{C}_{18}\text{H}_{17}\text{CuN}_5\text{S}$	Dark green	54.22 (54.19)	4.20 (4.29)	17.17 (17.55)
$\text{Cu}_2(\text{BpypTsc})_2\text{S}_2$ (9)	$\text{C}_{34}\text{H}_{36}\text{Cu}_2\text{N}_8\text{O}_5\text{S}_3$	Green	46.45(47.48)	4.02 (4.22)	12.83 (13.03)
CuBpypTscCl (10)	$\text{C}_{17}\text{H}_{17}\text{ClCuN}_4\text{S}$	Light green	49.86 (49.20)	4.27 (4.13)	23.95 (23.63)

3.2.2. Electronic spectra

The electronic spectra of copper(II) complexes is probably the most easily determined electronic property to obtain structural information due to flexible stereochemistry of copper(II) ion. The significant electronic absorption bands in the spectra of the complexes recorded in chloroform are presented in the Table 3.2. Figure 3.2 shows the electronic spectrum of the compound **1** in chloroform. The

spectrum of *HBpypTsc* and its complexes consisted of two broad bands in the regions ≈ 40300 & 29240 cm^{-1} . These bands remained almost unshifted in the complexes compared to *HBpypTsc* and are due to the $\pi \rightarrow \pi^*$ and $n \rightarrow \pi^*$ transitions of the thiosemicarbazone ligand. A second $n \rightarrow \pi^*$ band which is found below at $\approx 29760 \text{ cm}^{-1}$ in the spectrum of uncomplexed thiosemicarbazone was also slightly shifted due to complexation. This is an indication of the enolization followed by the coordination via thiolate sulfur. All complexes exhibit a $d \rightarrow d$ band as a weak shoulders in the visible region whose maximum of absorption lie in the visible region $\approx 17000 \text{ cm}^{-1}$. Such a feature is expected for a square planar chromophores in accordance with earlier reports^{44, 45}. For the square planar complexes with $d_{x^2-y^2}$ ground state, three spin allowed transitions are possible viz., ${}^2B_{1g} \rightarrow {}^2A_{1g}$ ($d_{x^2-y^2} \rightarrow d_{z^2}$), ${}^2B_{1g} \rightarrow {}^2B_{2g}$ ($d_{x^2-y^2} \rightarrow d_{xy}$) and ${}^2B_{1g} \rightarrow {}^2E_g$ ($d_{x^2-y^2} \rightarrow d_{xz}, d_{yz}$) and it is difficult to resolve it in to three bands. Since the four lower orbitals are so close together in energy that individual transitions cannot be distinguished resulting in a single absorption band.

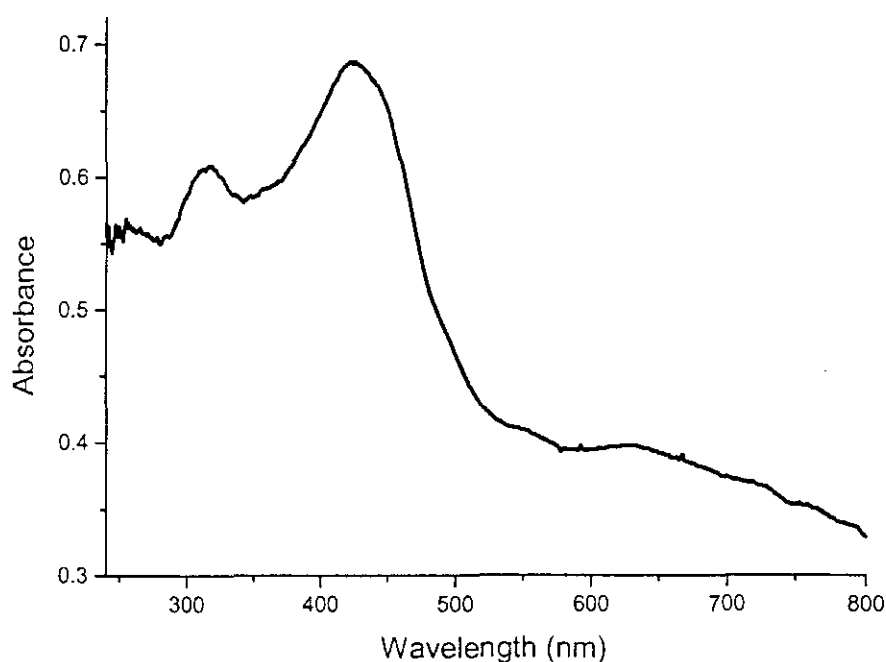


Figure 3.2. Electronic spectrum of the compound *CuBpypTscN₃ (1)* in CHCl_3

It is observed that the spectra of the complexes are dominated by intense intraligand and charge transfer bands. These intense bands cause the low energy bands to appear as weak shoulders. Metal to ligand charge transfer (CT) bands are found at $\approx 26000 \text{ cm}^{-1}$ to 21000 cm^{-1} in the complexes and in accordance with previous studies of copper(II) complexes of similar type of ligands, the higher energy bands are assignable to $S \rightarrow \text{Cu(II)}$ LMCT transition, tailing in to the visible region. The pyridyl $N(\pi) \rightarrow \text{Cu(II)}$ CT transition was observed in the at $\approx 23000 \text{ cm}^{-1}$ as a weak shoulder. The CT may occur from the p orbital of coordinated ketonic sulfur or nitrogen to the vacant d orbitals of copper(II). However the coordinated gegenions, $X(\pi) \rightarrow \text{Cu(II)}$ charge transfer was also observed $\approx 22000 \text{ cm}^{-1}$.

Table 3.2 Electronic spectral data of the complexes

Complex	$\pi \rightarrow \pi^*$	$n \rightarrow \pi^*$	LMCT	$d \rightarrow d$
<i>HBpypTsc</i>	40322 (2.69)	36231 (2.54), 29761 (2.25)	-	-
<i>CuBpypTscN₃</i> (1)	41666 (2.69)	37313 (2.42), 32467 (2.42)	24154 (2.28), 22123 (2.21), 21551 (1.67)	16949 (0.95)
<i>Cu₂(BpypTsc)₂Cl₂</i> (2)	41322 (2.64)	37878 (2.52), 31847 (2.57)	26737 (2.25), 22935 (2.57), 22123 (2.56)	16393 (0.96)
<i>CuBpypTscNO₃</i> (3)	41669 (2.65)	36764 (2.48), 31645 (2.5)	26881 (2.17), 23148(2.25), 22123 (2.56)	16835 (0.84)
<i>CuBpypTscNCS</i> (4)	40983 (2.65)	37313 (2.52), 32467 (2.50)	24390 (2.27), 23041 (2.01), 21834 (2.58)	17301 (0.85)
<i>CuBpypTscClO₄</i> (5)	40485 (2.54)	37313 (2.46), 31446 (2.55)	24572 (2.08), 22522 (2.26), 21739(1.98)	16205 (0.92)
<i>CuBpypTscBr</i> (6)	41322 (2.68)	36496 (2.33), 31847 (2.54)	26455 (2.03), 23401 (2.05), 22123 (2.40)	16891 (0.68)
<i>CuBpypTscSH</i> (7)	40322 (2.68)	37314 (2.57), 32051 (2.54)	25906 (2.32), 23148 (2.03), 22026 (2.56)	16611 (0.87)
<i>CuBpypTscCN</i> (8)	40816 (2.71)	37037 (2.41), 31847 (2.32)	26737 (2.17), 23696 (2.13), 21881 (2.45)	16447 (0.92)

All values are reported in cm^{-1} , log ϵ values are given in parentheses ($\text{Lmol}^{-1}\text{cm}^{-1}$)

3.2.3. Infrared spectra

The significant IR bands with the tentative assignments of the copper(II) complexes in the region $4000\text{-}50 \text{ cm}^{-1}$ are presented in the Table 3.3 and 3.4. On coordination of the azomethine nitrogen $\nu(\text{C}=\text{N})$ shifts to lower wavenumbers by $50\text{-}70 \text{ cm}^{-1}$. The occurrence of $\nu(\text{N}-\text{N})$ at higher wavenumbers in the spectra of the complexes compared to that of the ligand confirm the coordination of azomethine nitrogen². IR spectra of the complexes show a new sharp band at $\approx 1630 \text{ cm}^{-1}$ is

assigned to the newly formed $\nu(\text{N}=\text{C})$. This indicates that the ligand enolizes and coordinates in the thiolate form. Coordination *via* thiolate sulfur is also indicated by the ν/δ (C-S) bands found at ≈ 1294 and 786 cm^{-1} . The $\nu(\text{Cu}-\text{N})$ stretching frequencies for azomethine nitrogen are observed around 400 cm^{-1} and the $\nu(\text{Cu}-\text{N})$ for the pyridyl nitrogen is observed in the range $\approx 380-340 \text{ cm}^{-1}$. The presence of a new band in the $320-340 \text{ cm}^{-1}$ range which is assignable to $\nu(\text{Cu}-\text{S})$ is another indication of involvement of sulfur coordination. Figure 3.3 shows the IR spectrum of compound **1** and Figure 3.4 shows the far IR spectra of the copper complexes.

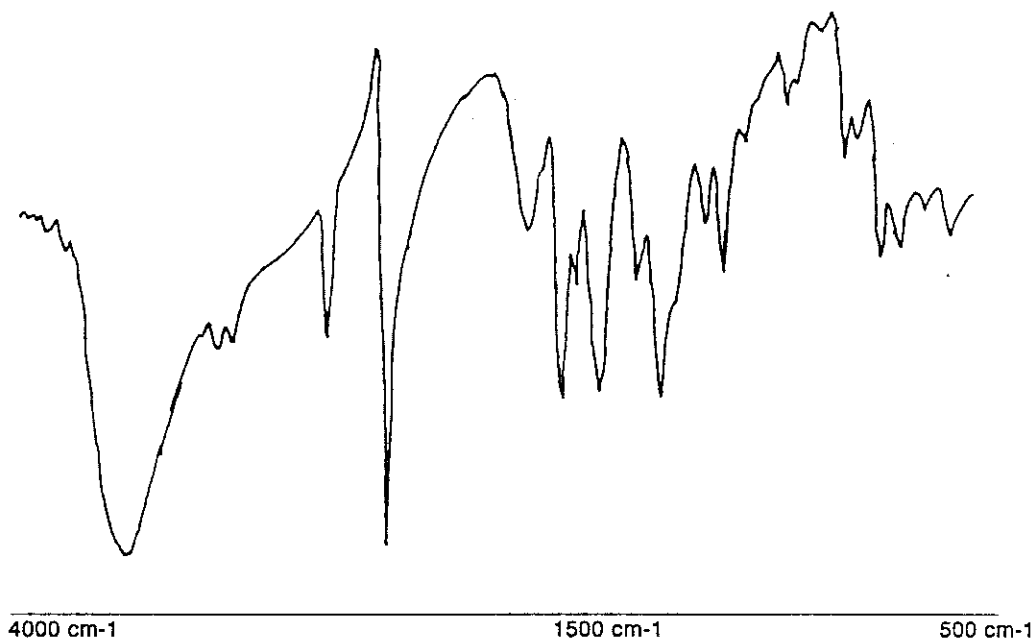


Figure 3.3. IR spectrum of the compound $\text{CuI}(\text{BpypTscN}_3)(1)$

Table 3.3. Ligand vibrations in the IR spectra of copper(II) complexes

Compound	$\nu(\text{C}=\text{N})$	$\nu(\text{N}=\text{C})$	$\nu(\text{N}-\text{N})$	pi.p	po.p	$\nu/\delta(\text{C}=\text{S})$
<i>HBpypTsc</i>	1630 s	-	1118 m	455w	649 w	1342 s, 842 m
$\text{Cu}(\text{BpypTscN}_3)$ (1)	1544 s	1633 s	1116 m	406 w	643 w	1342s, 842 m
$\text{Cu}_2(\text{BpypTsc})_2\text{Cl}_2$ (2)	1592 s	1634 s	1124 m	405 w	641 w	1334s, 785 m
$\text{Cu}(\text{BpypTscNO}_3)$ (3)	1575 s	1632 s	1119 m	410w	645 w	1278s, 790 m
$\text{Cu}(\text{BpypTscNCS})$ (4)	1547 s	1633 s	1114 m	411w	639 w	1287s, 786 m
$\text{Cu}(\text{BpypTscClO}_4)$ (5)	1540 s	1630 s	1129 m	408w	621 w	1294s, 783 m
$\text{Cu}(\text{BpypTscBr})$ (6)	1542 s	1628 s	1124 m	409w	641 w	1272 s, 783 m
$\text{Cu}(\text{BpypTscCN})$ (8)	1593 s	1634 s	1120 m	405w	644 w	1268s, 785 m
$\text{Cu}_2(\text{BpypTsc})_2\text{S}_2$ (9)	1596 s	1635 s	1116 m	398 w	642 w	1276 s, 785 m
$\text{Cu}(\text{BpypTscCl})$ (10)	1594 s	1636 s	1128 m	395 w	645 w	1336 s, 789 m

All values are reported in cm^{-1}

The azido complex (1) shows a single broad band 2044 cm^{-1} and a strong band at 1286 cm^{-1} . These are assigned to ν_a and ν_s of the coordinated azido group. The broad bands observed at 575 and 446 cm^{-1} are assigned to $\delta(\text{N-N-N})$ and $\nu(\text{Cu-N})$ bands. This suggests that Cu-N-N-N bond is linear. Compound 2 showed a sharp $\nu(\text{Cu-Cl})$ band at 304 cm^{-1} , along with the presence of a band at 162 cm^{-1} (ν_b) indicate the bridging character in the Cu-Cl bond. A band at 255 cm^{-1} for the compound 6 due to $\nu(\text{Cu-Br})$ is suggestive for terminally bonded bromine⁴⁶. The ratio of $\nu(\text{Cu-Br})/\nu(\text{Cu-Cl})$ is 0.77 is consistent with the usual values obtained for the complexes of first row transition metals.

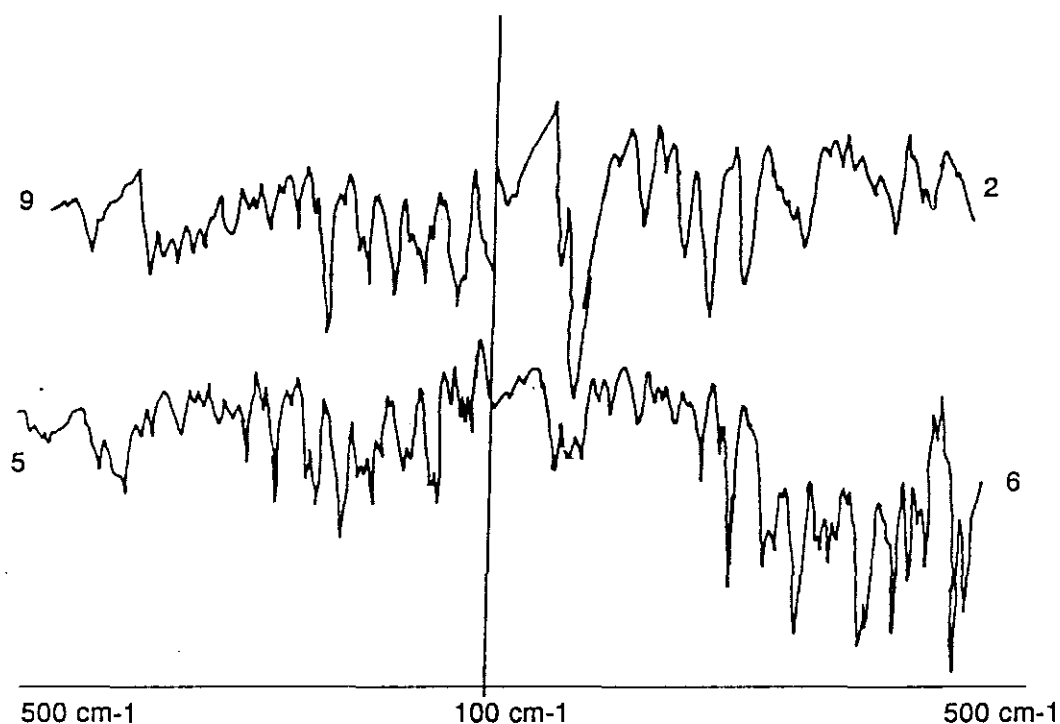


Figure 3.4. Far IR spectra of the compounds 2, 6, 5 and 8

We found that compound 3 has four strong bands at 1493 , 1379 , 1278 , and 1010 cm^{-1} corresponding to ν_1 , ν_2 , ν_4 and ν_5 of the nitrate group indicating the presence of a terminal monodentate coordination of the nitrate group⁴⁷. A combination band $\nu_1+\nu_4$ considered as diagnostic for the mono coordinate nitrate group has been observed at 1742 cm^{-1} . ν_3 and ν_6 could not be assigned due to the richness of the spectra of the complex. The $\nu(\text{Cu-N})$ of the N-nitrate compound is

found at 309 cm^{-1} . Compound **4** has a very strong band at 2076 cm^{-1} , a medium band at 916 cm^{-1} and a weak band at 506 cm^{-1} corresponding to $\nu(\text{CN})$, $\nu(\text{CS})$ and $\delta(\text{NCS})$ modes of the NCS group respectively. The intensity and position of these bands indicates the unidentate coordination of thiocyanate group through the nitrogen. The $\nu(\text{Cu-N})$ is observed at 321 cm^{-1} confirms that the N atom of the thiocyanate is coordinated to the metal.

Table 3.4. M-L and anionic vibrations for the copper(II) complexes

Compound	$\nu(\text{Cu-Npy})$	$\nu(\text{Cu-N}_{\text{azt}})$	$\nu(\text{X})^{\#}$	$\nu(\text{Cu-S})$
CuBpyppTscN_3 (1)	348 m	409 m	2044 s, 1286m, 575w	265 w
$\text{Cu}_2(\text{BpyppTsc})_2\text{Cl}_2$ (2)	345 m	392 m	303 s, 162 s	267 w
CuBpyppTscNO_3 (3)	350 m	398 m	1493s, 1278 s, 1379 s, 1010 m	264 w
CuBpyppTscNCS (4)	347 m	393 m	2076 s, 916m, 506 w	262 w
CuBpyppTscClO_4 (5)	345 m	398 m	1156s, 1092s, 908m, 381m	280 w
CuBpyppTscBr (6)	355 m	408 m	255s	279 w
CuBpyppTscCN (8)	357 m	421 m	2091s, 467m, 302m, 151m	281 w
$\text{Cu}_2(\text{BpyppTsc})_2\text{S}_2$ (9)	352 m	418 m	450b, 250 s	280 w
CuBpyppTscCl (10)	348 m	405 m	330 s	272 w

All values are reported in cm^{-1}
 $\# \text{ X} = \text{N}_3, \text{Cl}, \text{NO}_3, \text{NCS}, \text{ClO}_4, \text{Br}, \text{CN}, \text{S}$

The compound **5** showed single broad bands at 1156, 1092 and a strong band at 621, and a weak band at 908 cm^{-1} indicating the presence of coordinated perchlorate⁴⁸. The coordination is confirmed by a $\nu(\text{Cu-O})$ band at 385 cm^{-1} . The band at 1156 cm^{-1} is assignable to $\nu_3(\text{ClO}_4)$ and a band at 621 cm^{-1} assignable to $\nu_4(\text{ClO}_4)$. The compound **8** showed a sharp absorption near 2091 cm^{-1} indicating the $\nu(\text{CN})$ vibration. Coordination of Cu-CN is confirmed by the bands at 450 cm^{-1} $\nu(\text{Cu-C})$, 450 cm^{-1} $\delta(\text{Cu-C-N})$, and 151 cm^{-1} $\delta(\text{NC-Cu-S})$. The spectrum of the compound **9** showed a sharp band at 280 cm^{-1} indicating the $\nu(\text{Cu-S})$ along with a weak band near 450 cm^{-1} assignable to $\nu(\text{Cu-S-Cu})$ indicating thiometallic bridges in the compound. The far IR spectrum of the compound **10** showed a sharp absorption at 334 cm^{-1} indicating the presence of terminally bonded chlorine. All complexes showed the in-plane and out-of- plane ligand vibrations (ρ) of the thiosemicarbazone moiety approximately at ≈ 400 and 640 cm^{-1} respectively.

3.2.4. Electron paramagnetic resonance spectra

The EPR spectra of polycrystalline sample at 298 K, solution at 298 K and 77 K were recorded in the X band, using the 100-kHz field modulation; g factors were quoted relative to the standard marker TCNE ($g = 2.00277$). The EPR parameters of the copper(II) complexes are presented in Table 3.5. The copper(II) ion with a d^9 configuration, has an effective spin of $S = 3/2$ and associated with a spin angular momentum $m_s = \pm 1/2$, leading to a doubly degenerate spin state in the absence of a magnetic field. In a magnetic field this degeneracy is lifted and the energy difference between these states is given by $E = h\nu = g\beta H$ where h is the Planck's constant, ν is the frequency, g is the Lande splitting factor (equal to 2.0023 for free electron), β is the electronic Bohr magneton and H is the magnetic field. For the case of a $3d^9$ copper(II) ion the appropriate spin Hamiltonian assuming a B_{1g} ground state is given by⁴⁹

$$H = \beta[g_{\parallel}H_zS_z + g_{\perp}(H_xS_x + H_yS_y)] + A I_z S_z + B(I_x S_x + I_y S_y)$$

Table 3.5. EPR Spectral parameters of the copper(II) complexes

Compound	State	Temp	g_{iso}/g	g_{\parallel}	A_{iso}/A	A_{\parallel}	A_N
CuBpypTscN ₃ (1)	Polycrystalline	298 K	2.08	2.21	-	-	-
	CHCl ₃	298 K	2.087	-	-	-	-
	CHCl ₃	77 K	1.931	1.964	86.6	188.3	15.51
Cu ₂ (BpypTsc) ₂ Cl ₂ (2)	Polycrystalline	298 K	2.09	2.20	-	-	-
	CHCl ₃	298 K	2.107	-	110.6	-	10.25
	1:1 CHCl ₃ / Toluene	77 K	2.093	2.226	62.3	195.2	-
	DMF	77 K	2.090	2.195	-	-	-
CuBpypTscNO ₃ (3)	Polycrystalline	298 K	2.09	-	-	-	-
	CHCl ₃	298 K	2.134	-	112.3	-	17.51
	1:1 CHCl ₃ / Toluene	77 K	2.083	2.254	-	-	-
CuBpypTscNCS (4)	Polycrystalline	298 K	2.09	2.26	-	-	-
	CHCl ₃	298 K	2.092	-	-	-	-
	1:1 CH ₃ OH/ Toluene	77 K	2.077	2.228	-	-	-
CuBpypTscClO ₄ (5)	Polycrystalline	298 K	2.06	2.22	-	-	-
	CHCl ₃	298 K	2.147	-	102.3	-	17.45
	1:1 CHCl ₃ / Toluene	77 K	2.086	2.229	61.6	169.3	15.54
CuBpypTscBr (6)	Polycrystalline	298 K	2.12	-	-	-	-
	CHCl ₃	298 K	2.102	-	111.2	-	16.25
	1:1 Acetone/ Toluene	77 K	2.064	2.219	71.2	185.5	-
Cu ₂ (BpypTsc) ₂ S ₂ (9)	Polycrystalline	298 K	1.88	2.20	-	-	-
	CHCl ₃	298 K	2.099	-	108.6	-	15.85
	1:1 CH ₃ OH/ Toluene	77 K	2.084	2.190	56.6	192.5	17.52
CuBpypTscCN (8)	Polycrystalline	298 K	2.08	2.21	-	-	-
	CHCl ₃	298 K	2.097	-	112.6	-	15.25
	1:1 CHCl ₃ / Toluene	77 K	2.083	2.206	76.7	193.3	13.75
	DMF	77 K	2.090	2.215	-	-	-

A values are reported in $\times 10^{-4} \text{ cm}^{-1}$

The EPR spectra of compounds **3** & **6** in the polycrystalline state (298 K) show only one broad signal at $g \approx 2.09$. Such isotropic spectra, consisting of a broad signal, and hence only one g value, arise from extensive exchange coupling through misalignment of the local molecular axes between different molecules in the unit cell (dipolar broadening) and enhanced spin lattice relaxation. This type of spectra unfortunately gives no information on the electronic ground state of Cu(II) ion present in the complexes. However the spectra of the compounds **1**, **2**, **4**, **5**, **7** and **8** show typical axial spectra with well defined g_{\parallel} feature and g_{\perp} feature at values ≈ 2.22 and 2.09 . Figure 3.5 and 3.6 shows the EPR spectra of two representative samples in the polycrystalline state. The variation in the g_{\parallel} and g_{\perp} values indicate that the geometry of the compounds in the solid state is affected by the nature of the coordinating ligands. The geometric parameter G , which is a measure of exchange interaction between copper centers in the polycrystalline compound, is calculated using the equation

$$G = \frac{g_{\parallel} - 2.002}{g_{\perp} - 2.002} = \frac{4k_{\parallel}^2 \Delta E_{xy}}{k_{\perp}^2 \Delta E_{xz}}$$

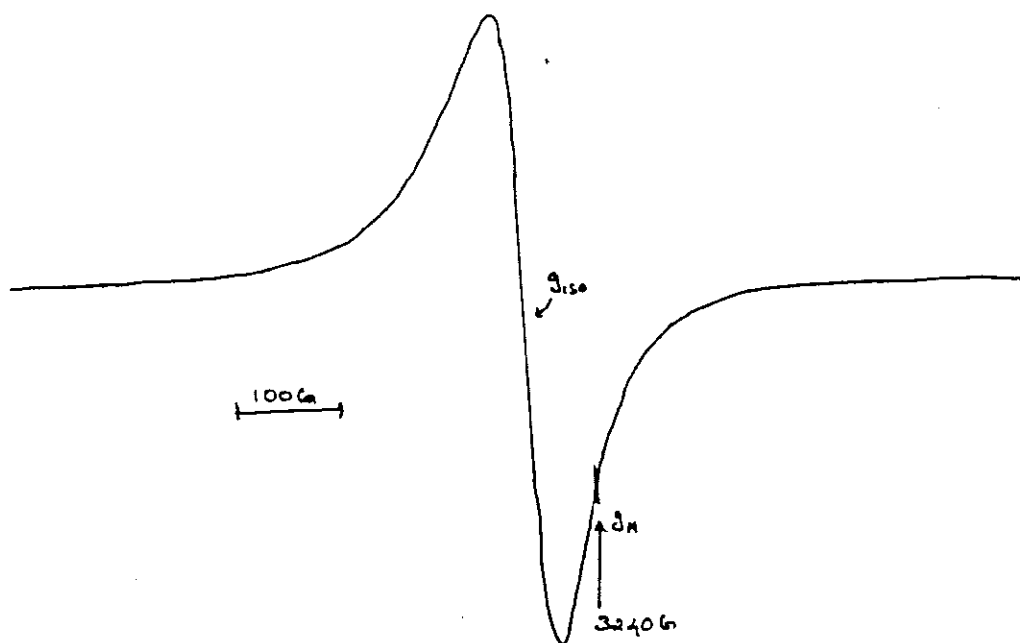


Figure 3.5. EPR spectrum of the compound **3** in polycrystalline state (298K)

If $G > 4$, exchange interaction is negligible and if it is less than 4, considerable exchange interaction is indicated in the solid complex. The geometric parameter G for the complexes is found to be in the range $\approx 2.1-3.8$ indicating that the g value obtained in the polycrystalline samples are near to the molecular g values which indicate the fact that the unit cell of the compounds contains magnetically equivalent sites. For all complexes with $g_{\parallel} > g_{\perp} > 2$ and G value fall within these range, is consistent with a $d_{x^2-y^2}$ ground state. Hence we assigned a square planar environment in all the complexes⁵⁰.

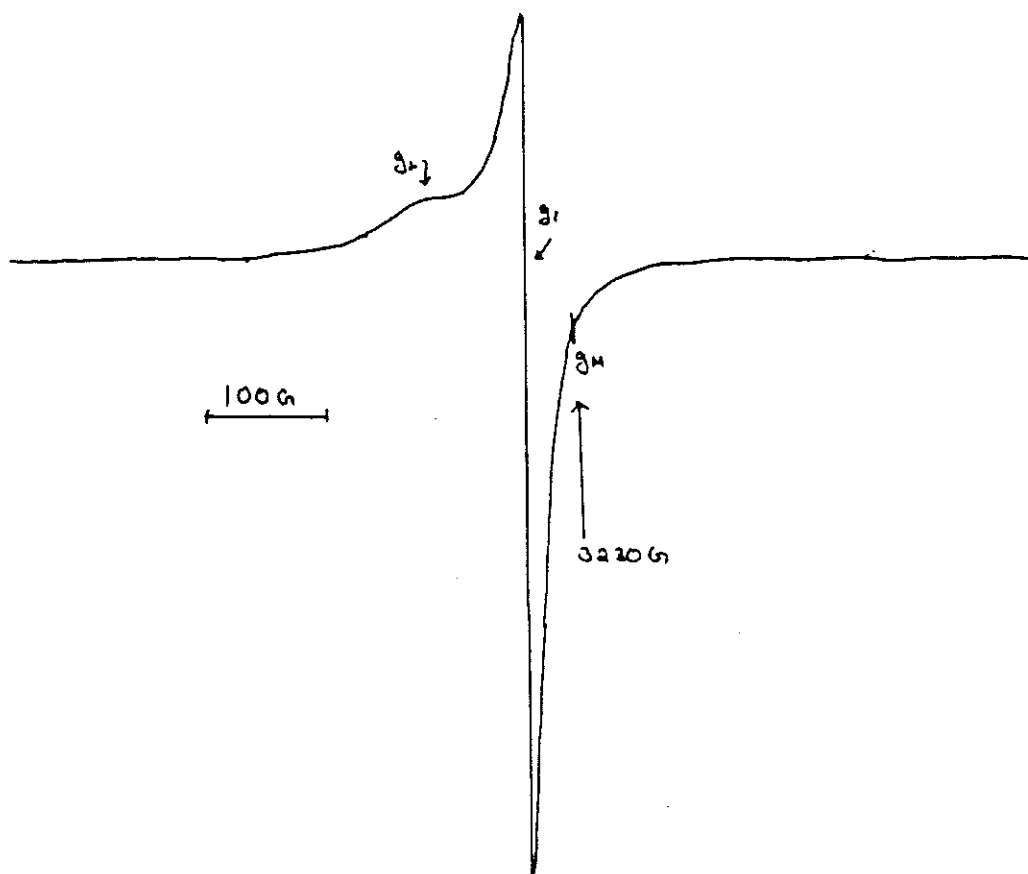


Figure 3.6. EPR Spectrum of the compound 5 in the polycrystalline state (298 K)

The solid state EPR spectra have low values of g suggesting considerable amount of covalency in the bonding⁵¹. Low values of g suggests the less interaction of neighboring sites indicating a magnetically dilute system.

The solution spectra of all complexes were recorded in CHCl_3 at 298 K. For all complexes spectra with isotropic features were obtained. It is assumed to be due to tumbling motion of the molecules in solution. The spectral features of all the complexes clearly show four fairly resolved hyperfine lines (^{65}Cu , $I = 3/2$) corresponding to $-3/2, -1/2, 1/2, 3/2$ transitions ($\Delta M_s = \pm 1$). The signal corresponding $M_I = -3/2$ splits clearly in to five peaks with a superhyperfine (shf) or ligand hyperfine coupling constant $A = 15$ G in the spectra of the complexes due to azomethine nitrogen and pyridyl nitrogen atoms⁵². In the case of compound 2 (Figure 3.7) this signal splits into nine shf lines showing the differences between the pyridyl and azomethine nitrogen due to the bridging of chlorine atom. The absence of a signal corresponding to ($\Delta M_s = \pm 2$) in the half field rules out the possibility of any Cu-Cu interactions in compound 2 and 9. In the case of compound 8 (Figure 3.8) all signals except to that corresponding to $M_I = +3/2$ showed five intense superhyperfine lines with $A = 16$ G. These features are characteristic of compounds bound through azomethine nitrogen and an indication that the bonding in solution state is dominated by the thiosemicarbazones moiety rather than the mono or polyatomic gegenions.

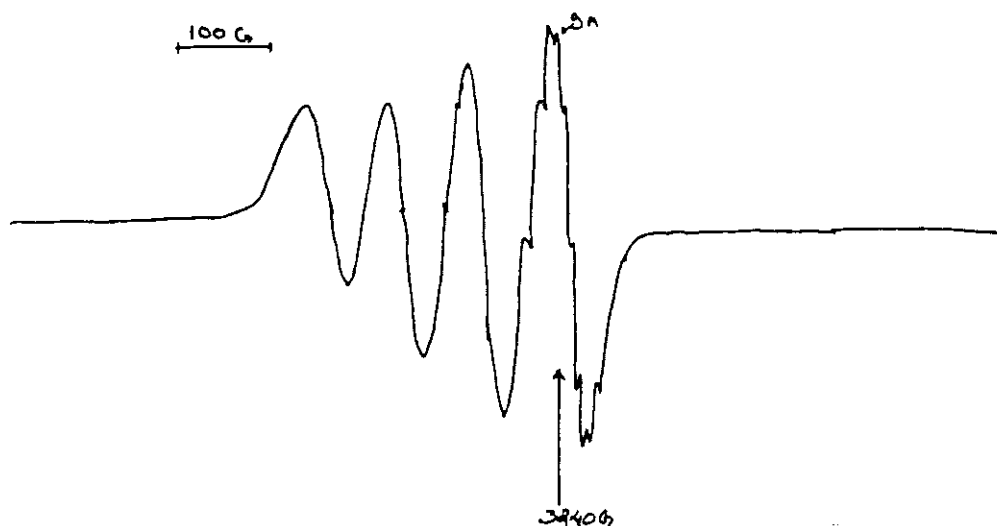


Figure 3.7 EPR spectrum of compound 2 in chloroform (298K)

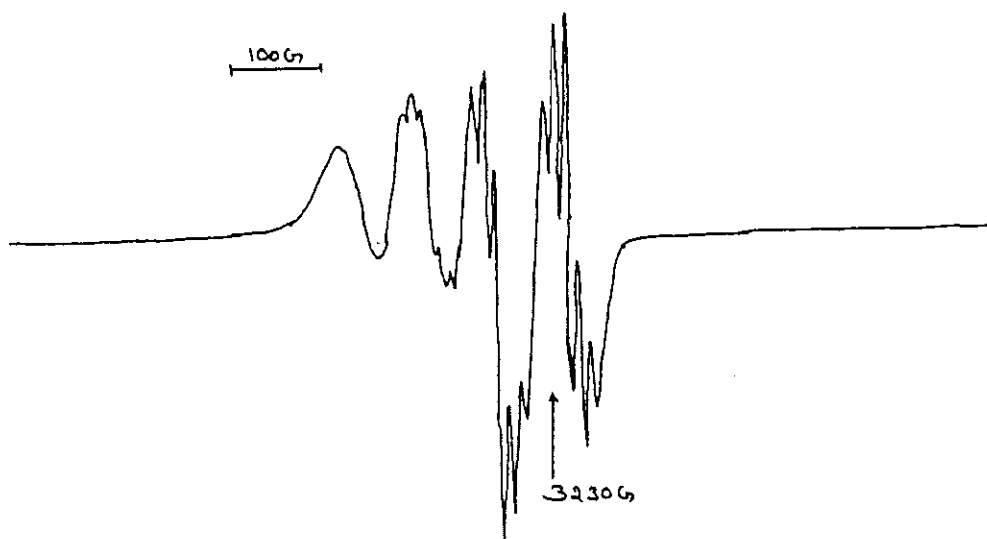


Figure 3.8. EPR spectrum of the compound 8 in chloroform (298 K)

The smaller variation in the g_{iso} values calculated when compared to the values from the polycrystalline spectra can be attributed to the variation in the geometric environment of the compounds upon dissolution. Spectra of all complexes show similar g and A values indicate the similarity in bonding of the thiosemicarbazone moiety.

The EPR spectra of the complexes in glassy state at 77 K was recorded in different solvents like CHCl_3 , DMF, CHCl_3 +toluene (1:1), acetone+toluene (1:1), and methanol+toluene (1:1). However we were unable to get clearly resolved spectra in many cases due to poor glass formation. Figure 3.9 and 3.10 show the spectra at 77 K of the representative samples. Some spectra showed three well-resolved peaks of low intensity in the low field region and intense unresolved peaks are obtained in the high field region. The g_{\parallel} , g_{\perp} , A_{\parallel} and A_{\perp} values were calculated accurately from the spectra, while g_{\perp} and A_{\perp} values were confirmed by using the following equations⁵³.

$$g_{\perp} = \frac{(3g_{\text{iso}} - g_{\parallel})}{2} \quad \text{and} \quad A_{\perp} = \frac{(3A_{\text{iso}} - A_{\parallel})}{2}$$

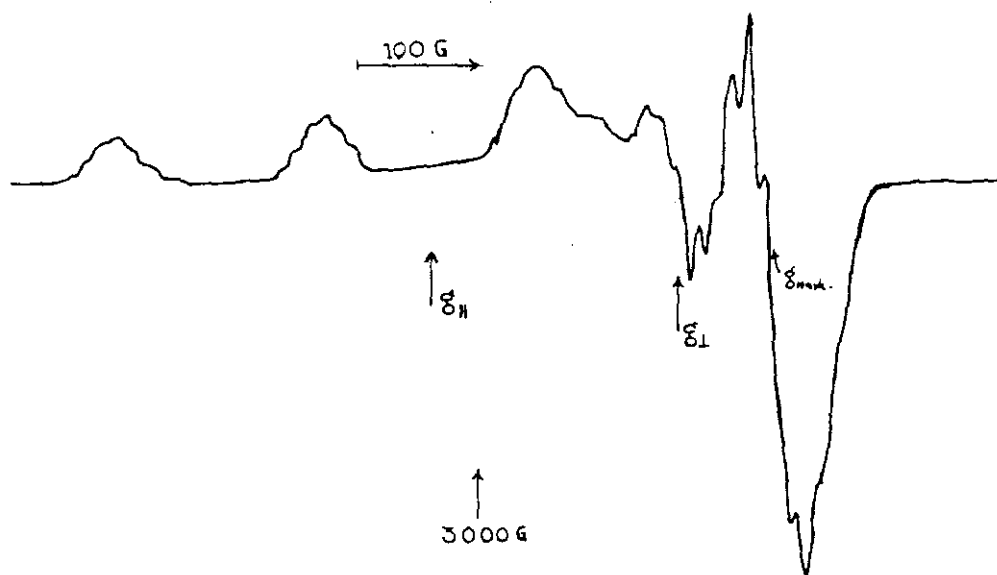


Figure 3.9. EPR spectrum of the compound 1 in 1:1 CHCl₃/Toluene (77 K)

In the parallel region, three of the four copper hyperfine lines are moderately resolved while the fourth one overlaps with the perpendicular features. As is evident from the analysis of the parallel part of the spectra, the line width of the $M_I = -3/2$, component is small compared with the nitrogen coupling constants, leading to the appearance of nitrogen superhyperfine pattern. The splitting in the perpendicular region of the spectra can be attributed to interaction of an unpaired electron spin with the copper nuclear spin and two ^{14}N ($I=1$) donor nuclei. The smaller $g_{||}$ values for the complexes indicates delocalization of the unpaired electron spin density away from the copper nucleus and may be interpreted in terms of increased covalency of the M-L bond. There is little difference between the solution spectra obtained at 77 K indicating that the stereochemistry of the complexes is retained on cooling. The $g_{||} > g_{\perp}$ values suggest a square planar geometry. The $g_{||}$ values are almost the same for all the compounds, which indicate that the bonding is dominated by the thiosemicarbazones moiety but are slightly different from that in the solid state. Kivelson and Neiman⁴⁹ have reported that the $g_{||}$ values less than 2.3 indicate considerable covalent character to M-L bond and greater than 2.3 indicate ionic character.

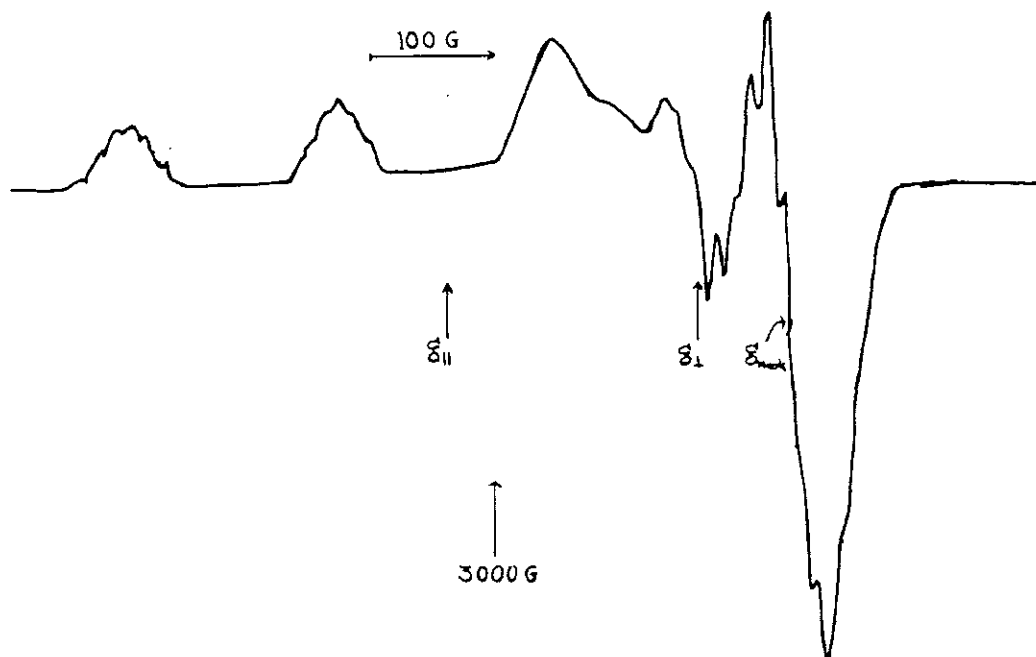


Figure 3.10. EPR Spectrum of the compound 6 in DMF (77 K)

The tendency of A_{\parallel} to decrease with increase of g_{\parallel} is an index of an increase of the tetrahedral distortion in the coordination sphere of copper. The $g_{\parallel} > g_{\perp}$ values suggest a square planar environment around the metal atom in all the complexes. Moderately resolved five superhyperfine lines in the g_{\parallel} feature show that the coordinated pyridyl and azomethine nitrogens are coplanar. The EPR parameters g_{\parallel} , g_{\perp} , A_{\parallel} , A_{\perp} , g_{iso} , and energies of d-d transitions were used to evaluate the bonding parameters⁵⁴⁻⁵⁸ α^2 , β^2 and γ^2 which are regarded as the measures of covalency of the in-plane σ bond, in-plane π bond and out-of-plane π bond respectively. Table 3.6 presents the calculated spin Hamiltonian parameters.

Table 3.6. Magnetic and spin Hamiltonian parameters of the complexes.

Compounds	α^2	β^2	γ^2	K_{\parallel}	K_{\perp}	f_{cm}	P	G
CuBpypTscN ₃ (1)	0.771	0.829	0.84	0.638	0.652	112.6	0.0248	3.038
Cu ₂ (BpypTsc) ₂ Cl ₂ (2)	0.578	0.852	0.81	0.495	0.542	134.8	0.0225	2.431
CuBpypTscNO ₃ (3)	0.736	0.773	0.88	0.628	0.659	116.5	0.0229	3.175
CuBpypTscNCS (4)	0.784	0.871	0.93	0.710	0.721	121.8	0.0192	2.652
CuBpypTscClO ₄ (5)	0.567	0.921	0.83	0.671	0.616	133.8	0.0241	2.971
CuBpypTscBr (6)	0.689	0.856	0.85	0.404	0.492	136.1	0.0194	3.172
Cu ₂ (BpypTsc) ₂ S ₂ (9)	0.611	0.705	0.79	0.497	0.486	112.7	0.0251	2.375
CuBpypTscCN (8)	0.566	0.811	0.67	0.466	0.665	119.4	0.0233	2.562

The value of the in-plane σ -bonding parameter α^2 is estimated from the expression $\alpha^2 = -A_{\parallel} / 0.036 + [g_{\parallel} - 2.0023] + 3/7[g_{\perp} - 2.0023] + 0.04$. This can also be calculated by using another expression reported by Pilbrow et. al.⁵⁹, $\alpha^2 = 1/8[-14(A + K)/p + 11(g_{\perp} - g_e) + 9(g_0 - g_e)]$ where p is the dipolar interaction coefficient (0.036 cm^{-1}) for Cu(II) ion, K represents the Fermi contact interaction term calculated as $K = -A_0 + P(g_0 - g_e)$. The values of α^2 varies from 0.5 to 1.0 for purely covalent to ionic bonding. The values obtained from the calculation points to a covalent nature of the in plane σ -bonding in all complexes.

The value of in plane π bonding β^2 for copper(II) vary from 0.79 to 0.90. The trend of β^2 values is opposite to that observed for α^2 which are indicative of competitive mechanism of in-pane σ and π bonding. The value of out-of-plane π bonding γ^2 vary in the range of 0.83-0.93 showing little to appreciable out-of-plane bonding. The extent of departure from these coefficients from unity measures the extent of delocalization of the metal electron due to M-L bonding. The orbital reduction factors $K_{\parallel} = \alpha^2 \beta^2$ and $K_{\perp} = \alpha^2 \gamma^2$ were estimated from the following expressions.

$$K_{\parallel}^2 = (g_{\parallel} - 2.0023)\Delta E(d_{xy} \rightarrow d_{x^2-y^2}) / 8\lambda_0$$

$$K_{\perp}^2 = (g_{\perp} - 2.0023)\Delta E(d_{xy} \rightarrow d_{x^2-y^2}) / 2\lambda_0$$

where λ_0 is the spin orbit coupling constant and has a value of -828 cm^{-1} for copper(II) d^9 systems. The spin orbit coupling constants were also calculated from the following expressions.

$$\lambda_{\parallel} = 2.0023 - 8\lambda(\alpha^2\beta^2) / \Delta E_{d \leftarrow d} \text{ and } \lambda_{\perp} = 2.0023 - 2\lambda(\alpha^2\gamma^2) / \Delta E_{d \rightarrow d}$$

The values of λ_{\parallel} and $\lambda_{\perp} \sim -789.87$ and -785.12 cm^{-1} respectively suggest a greater contribution from out-of-plane π bonding than in-plane π bonding. According to Hathaway^{60,61} for pure σ bonding $K_{\parallel} \approx K_{\perp} \approx 0.77$, and for out-of-plane π bonding $K_{\parallel} > K_{\perp}$. This is observed for the values calculated for all the complexes confirming the domination of out-of-plane π bonding in the compounds⁶². The empirical factor f calculated as $g_{\parallel}/A_{\parallel} \text{ cm}^{-1}$ is an index of tetrahedral distortion, and distortion from planarity. The value ranges from 105 to 135 cm^{-1} for smaller to larger distortion in

square planar species. All complexes show values near to 120 cm^{-1} indicating moderate out-of-plane distortion in the molecules.

The identification of bonding groups can be suggested from the values of the dipolar term P . The small reduction in P values from the free ion (0.036 cm^{-1}) might be attributable to significant covalent bonding character. The P value calculated for the complexes is found in the range of 0.02 cm^{-1} indicates significant covalent character in the molecules. All these arguments are mutually supporting. The parameter P can be treated as a variable to observe the effects of electron delocalization and can be calculated by using the expression, $P = (A_{\parallel} - A_{\perp}) / [(g_{\parallel} - 2) - 5/14(g_{\perp} - 2) - 6/7]$.

The identification of the bonding groups can be obtained by looking at the values of P . The observed values for the complexes favor the bonding of nitrogen to copper⁶³.

3.2.5. Molecular and crystal structure of compound 2

The compound $\text{Cu}_2(\text{BpypTsc})_2\text{Cl}_2$ (**2**) crystallizes into a triclinic lattice with $P1$ space group symmetry. Table 3.7 reports the crystallographic refinement parameters for the structural determination; Table 3.8 presents the selected bond lengths and angles of the compound.

Table 3.7. Crystallographic refinement parameters of the compound 2

Empirical formula	$\text{C}_{34}\text{H}_{34}\text{Cl}_2\text{Cu}_2\text{N}_8\text{S}_2$
Formula weight (M)	816.79
Temperature (T) K	298(2)
Wave length (Mo $K\alpha$), Å	0.70930 Å
Crystal system/ Space group	Triclinic/ $P1$
Unit cell dimensions	
a, Å, α°	7.5440(8), 65.924(14)
b, Å, β°	11.0990(18), 72.261(12)
c, Å, γ°	12.258(2), 76.244(11)
Volume (V), Å ³ / F(000)	884.9(2)/ 416
Z, Calculated density (ρ), Mgm^{-3}	1, 1.533
Absorption coefficient (μ) mm^{-1}	1.509
Crystal size	0.315×0.20×0.10 mm
θ Range for data collection	1.87-24.93°
Limiting indices	-8 ≤ h ≤ 8, -12 ≤ k ≤ 13, 0 ≤ l ≤ 14
Reflections collected/ Unique	2889/ 2889 [R(int) = 0.000]
Completeness to 2θ	24.93°, 88.5%
Max and min transmission	1.000 and 0.957
Goodness-of-fit on F^2	1.072
Final R indices [$I > 2 \sigma(I)$]	R1 = 0.0392, wR2 = 0.0965
R indices (all data)	R1 = 0.0512, wR2 = 0.1086
Largest diff. peak and hole	0.560 and -0.537 e. Å ⁻³

Table 3.8 Selected bond lengths and angles of the compound **2**

Bond lengths (Å)		Bond angles (°)	
Cu1-N1	2.058 (14)	N1-Cu1-N2	82.9(5)
Cu1-N2	2.247(5)	N1-Cu1-S1	164.4(4)
Cu1-S1	2.253(5)	S1-Cu1-Cl1	96.81(18)
Cu1-Cl1	1.280 (2)	N1-Cu1-Cl1	95.5(4)
C6-N2	1.307 (19)	S1-Cu1-N2	83.9 (4)
N3-N2	1.734 (17)	N2-Cu1-Cl1	174.3(4)
C13-S1	1.337 (19)	N6-Cu2-N5	79.2(5)
C13-N3	2.055 (11)	C13-S1-Cu1	93.7(5)

The asymmetric unit of the crystal of the compound **2** consist of two molecules characterized by a two-fold axis perpendicular to the Cu1-Cl1-Cu2-Cl2 plane resulting in a centrosymmetric closely associated crystallographically equivalent molecules strongly bridged via chlorine atoms Cl1 and Cl2. The molecular structure along with the atom numbering scheme is presented in Figure 3.11.

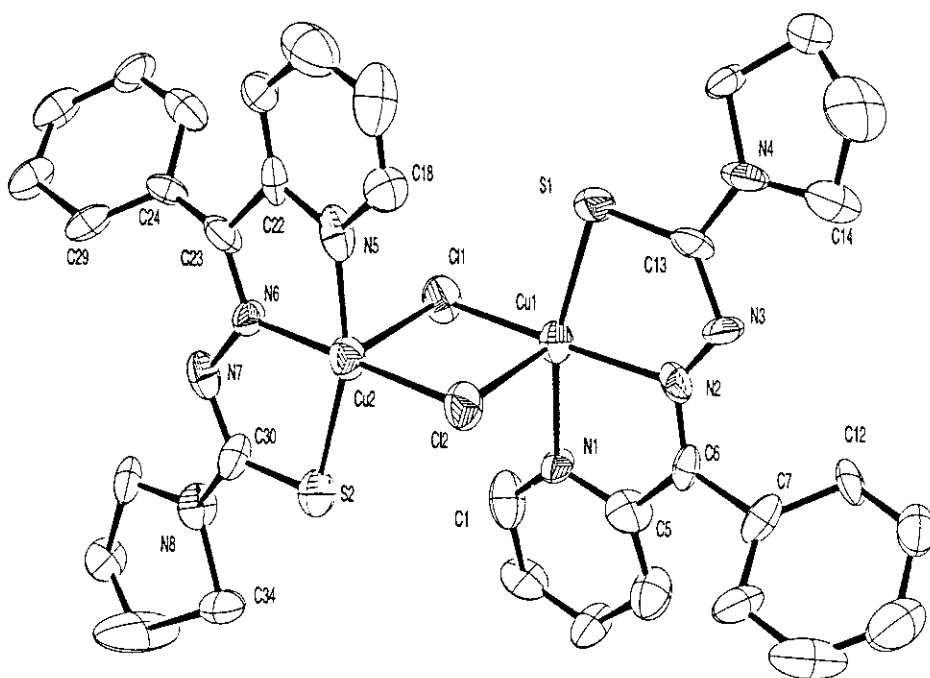


Figure 3.11. ORTEP diagram for compound $\text{Cu}_2(\text{BpypTsc})_2\text{Cl}_2(\mathbf{2})$, displacement ellipsoids are drawn at 55% probability level and hydrogen atoms are shown as small spheres of arbitrary radii.

The comparison of bond distances Cu(2)-Cl(2) (2.253 Å), Cu(2)-Cl(1) (2.776 Å), Cu(1)-Cl(1) (2.253 Å) and Cu(1)-Cl(2) (2.811 Å) confirms the possibility of a bridging dinuclear structure, the Cu(1)-Cu(1) distance is also moderate (3.375 Å). These observations agree with the far-IR assignments that the chlorine atoms interact strongly with the metal centre of the neighboring molecule for a bridging bond. This is further confirmed by including the four membered ring Cg(2) = Cu1-Cl1-Cu2-Cl2 in the analysis of short ring interactions with the program PLATON which indicated that the ring Cg(2) interacts strongly with the pyridyl ring of the ligand. The distance between the Cg(2) ring and the pyridyl rings is small (~3.9 Å) which can be considered as a strong π - π interaction indicating considerable amount of π electron delocalization in the Cg(2) ring. Figure 3.12 shows the molecular packing of the compound.

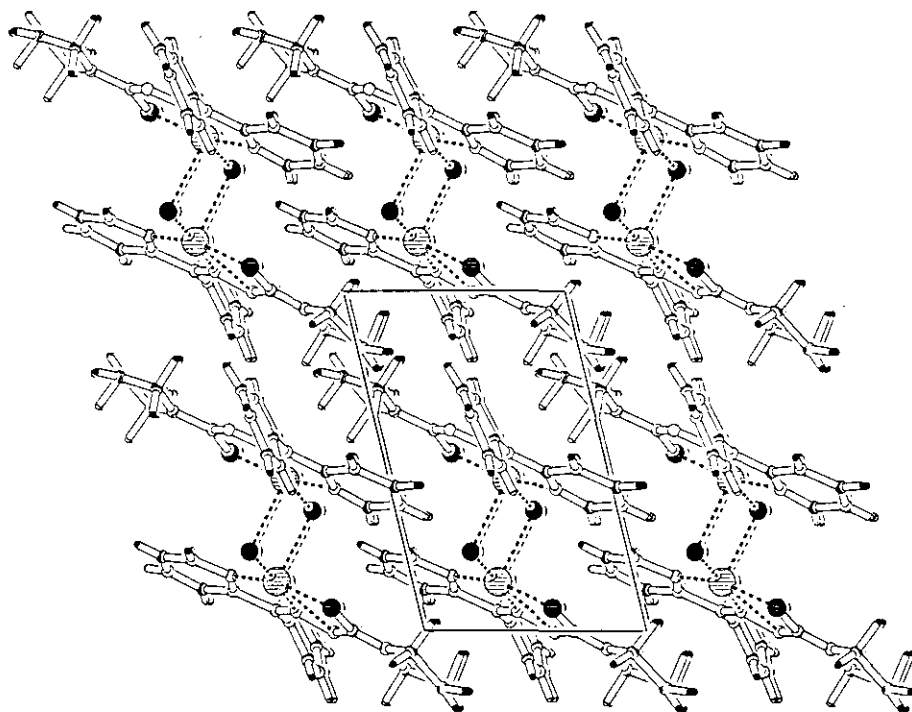


Figure 3.12. Packing of the compound 2, viewed along c axis.

Coordination lengthens the thiosemicarbazone moiety's C(13)-S(1) bond length⁶⁴ from 1.681 to 1.750 Å which is consistent with the C-S single bond length. Copper atom is in the same plane with the coordinating Cl(1), azomethine nitrogen N(2), pyridyl nitrogen N(1), and thiolate sulfur S(1) indicated by the bond angles

N(1)-Cu(1)-N(2) (82.9°), N(2)-Cu(1)-Cl(1) (174.3°), N(1)-Cu(1)-Cl(1) (95.5 °). The bond angles are quiet far from a perfect square planar geometry around copper atom. The Cu-N and Cu-S bond lengths are smaller ~ 2.058 and 2.253 Å indicating the domination of thiosemicarbazone moiety in the bonding. It is found that copper atom is closer to thiosemicarbazone moiety than the chloride.

The compound **2** packs in to an offset π stacked fashion with intermolecular π - π stacking interactions between the pyridine rings of both molecule and the four membered ring formed between the two chlorine and copper atoms of the molecule. The interaction is more related to a π -deficient- π -deficient interaction and will lead to a stable structure⁶⁵. The packing is stabilized by the H- bonding and CH... π interactions in the molecule presented in Table 3.9.

Table 3.9. Crystallographic interaction parameters for compound 2

D-H...A	D-H (Å)	H...A (Å)	D...A (Å)	\angle D-H...A (°)
Intra C(1)-H(1)...Cl(1)	0.93	2.79	3.329	118
C(9)-H(9).....Cl(1) ^a	0.93	2.55	3.697	157
Intra C(12)-H(12).....N(3)	0.93	2.55	2.899	103
C(17)-H(17).....Cl(1) ^b	1.30	2.78	3.949	149
Intra C(18)-H(18).....Cl(2)	0.93	2.76	3.330	120
C(26)-H(26).....Cl(2) ^c	0.93	2.77	3.656	160
Intra C(29)-H(29).....N(7)	0.93	2.53	2.954	108
C(34)-H(34A).....Cl(2) ^d	1.19	2.80	3.886	152
Equivalent Position Code a = x, 1+y, z; b = 1+x, y, z; c = x, -1+y, z; d = -1+x, y, z				
π...π interactions				
Cg(I)-Res(I)...Cg(J)	Cg-Cg (Å)	α (°)	β (°)	
Cg(2)-[1]....Cg(11) ^e	3.9765	84.15	33.50	
Cg(2)-[1]....Cg(12) ^e	3.9513	87.07	33.28	
Equivalent Position Code e = x, y, z		Cg(2) = Cu(1), Cl(1), Cu(2), Cl(2) Cg(11) = N(1), C(1), C(2), C(3), C(4), C(5), C(6)		
CH...π interactions				
X-H(I)---Cg(J)	H...Cg (Å)	X....Cg (Å)	\angle X-H...Cg (°)	
C(1)-H(1).....Cg(2) ^f	3.0519	3.2714	95.29	
C(3)-H(3)....Cg(13) ^g	2.8591	3.4937	126.54	
C(14)-H(14A)....Cg(11) ^h	2.9284	4.0098	174.56	
Equivalent position code f = x, y, x g = -1+x, y, z; h = 1+x, y, z		Cg(12) = N(5), C(18), C(19), C(20), C(21), C(22) Cg(13) = C(7), C(8), C(9), C(10), C(11), C(12)		
D= donor, A= acceptor, Cg= Centroid, α = dihedral angles between planes I&J, β = angle				

The molecules connect with one another *via* aromatic C-H... π interactions leading to a honeycomb like arrangement in the crystal lattice. Interestingly the referred intra- and intermolecular π ... π stacking interactions coexist with an

extensive 3D hydrogen bonding network between the molecules. The above facts aims at considerable amount of π - electron delocalization in the metal containing four membered ring Cg(2). These exists a strong pulling effect on the chlorine atoms from two hydrogen bonds, one intra and one intermolecular.

3.2.6. Molecular and crystal structure of compound 6

The compound CuBpypTscBr (6) crystallizes in to a monoclinic lattice with P21/n space group symmetry. Table 3.10 illustrates the experimental refinement parameters for the compound. Asymmetric unit of a unit cell contains crystallographically equivalent molecules of 6 with square planar environment around copper atom.

Table 3.10. Crystallographic refinement parameters for compound 6

Empirical formula	C ₁₇ H ₁₇ BrCuN ₄ S
Formula weight (M)	452.86
Temperature (T) K	293(2)
Wave length (Mo K α), Å	0.70930Å
Crystal system	Monoclinic
Space group	P21/n
Unit cell dimensions	
a, Å, α°	11.1600(8), 90.000(7)
b, Å, β°	8.4050(6), 97.931(7)
c, Å, γ°	18.534(2), 90.000(6)
Volume (V), Å ³	1721.9(3)
Z, Calculated density (ρ), Mgm ⁻³	4, 1.747
Absorption coefficient (μ) mm ⁻¹	3.716
F(000)	908
Crystal size	0.35×0.25×0.15 mm
θ Range for data collection	2.01-24.92°
Limiting indices	0 ≤ h ≤ 13, 0 ≤ k ≤ 9, -22 ≤ l ≤ 21
Reflections collected/ Unique	2763/ 2763 [R(int) = 0.000]
Completeness to 2 θ	24.92°, 85.3%
Max and min transmission	1.000 and 0.980
Goodness-of-fit on F ²	1.080
Final R indices [I > 2 σ (I)]	R1= 0.0275, wR2= 0.0631
R indices (all data)	R1= 0.0359, wR2= 0.0699
Largest diff. peak and hole	0.578 and -0.346 e. Å ⁻³

The molecular structure along with atom numbering scheme is presented in Figure 3.13, and selected bond lengths and angles are presented in Table 3.11. Coordination lengthens the thiosemicarbazone moiety's C(13)-S(1) bond length from 1.681 to 1.749 Å which is consistent with the C-S single bond length. Copper atom is in the same plane with the coordinating Br(1), azomethine nitrogen N(2),

pyridyl nitrogen N(1), and thiolate sulfur S(1) indicated by the bond angles N(1)-Cu(1)-N(2) (80.61°), N(2)-Cu(1)-Br(1) (169.02°), N(1)-Cu(1)-Br(1) (97.94°). The bond angles are quiet far from a perfect square planar geometry around copper atom. The Cu-N and Cu-S bond lengths are smaller ~ 2.055 and 2.247 Å indicating the domination of thiosemicarbazone moiety in the bonding. It is found that copper atom is closer to thiosemicarbazone moiety than the bromide.

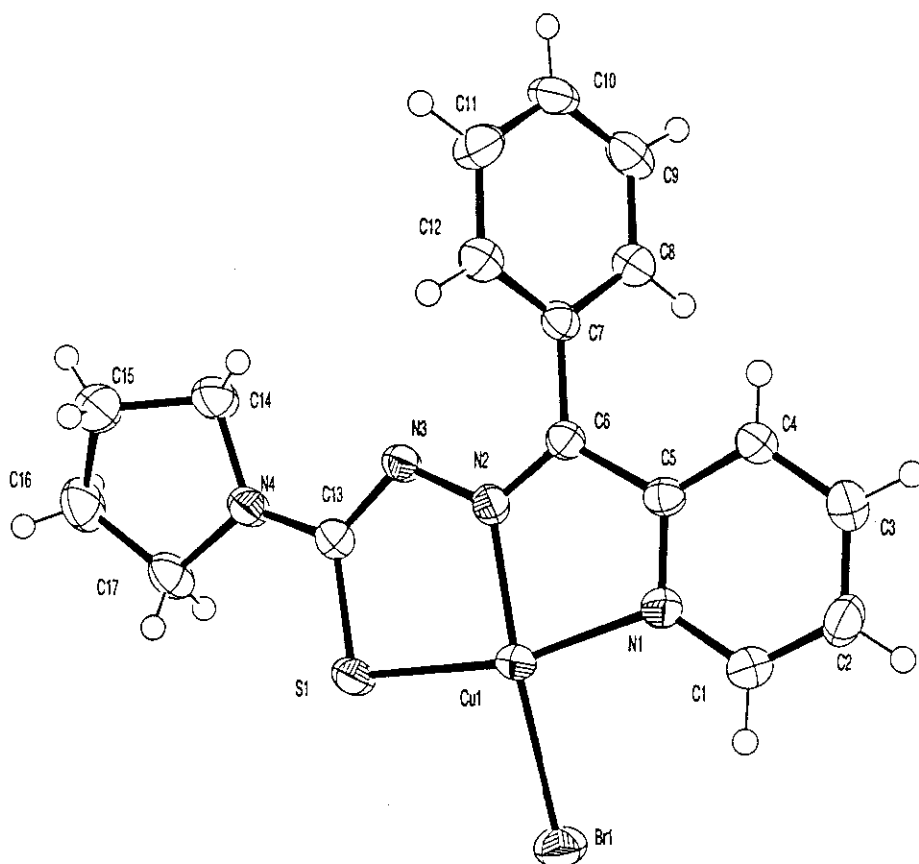


Figure 3.13. ORTEP diagram for compound CuBpypTscBr(6), displacement ellipsoids are drawn at 55% probability level and hydrogen atoms are shown as small spheres of arbitrary radii.

As Figure 3.14 shows the molecules packs in an face-to-face offset fashion with edge-on or T-shaped geometry due to π - σ attraction between the metal containing chelate rings and aromatic hydrogen atoms of the thiosemicarbazone moiety of the neighboring molecules. Table 3.12. Presents the intermolecular interaction parameters of the compound.

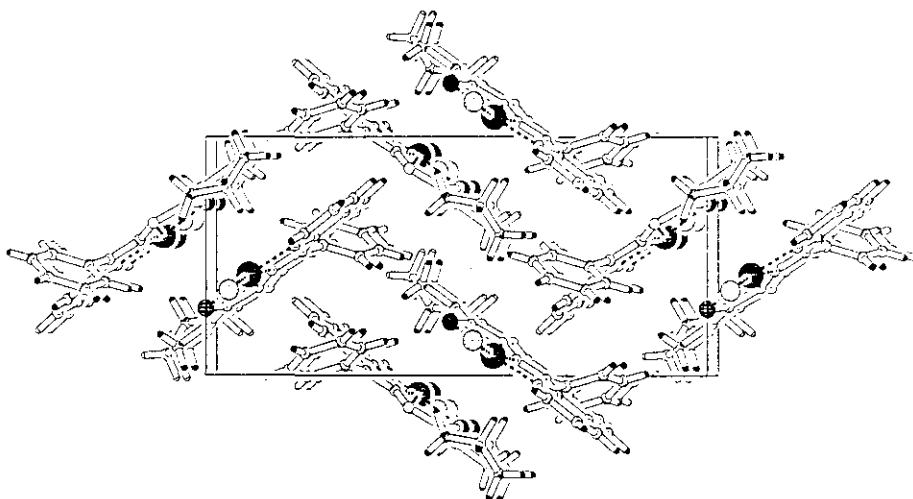


Figure 3.14. Packing of the compound 6 in a unit cell, view along *b* axis.

Table 3.11. Selected bond lengths and angles of the compound 6

Bond lengths (Å)		Bond angles (°)	
Cu1-N1	2.017(3)	N1-Cu1-N2	80.61(10)
Cu1-N2	1.977(3)	N1-Cu1-S1	165.20(8)
Cu1-S1	2.2461(9)	S1-Cu1-Br	95.83(3)
Cu1-Br	2.381(5)	N1-Cu1-Br	97.94(7)
C6-N2	1.301(4)	S1-Cu1-N2	84.84(8)
N3-N2	1.357(4)	N2-Cu1-Br	169.02(8)
C13-S1	1.749(3)		
C13-N3	1.339(4)		

Table 3.12. Interaction parameters of the compound 6

D-H...A	D-H (Å)	H...A (Å)	D...A (Å)	∠D-H...A (°)
Intra C(1)-H(1).....Br(1)	0.90	2.86	3.4559	124
π...π interactions				
Cg(I)-Res(I)....Cg(J)	Cg-Cg (Å)	α (°)	β (°)	
Cg(2)....Cg(2) ^a	3.8238	0.03	37.71	
Cg(2)....Cg(3) ^a	3.8773	0.67	38.93	
Cg(3)....Cg(3) ^a	3.9557	0.02	40.23	
Cg(3)....Cg(8) ^b	3.8910	16.26	19.85	
Cg(4)....Cg(8) ^b	3.9295	17.80	19.30	
Equivalent position code a = -x, 1-y, -z; b = ½-x, -½+y, ½-z	Cg(2) = Cu(1), S(1), C(13), N(3); Cg(3) = Cu(1), S(1), C(13), N(3), N(2); Cg(4) = Cu(1), N(1), C(5), C(6), N(2); Cg(8) = C(7), C(8), C(9), C(10), C(11), C(12)			
CH...π interactions				
X-H(I)....Cg(J)	H.....Cg (Å)	X.....Cg (Å)	∠X-H...Cg (°)	
C(4)-H(4).....Cg(8) ^c	3.1905	3.4114	98.03	
C(9)-H(9).....Cg(2) ^d	3.1444	3.3379	96.09	
Equivalent position code c = ½-x, ½+y, ½-z; d = ½+x, ½-y, -½+z				

The C1-H1 forms a six membered ring through hydrogen bonding with bromine atom existing at a distance of 0.90 Å. It has been observed that there exists strong π - π interactions between the metal containing chelate rings Cg(2) (Cu1, S1, C13, N3) and Cg(3) (Cu1, S1, C13, N3, N2) of the face-to face packed molecules of compound 6. Interestingly the chelate rings Cg(3) of the two neighboring molecules are at a distance of 3.9 Å with a strong π - π interaction between them. The same centroid interacts strongly with the phenyl ring Cg(8) of the near by offset- π -stacked molecule at a distance of 3.89Å and with a small β angle (19.85°). There exists a similar type of π - π interaction between the Cg(8) and Cg(4) (Cu1, N1, C5, C6, N2) at a distance of 3.92 Å. All these observations along with the C-H... π interactions stabilize the molecular packing and points to considerable amount of π -electron delocalization in the metal containing chelate rings.

3.2.7. Molecular and crystal structure of compound 7

The compound CuBpypTscSH (7) crystallizes in to a monoclinic space group with P21/n space group symmetry. Table 3.13 presents the crystallographic refinement parameters and Figure 3.15 shows the molecular structure of compound 7.

Table 3.13 crystallographic refinement parameters of compound 7

Empirical formula / FW (M)	C ₁₇ H ₁₈ CuN ₄ S ₂ / 406.01
Temperature (T) K	293(2)
Wave length (Mo K α), Å	0.70930Å
Crystal system/ Space group	Monoclinic / P21/n
Unit cell dimensions	
a, Å, α°	11.1160(9), 90.000(4)
b, Å, β°	8.3010(4), 98.012(6)
c, Å, γ°	18.6780(11), 90.000(5)
Volume (V), Å ³	1706.67(19)
Z, Calculated density (ρ), Mmg ⁻³	4, 1.580
Absorption coefficient (μ) mm ⁻¹	1.530
F(000)	836
Crystal size	0.40×0.25×0.25 mm
θ Range for data collection	2.01-24.93°
Limiting indices	0 ≤ h ≤ 13, 0 ≤ k ≤ 9, -22 ≤ l ≤ 21
Reflections collected/ Unique	2844/ 2844 [R(int) = 0.000]
Completeness to 2 θ	24.93°, 88.0%
Max and min transmission	1.000 and 0.971
Goodness-of-fit on F ²	1.087
Final R indices [I > 2 σ (I)]	R1= 0.0276, wR2= 0.0734
Largest diff. peak and hole	0.442 and -0.504 e. Å ⁻³

Coordination lengthens the thiosemicarbazone moiety's C(13)-S(1) bond length from 1.681 to 1.749 Å which is consistent with the C-S single bond length. Copper atom is in the same plane with the coordinating S2, azomethine nitrogen N(2), pyridyl nitrogen N(1), and thiolate sulfur S(1) as indicated by the bond angles N(1)-Cu(1)-N(2) (80.44°), N(2)-Cu(1)-S(2) (169.02°), N(1)-Cu(1)-S(2) (97.94°). The bond angles are quiet far from a perfect square planar geometry around copper atom. The Cu-N and Cu-S bond lengths are smaller ~ 2.055 and 2.247 Å indicating the domination of thiosemicarbazone moiety in the bonding. It is found that copper atom is closer to thiosemicarbazone moiety than the mercapto sulfur. Selected bond lengths and angles are listed in Table 3.14 and interaction parameters are presented in Table 3.15.

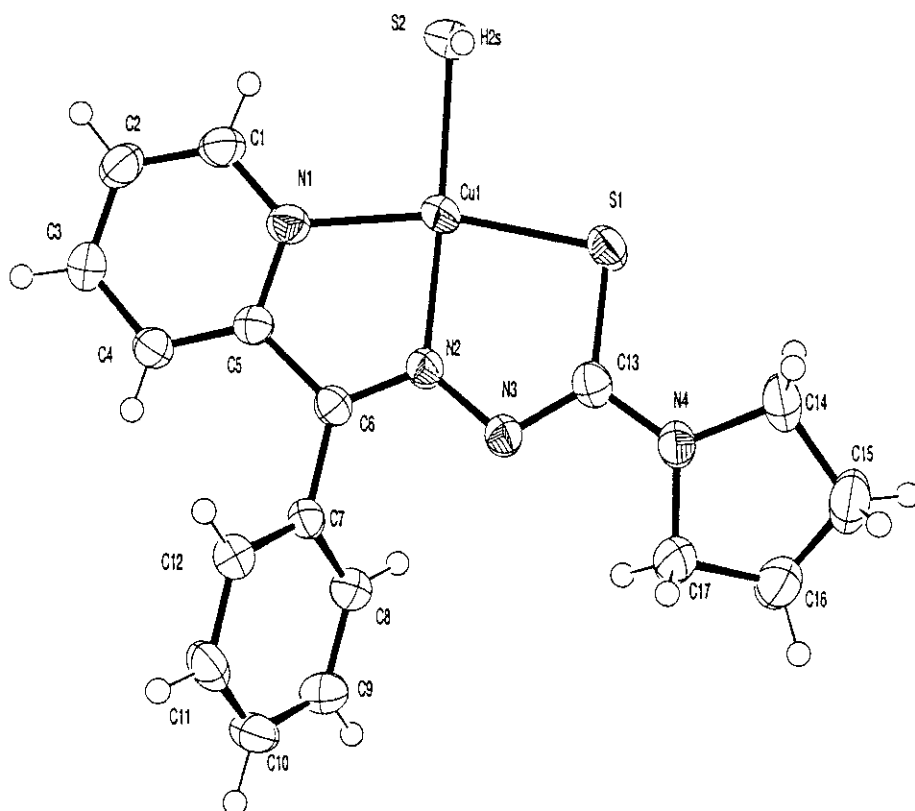


Figure 3.15. ORTEP diagram for compound CuBpypTscSH(7), displacement ellipsoids are drawn at 55% probability level and hydrogen atoms are shown as small spheres of arbitrary radii.

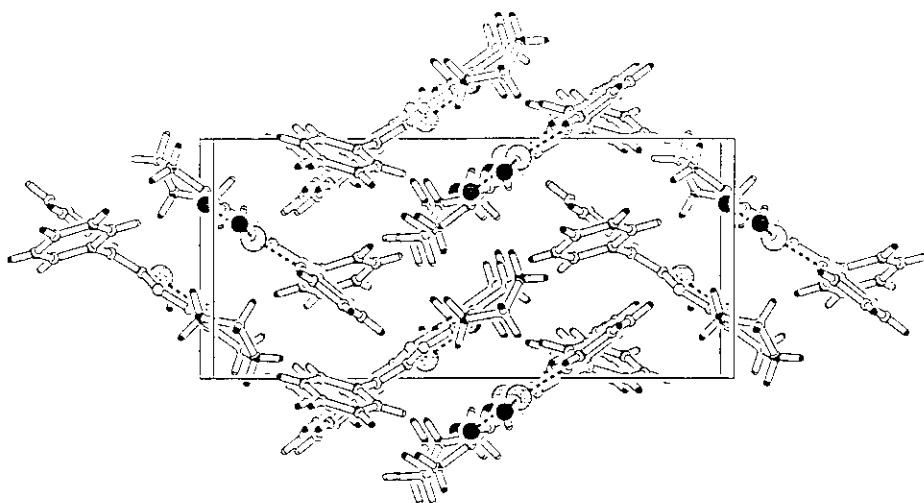


Figure 3.16 Packing of the compound 7 viewed along b axis

The C1-H1 forms a six membered ring through hydrogen bonding with mercapto sulfur atom existing at a distance of 0.90 Å. It has been observed that there exists strong π - π interactions between the metal containing chelate rings Cg(2) (Cu1, S1, C13, N3) and Cg(3) (Cu1, S1, C13, N3, N2) of the face-to-face packed molecules of compound 7. Interestingly the chelate rings Cg(3) of the two neighboring molecules are at a distance of 3.9 Å with a strong π - π interaction between them. The same centroid interacts strongly with the phenyl ring Cg(8) of the near by offset- π -stacked molecule at a distance of 3.89 Å and with a small β angle (19.85°). There exists a similar type of π - π interaction between the Cg(8) and Cg(4) (Cu1, N1, C5, C6, N2) at a distance of 3.92 Å. All these observations along with the C-H... π interactions stabilizes the molecular packing and points to considerable amount of π -electron delocalization in the metal containing chelate rings. It was interesting to note a ring-metal interaction between the Cu1 and Cg(2) and Cg(3) of the face-to-face packed molecules in compound 7. The metal chelate ring Cu1-S1-C13-N3-N2 is at a distance of 3.46 Å with the Cu1 of the next molecule. To our knowledge these weak intramolecular interactions - π ... π , CH... π or chelate ring...metal interactions- involving metal chelate rings can be evidenced for metalloaromaticity - a classic concept recently reviewed by Masui⁶⁶.

Table 3.14. Selected bond lengths and angles of the compound 7

Bond lengths (Å)		Bond angles (°)	
Cu1-N1	2.027(19)	N1-Cu1-N2	80.44(7)
Cu1-N2	1.977(18)	N1-Cu1-S1	165.01(6)
Cu1-S1	2.257(7)	S1-Cu1-S2	97.36(7)
Cu1-S(2)	2.247(18)	N1-Cu1-S2	96.73(8)
C6-N2	1.304(3)	S1-Cu1-N2	84.80(2)
N3-N2	1.358(3)	N2-Cu1-S2	169.81(9)
C13-S1	1.751(2)		
C13-N3	1.337(3)		

Table 3.15. Crystallographic interaction parameters of the compound 7

D-H...A	D-H (Å)	H...A (Å)	D...A (Å)	∠D-H-A (°)
C(1)-H(1)....S(2)	0.90	2.76	3.3465	124
π...π interactions				
Cg(I)-Res(I)....Cg(J)	Cg-Cg (Å)	α (°)	β (°)	
Cg(2)-[1].....Cg(2)a	3.7862	0.02	35.93	
Cg(2)-[1].....Cg(3)a	3.8418	0.67	37.28	
Cg(2)-[1].....Cg(8)b	3.9977	16.33	24.92	
Cg(3)-[1].....Cg(2)a	3.8418	0.67	37.05	
Cg(3)-[1].....Cg(3)a	3.9226	0.02	38.71	
Cg(3)-[1].....Cg(8)b	3.8833	16.88	19.96	
Cg(4)-[1].....Cg(8)b	3.8913	17.90	18.74	
Ring metal interactions				
M....Cg(J)	Cg-Cg (Å)	α (°)	β (°)	
Cu(1)....Cg(2) ^a	3.336	3.067	23.16	
Cu(1)....Cg(3) ^a	3.460	3.076	27.26	
Equivalent position code a = 1-x, 1-y, z; b = 3/2-x, 1/2+y, 1/2-z	Cg(2) = Cu(1), S(1), C(13), N(3); Cg(3) = Cu(1), S(1), C(13), N(3), N(2); Cg(4) = Cu(1), N(1), C(5), C(6), N(2); Cg(8) = C(7), C(8), C(9), C(10), C(11), C(12);			
CH...π interactions				
X-H(I)---Cg(J)	H....Cg (Å)	X.....Cg (Å)	∠X-H-Cg (°)	
C(4)-H(4).....Cg(8)c	3.1918	3.3852	96.02	
C(11)-H(11).....Cg(2)c	3.1106	3.3185	95.60	
C(11)-H(11).....Cg(3)c	3.1896	3.3115	89.98	
Equivalent position code c = 3/2-x, -1/2+y, 1/2-z				
D= donor, A= acceptor, Cg = Centroid, α = dihedral angles between planes I&J, β= angle Cg(I)=Cg(J)				

3.2.8. Molecular and crystal structure of compound 9

The compound 9 crystallizes in to a monoclinic lattice with a Cc point group symmetry. The structural refinement parameters are listed in Table 3.16 and selected bond lengths and angles along with interaction parameters are listed in Table 3.17.

The structure of compound 9 was interesting compared with the other complexes. The unit cell of the compound contain three different structures of a homothiometallic μ_2 -S bridged compound. All the three compounds have the same composition and are crystallographically equivalent and is co-crystallized into the monoclinic lattice with an approximate 54%: 34%:12% ratio of the structures 9A, 9B and 9C. The differences are in the extend of bridging in these compounds. The bond lengths and angles are listed in the Table 3.18. Figure 3.16 show the co-crystallized structure of the compound, Figures 3.17-3.19 shows the individual structures 9A, 9B and 9C and Figure 3.20 shows the packing of the molecule in a unit cell. The molecular packing as well as the co-crystallization is favored by strong C-H..... π interactions existing in the unit cell lattice. It is notable that the metal containing chelate ring does not interact with neighboring moieties. The extensive 3D network formed due to co-crystallization is stabilized by C-H..... π Interactions provided by the aromatic rings of the ligand moiety. This is evident from the packing diagram, which shows the molecules are stacked in to zigzag columns in a honey comb like pattern where the aromatic rings interacts in a T-shaped geometry.

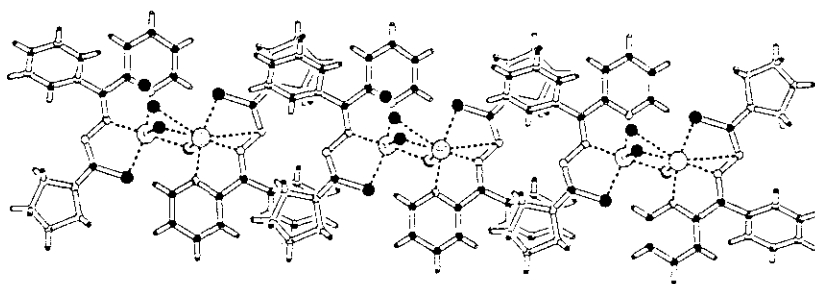


Figure 3.16. PLATON view of the compound 9 co-crystallized structures A, B and C, in 30% probability level. Hydrogen atoms are arbitrarily assigned.

Table 3.16. Crystallographic parameters of the compound 9

Empirical formula	C ₃₄ H ₃₄ Cu ₂ N ₈ S ₄
Formula weight (M)	810.01
Crystal system/ Space group	Monoclinic/ Cc
a, Å, α°	23.317(2), 90.00
b, Å, β°	7.5745(7), 113.162(2)
c, Å, γ°	22.000(2), 90
Z, Calculated density (ρ), Mgm ⁻³	4, 1.506
Absorption coefficient (μ) mm ⁻¹	1.462
F(000)	1664
Crystal size	0.40 x 0.34 x 0.14 mm
Limiting indices	-22 ≤ h ≤ 27, -8 ≤ k ≤ 8, -26 ≤ l ≤ 25
Reflections collected/ Unique	8127 / 4689 [R(int) = 0.0316]
Goodness-of-fit on F ²	1.099
Final R indices [I > 2 σ (I)]	R1 = 0.0802, wR2 = 0.2052
Largest diff. peak and hole	1.531 and -1.248 e. Å ⁻³

Table 3.17. Bonding parameters of the compound 9

Bond lengths (Å)		Bond angles (°)	
Cu(1)-N(2)	1.970(12)	N(2)-Cu(1)-S(3)	172.6(3)
Cu(1)-N(1)	2.002(13)	N(1)-Cu(1)-S(3)	98.7(3)
Cu(1)-S(3)	2.238(4)	N(2)-Cu(1)-S(1)	84.8(3)
Cu(1)-S(1)	2.243(4)	N(1)-Cu(1)-S(1)	163.6(3)
Cu(2)-N(6)	1.964(9)	S(3)-Cu(1)-S(1)	94.64(16)
Cu(2)-N(5)	2.020(11)	N(6)-Cu(2)-N(5)	81.6(4)
Cu(2)-S(2)	2.233(4)	N(6)-Cu(2)-S(4)	166.2(5)
Cu(2)-S(4)	2.56(2)	N(5)-Cu(2)-S(4)	108.1(5)
Cu(2)-S(3)	2.793(4)	S(2)-Cu(2)-S(4)	83.9(4)
S(1)-C(13)	1.746(12)	N(6)-Cu(2)-S(3)	90.4(3)
S(2)-C(30)	1.739(12)	S(2)-Cu(2)-S(3)	103.38(16)
CH....π interactions			
X-H(I)—Cg(J)	H.....Cg (Å)	X.....Cg (Å)	∠X-H...Cg (°)
C(3)-H(3B).....Cg(12) ^a	2.8621	3.5331	130.06
C(17)-H(17B)....Cg(10) ^b	2.8153	3.7480	161.53
C(20)-H(20A)....Cg(13) ^b	2.9597	3.5967	126.98
C(31)-H(31B)....Cg(11) ^a	2.9333	3.8358	155.27
Equivalent position code a= x, 1+y, z; b= x, -1+y, z Cg= Centroid			
Cg(13) = C(24), C(25), C(26), C(27), C(28), C(29)			
Cg(12) = C(7), C(8), C(9), C(10), C(11), C(12)			
Cg(11) = N(5), C(18), C(19), C(20), C(21), C(22)			
Cg(10) = N(1), C(1), C(2), C(3), C(4), C(5)			

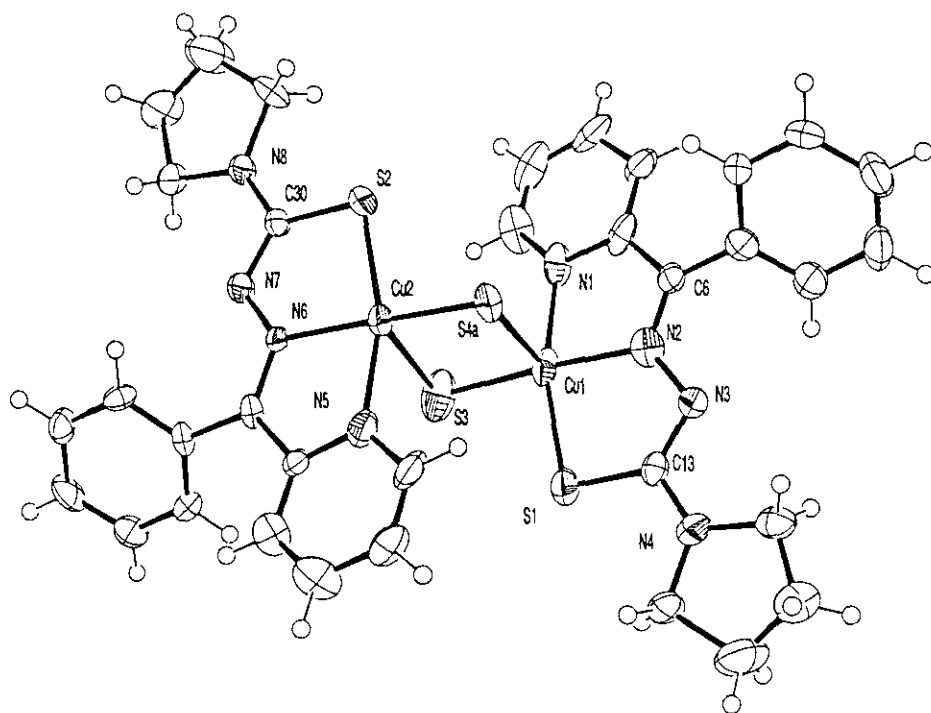


Figure 3.17. ORTEP diagram of Compound 9A displacement ellipsoids are drawn at 55% probability level and hydrogen atoms are shown as small spheres of arbitrary radii.

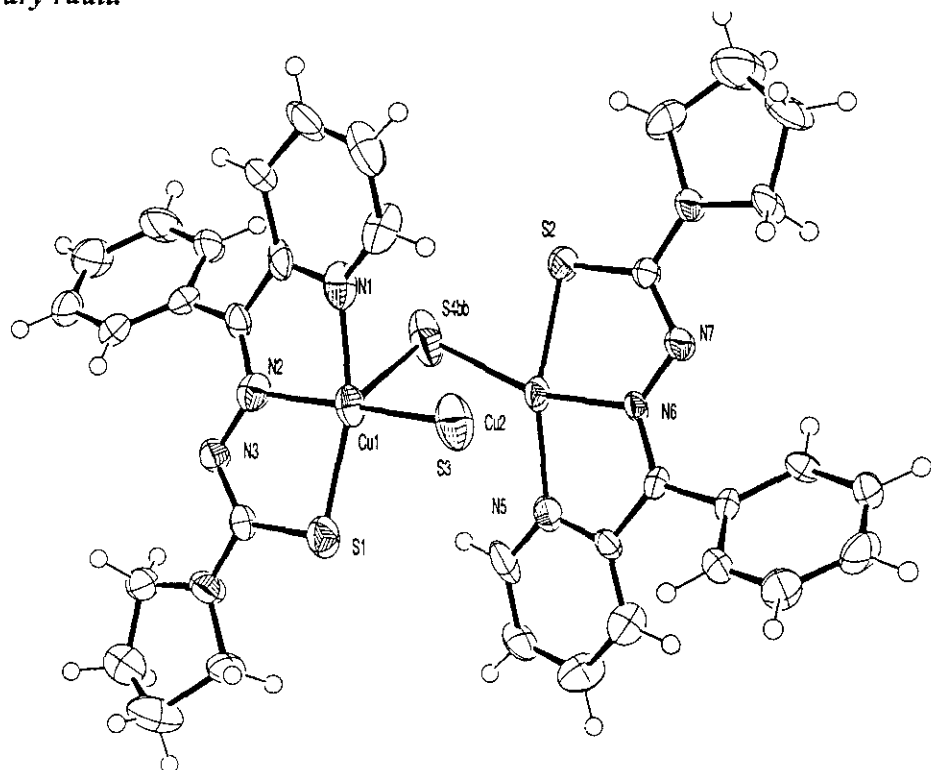


Figure 3.18. ORTEP diagram of Compound 9B displacement ellipsoids are drawn at 55% probability level.

3.2.9. Molecular and crystal structure of compound 10

The compound CuBpypTscCl (**10**) crystallizes in to a monoclinic lattice with P21/n space group symmetry. Selected bond lengths and angles are listed in Table 3.18. Figure 3.21 presents the molecular structure of the compound. The bond lengths and angles are comparable to that of the compound **2** but the salient feature is the absence of bridging and mode of packing in the unit cell. Though the compounds **2** and **10** were formed from the same reaction medium, the very existence of the compound **10** can be inferred from the differences in the Cu1-Cl1 bond lengths which is very small in compound **10** (2.240 Å) compared to compound **2** (2.280 Å) where it is elongated due to bridging. All other bond lengths and angles are in the normal range when compared with an isostructural compound **6**. As observed the Cu1-N1 bond stronger than the azomethine Cu1-N2 bonding. Cu1-S1 bond length is also large compared to similar type of compounds points to a least deviation from the perfect square planar geometry.

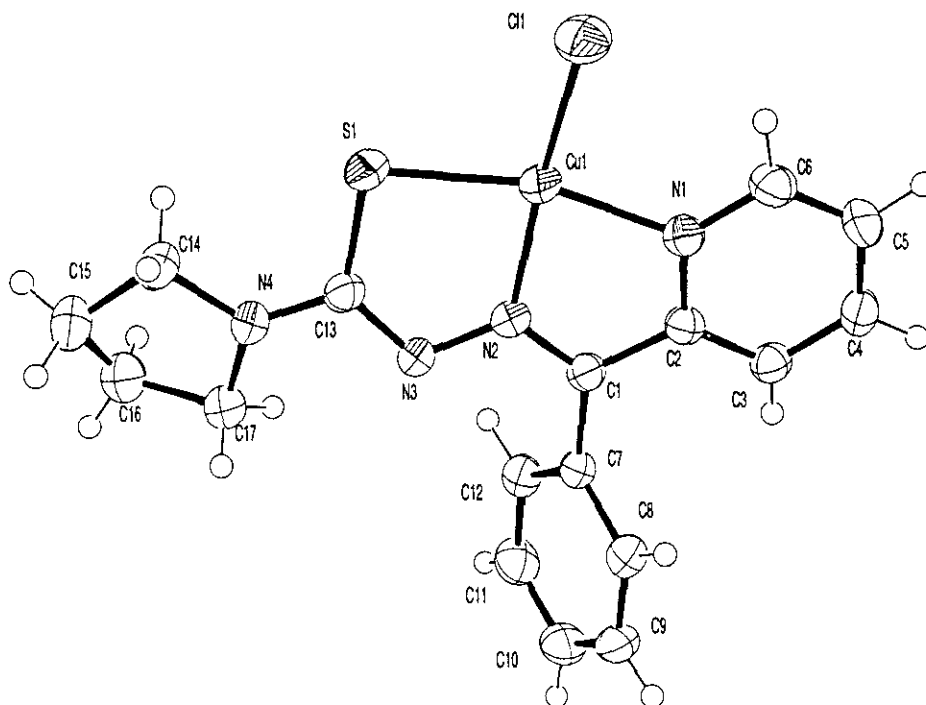


Figure 3.21. ORTEP diagram of Compound 10, displacement ellipsoids are drawn at 55% probability level and hydrogen atoms are shown as small spheres of arbitrary radii.

Table 3.18. Selected Bond lengths and Angles of the compound 10

Bond lengths (Å)		Bond angles (°)	
Cu1-N1	1.976	N1-Cu1-N2	80.48
Cu1-N2	2.027	N1-Cu1-S1	164.98
Cu1-S1	2.255	S1-Cu1-Cl1	97.26
Cu1-Cl(1)	2.240	N1-Cu1-Cl1	96.84
C6-N2	1.305	S1-Cu1-N2	84.73
N3-N2	1.355	N2-Cu1-Cl1	169.58
C13-S1	1.746		

Table 3.19. Crystallographic interaction parameters of the compound 10

D-H...A	D-H (Å)	H...A (Å)	D...A (Å)	∠D-H...A (°)
C(11)-H(1)...Cl(1)	0.92	2.71	3.3485	128
π ... π interactions				
Cg(I)-Res(I)...Cg(J)	Cg-Cg (Å)	α (°)	β (°)	
Cg(2)...Cg(2)a	3.7814	0.03	35.91	
Cg(2)...Cg(3)a	3.8367	0.06	37.02	
Cg(2)...Cg(8)b	3.9891	16.22	39.97	
Cg(3)...Cg(3)a	3.9173	0.03	38.68	
Cg(3)...Cg(8)b	3.8748	16.77	35.87	
Cg(4)...Cg(8)b	3.8845	17.78	28.44	
Ring metal interactions				
Cu(1)...Cg(2) ^a	3.332	3.064	23.10	
Cu(1)...Cg(3) ^a	3.455	3.073	27.20	
Equivalent position code	Cg(2) = Cu(1), S(1), C(13), N(3);			
a = 1-x, 1-y, 1-z;	Cg(3) = Cu(1), S(1), C(13), N(3), N(2);			
b = 1/2-x, -1/2+y, 1/2-z	Cg(4) = Cu(1), N(1), C(5), C(6), N(2);			
	Cg(8) = C(7), C(8), C(9), C(10), C(11), C(12);			
D= donor, A= acceptor, Cg = Centroid, α = dihedral angles between planes I&J, β = angle Cg(I)=Cg(J)				

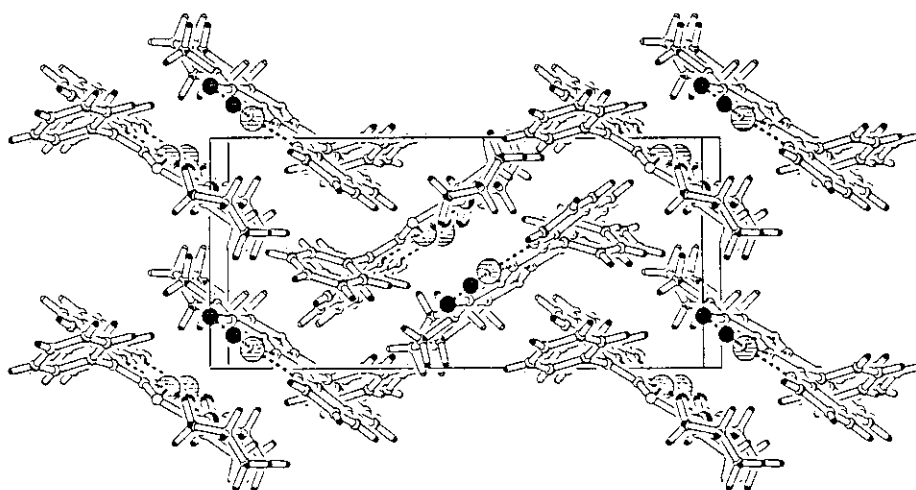
Figure 3.22. packing of the compound 10 viewed along *c* axis

Figure 3.22 shows the packing of the molecule and the intermolecular interactions are listed in Table 3. 20. The compound packs in to a zigzag arrangement with pairs of molecules arranged into a face-to-face fashion. The compound shows considerable amount of electron delocalization observed through $\pi \dots \pi$ interactions through and between the metal containing chelate rings. There exist dipolar interactions in the form of chelate ring-metal interactions as observed in the case of compound 7. All these interactions were supported in the crystal lattice by extensive C-H... π interaction networks.

3.3. Antimicrobial studies of the complexes

The details of experimental methods are discussed in detail in chapter 2. For past two decades of research in the biological activities of copper(II) complexes of thiosemicarbazones point to a redox mechanism involving thiol as the main cause of the biological activity of these compounds. Though the results of activity against the five organisms shows more activity compared to the ligand HBpypTsc, these compounds are less active compared to their 2-acetylpyridine analogs. This may be due to the additional phenyl substitution in the 2-benzoylpyridine compounds which may impose steric factors during the course of their activity. The chelation introduces significant changes in the cytotoxicity of the ligand. All the compounds exhibited good activity against *Salmonella paratyphi* and *Vibrio Cholerae O1*. None of them inhibited *Escherichia Coil* and the activities against *Bacillus Sp* and *Staphylococcus aureus* are moderate. Table 3.21 lists the diameters of the microbial inhibition zones while Figure 3.23 shows the inhibition zones of the compounds against *Salmonella paratyphi*.

Among the complexes **1**, **2**, **3** and **5** were found to be hyperactive. Others were having a less but equal activity against the two bacteria. It is thought to be due to more distortion from the square planar geometry as indicated by the crystallographic data of some of the compounds. A possible mechanism of the lower activity may be attributed to the inability to form extensive H-bonding with the active centers of cell structures, resulting in an interference with the normal cell cycle.

Chapter 4 Synthesis and studies of iron(III) complexes

Table 3.21. Antimicrobial studies of the compounds

Compounds	1 [#]	2 [#]	3 [#]	4 [#]	5 [#]
CuBpypTscN ₃ (1)	+14 mm	+19 mm	-	+13 mm	+14 mm
Cu ₂ (BpypTsc) ₂ Cl ₂ (2)	+9 mm	+11 mm	-	+14 mm	+11 mm
CuBpypTscNO ₃ (3)	+14 mm	+11 mm	-	+13 mm	+15 mm
CuBpypTscNCS (4)	+11 mm	+10 mm	-	+12 mm	+12 mm
CuBpypTscClO ₄ (5)	+11 mm	+11 mm	-	+13 mm	+11 mm
CuBpypTscBr (6)	+10 mm	+11 mm	-	+11 mm	+10 mm
Cu ₂ (BpypTsc) ₂ S ₂ (9)	+11 mm	+12 mm	-	+12 mm	+13 mm

1) *Staphylococcus aureus*, 2) *Bacillus* sp (Gram positive); 3) *Escherichia coli*,
4) *Salmonella paratyphi*, 5) *Vibrio cholerae O1* (Gram negative)

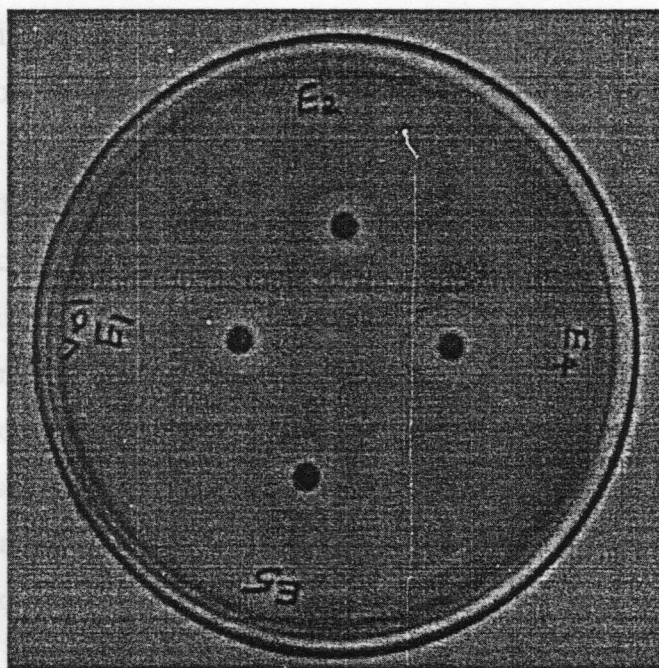


Figure 3.23. Zone of inhibitions of the compounds 1, 2, 3 and 4 against *Vibrio cholerae O1*

4.1. Experimental

4.1.1. General

Ferric chloride (Merck) and Ferric nitrate (Merck) were used as received. Ferric perchlorate was prepared by from ferric carbonate by digesting it with perchloric acid followed by evaporating the solution. The ligands HBpypTsc and HPranThas were synthesized as described in chapter 2. All solvents were distilled before use.

Chapter 4

Synthesis and studies of iron(III) complexes

Iron is the most wide spread and important transition metal which has a vital role in the living systems. Iron is an essential element in the dioxygen transport, nitrogen fixation and DNA synthesis. Physiologically iron is stored in a ubiquitous protein called ferritin, which can hold up to 4500 iron atoms. The two main functions of iron containing proteins are dioxygen transport (Hemoglobin) and electron transfer (Cytochrome c). Iron is well known to be an important initiator of free radical oxidation such as lipid peroxidation. These remarkable properties make the coordination chemistry of iron important so as to understand the biological functions. Iron complexes of thiosemicarbazones are known for past two decades exhibiting outstanding *in vitro* antitumor type activity. Iron has five 3d electron and is known to exist in three spin states *viz.*, 1/2, 3/2 and 5/2 and the dithiocarbamate complexes of iron(III) are long known to exhibit all the three states while varying the temperature. Understanding of such spin-crossover phenomenon is very important while searching for potential candidates for memory storage devices. This chapter discusses the synthesis and structural and spectroscopic characterization of four low spin iron(III) complexes of HBpypTsc and HPranThas. The spin properties of the complexes were assigned by variable temperature Mössbauer spectroscopy. All complexes were screened against clinical pathogens to understand the microbial inhibitory activity.

4.1. Experimental

4.1.1. General

Ferric chloride (Merck) and Ferric nitrate (Merck) were used as received. Ferric perchlorate was prepared by from ferric carbonate by digesting it with perchloric acid followed by evaporating the solution. The ligands HBpypTsc and HPranThas were synthesized as described in chapter 2. All solvents were distilled before use.

4.1.2. Synthesis of $[Fe(BpypTsc)_2]ClO_4$ (11)

To a methanolic solution of ferric perchlorate (1 mmol) was added a solution of HBpypTsc (2 mmol) in chloroform and refluxed for 30 minutes. The resulting deep green colored solution was evaporated to half its volume. On cooling dark brown shining crystals of the compound 11 separated out was washed with ether and dried over P_4O_{10} *in vacuo*.

4.1.3. Synthesis of $[Fe(PranThas)_2]FeCl_4$ (12)

To a methanolic solution of ferric chloride (1 mmol) was added a solution of HPranThas (1 mmol) in chloroform and refluxed for 30 minutes. The resulting deep green colored solution was evaporated to half its volume. On cooling dark brown shining crystals of the compound 12 separated out was washed with ether and dried over P_4O_{10} *in vacuo*. X-Ray quality single crystals were grown by the slow evaporation of a methanolic solution of the complex in 7 days.

4.1.4. Synthesis of $[Fe(BpypTsc)_2]NO_3$ (13)

To a methanolic solution of ferric nitrate (1 mmol) was added a solution of HBpypTsc (2 mmol) in chloroform and refluxed for 30 minutes. The resulting deep green colored solution was evaporated to half its volume. On cooling dark brown shining crystals of the compound 13 separated out was washed with ether and dried over P_4O_{10} *in vacuo*.

4.1.5. Synthesis of $[Fe(BpypTsc)_2]FeCl_4$ (14)

To a methanolic solution of ferric chloride (1 mmol) was added a solution of HBpypTsc (1 mmol) in chloroform and refluxed for 30 minutes. The resulting deep green colored solution was evaporated to half its volume. On cooling dark brown shining crystals of the compound 14 separated out was washed with ether and dried over P_4O_{10} *in vacuo*. X-Ray quality single crystals were grown by the slow evaporation of a methanolic solution of the complex in 7 days.

4.2. Results and discussions

4.2.1. Syntheses

All complexes were dark brown and are readily soluble in chloroform and methanol. Their stoichiometries and partial elemental analysis data are shown in Table 4.1. Analytical data shows a 1:2:1 ratio of iron, ligand and anions with FeL_2X [$\text{X} = \text{ClO}_4, \text{FeCl}_4, \text{NO}_3$]. The formation of complexes **12** and **14** were highly interesting due to the formation of FeCl_4^- in the reaction medium. A previously reported complex of a 2-acetylpyridine thiosemicarbazone prepared from FeCl_3 , gave a stoichiometry FeLCl_2 suggested it to be a 5-coordinate iron(III) having an intermediate spin state⁶⁸. However the structural information as well as the spectral information obtained for both compounds **12** and **14** in our case confirmed that the previous report could be incorrectly formulated. The compounds were 1:1 electrolytes in DMF⁶⁹ with Λ_m values near to $95 \Omega^{-1}\text{cm}^2\text{mol}^{-1}$. The cation centre of all the complexes are expected to contain two deprotonated ligands attached to iron(III) centers.

Table 4.1. Stoichiometries and partial elemental analysis of the complexes

Compounds	Anal: Calcd(Found) %			μ BM
	C	H	N	
$[\text{Fe}(\text{BpypTsc})_2]\text{ClO}_4$ (11)	52.74 (52.75)	4.40 (4.43)	14.45 (14.48)	1.59
$[\text{Fe}(\text{PranThas})_2]\text{FeCl}_4$ (12)	38.54 (38.53)	4.00 (4.04)	14.91 (14.98)	4.44
$[\text{Fe}(\text{BpypTsc})_2]\text{NO}_3$ (13)	55.40 (55.43)	4.65 (4.65)	17.09 (17.11)	2.33
$[\text{Fe}(\text{BpypTsc})_2]\text{FeCl}_4$ (14)	46.80 (46.81)	3.93 (3.93)	12.85 (12.85)	4.38

Magnetic moments have been determined for all the complexes at room temperature in the polycrystalline state. Iron(III) is known to exist in three states with $S = 5/2$ (${}^6\text{A}_1$, $\mu = 5.92$ BM), $3/2$ (${}^4\text{A}_2$, $\mu = 4.00$ BM) and $1/2$ (${}^2\text{T}_2$, $\mu = 2.6$ BM). The magnetic moments of the compounds **11** and **13** are 1.59 and 2.33 BM respectively indicating these compounds are typical low spin compounds. The high values of susceptibility for the compounds **12** and **14** indicate the presence of a high spin centre in the molecule⁷⁰. The complete assignment of the spin states of the complexes were done on the basis of EPR and Mössbauer measurements. The slightly lower values than the expected ones may be due to the effective quenching of orbital angular momentum.

4.2.2. Molecular and crystal structure of compound 12

The compound $\text{Fe}(\text{PranThas})_2\text{FeCl}_4$ (12) was found to crystallize into a triclinic lattice with P-1 space group symmetry. The crystal data and structural refinement parameters are listed in Table 4.2 and selected bond lengths and angles are listed in Table 4.3. Figure 4.1 shows the molecular structure of the compound. The iron(III) ion pair has a distorted octahedral coordination in the complex. The two molecules of monodeprotonated ligand, coordinate to iron via pyridyl nitrogens, azomethine nitrogens and thiolato sulfur atoms to form four five membered chelate rings. The pattern of coordination is similar to that observed in similar type of complexes⁷¹. The crystallographic asymmetric unit contains $[\text{Fe}(\text{PranThas})_2]$ cation and a tetrachloroferrate (FeCl_4) anion. The FeCl_4 anion is having a tetrahedral structure.

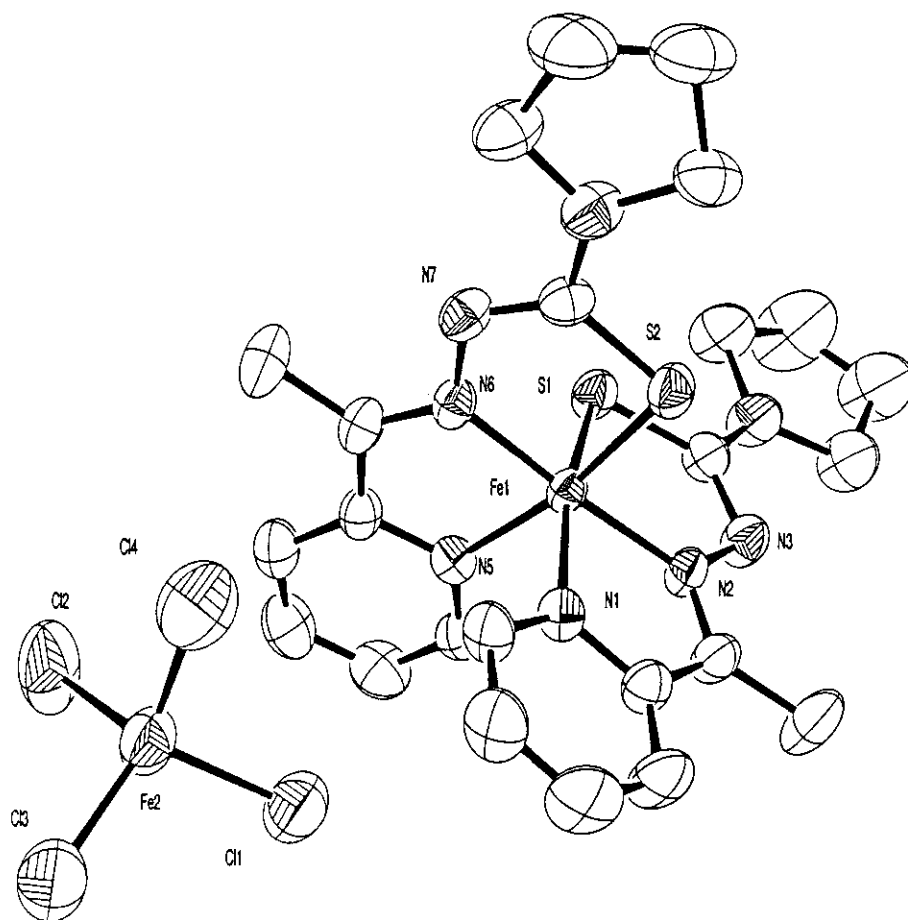


Figure 4.1. ORTEP diagram of the compound $\text{Fe}(\text{PranThas})_2\text{FeCl}_4$ (12) in 50% probability level. All hydrogen atoms are removed for clarity.

Table 4.2. Structural refinement parameters of compound 12

Empirical formula	C ₂₄ H ₃₀ Cl ₄ Fe ₂ N ₈ S ₂
Formula weight	748.18
Temperature	293(2) K
Wavelength	0.71073
Crystal system, space group	Triclinic, P-1
Unit cell dimensions	a = 8.7431(7) Å α = 82.619(2)° b = 13.4881(11) Å β = 87.482(2)° c = 14.4522(12) Å γ = 75.535(2)°
Volume, Z, Calculated density, Mg/m ³	1636.5(2) Å ³ , 2, 1.518
Absorption coefficient	1.370 mm ⁻¹
F(000)	764
Crystal size	0.44 x 0.26 x 0.26 mm
Limiting indices	-8 ≤ h ≤ 10, -15 ≤ k ≤ 16, -17 ≤ l ≤ 15
Reflections collected / unique	8073 / 5634 [R(int) = 0.0252]
Goodness-of-fit on F ²	1.095
Final R indices [I > 2σ(I)]	R1 = 0.0564, wR2 = 0.1175
Largest diff. peak and hole	0.507 and -0.372 e.Å ⁻³

Table 4.3. Selected bond lengths and angles of compound 12

Bond lengths (Å)		Bond angles (°)	
Fe(1)-N(6)	1.918(3)	N(6)-Fe(1)-N(2)	176.48(16)
Fe(1)-N(2)	1.928(3)	N(6)-Fe(1)-N(5)	80.47(15)
Fe(1)-N(5)	1.986(3)	N(2)-Fe(1)-N(5)	103.03(15)
Fe(1)-N(1)	1.986(3)	N(6)-Fe(1)-N(1)	98.98(14)
Fe(1)-S(1)	2.2151(13)	N(6)-Fe(1)-S(1)	95.42(11)
Fe(1)-S(2)	2.2194(13)	N(2)-Fe(1)-S(1)	85.12(11)
Fe(2)-Cl(2)	2.1820(19)	N(5)-Fe(1)-S(1)	89.18(10)
Fe(2)-Cl(3)	2.1831(19)	N(1)-Fe(1)-S(1)	164.56(11)
Fe(2)-Cl(4)	2.187(2)	N(6)-Fe(1)-S(2)	85.52(11)
Fe(2)-Cl(1)	2.1929(17)	N(2)-Fe(1)-S(2)	90.97(11)
S(1)-C(8)	1.741(4)	N(5)-Fe(1)-S(2)	165.57(11)
C-H.....π interactions		H.....Cg	X.....Cg
C(1)-H(1A).....Cg(4) ^a	2.7738	3.1062	102.19
C(13)-H(13A).. Cg(1) ^a	3.0009	3.2959	100.24
C(13)-H(13A)...Cg(3) ^a	2.9469	3.2420	100.10
C(14)-H(14A)...Cg(7) ^b	3.0917	3.9134	148.28
C(21)-H(21B)...Cg(8) ^c	3.0146	3.8528	145.42
H-Bonding interactions		D.....A	H....A
C(4)-H(4A)..... Cl(3)	2.82	3.6626	152
Equivalent position code	Cg(1) = Fe(1), S(1), C(8), N(3), N(2)		
a = x, y, z, b = -1+x, y, z,	Cg(3) = Fe(1), N(1), C(5), C(6), N(2)		
c = 1+x, y, z	Cg(4) = Fe(1), N(5), C(17), C(18), N(6)		
	Cg(7) = N(1), C(1), C(2), C(3), C(4), C(5)		
	Cg(8) = N(5), C(13), C(14), C(15), C(16), C(17)		

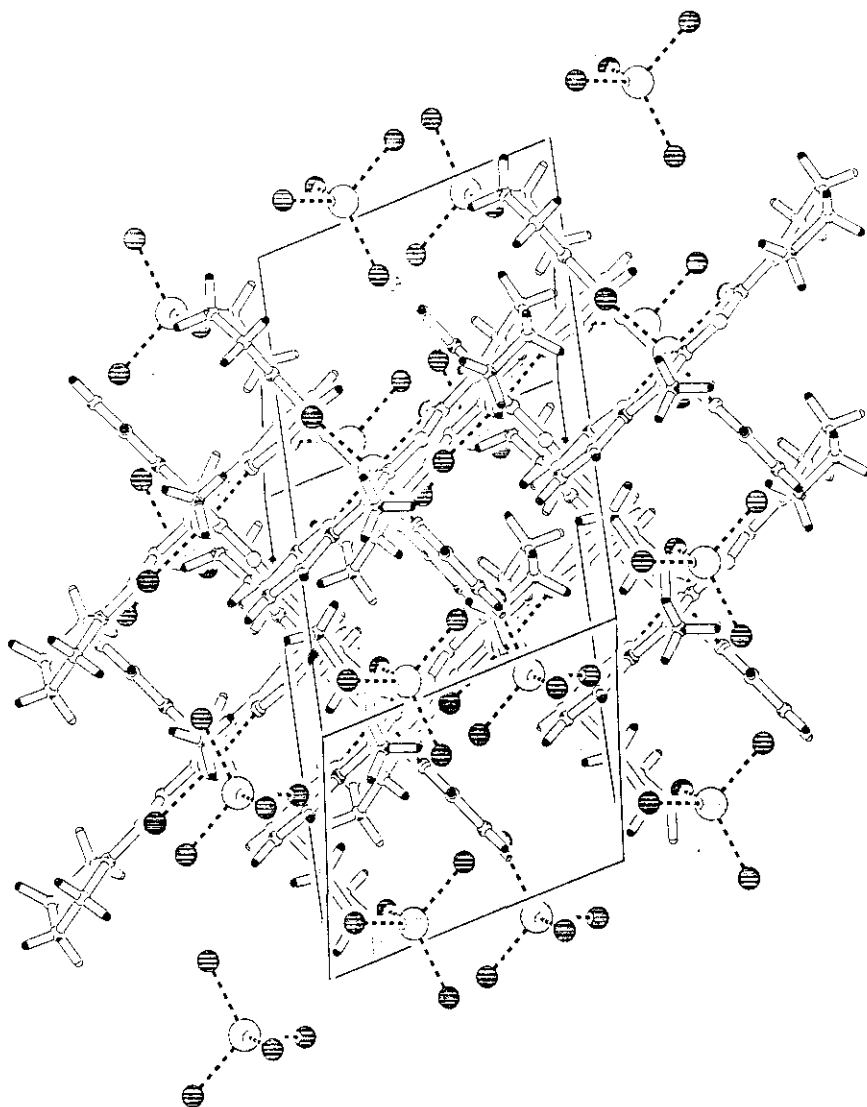
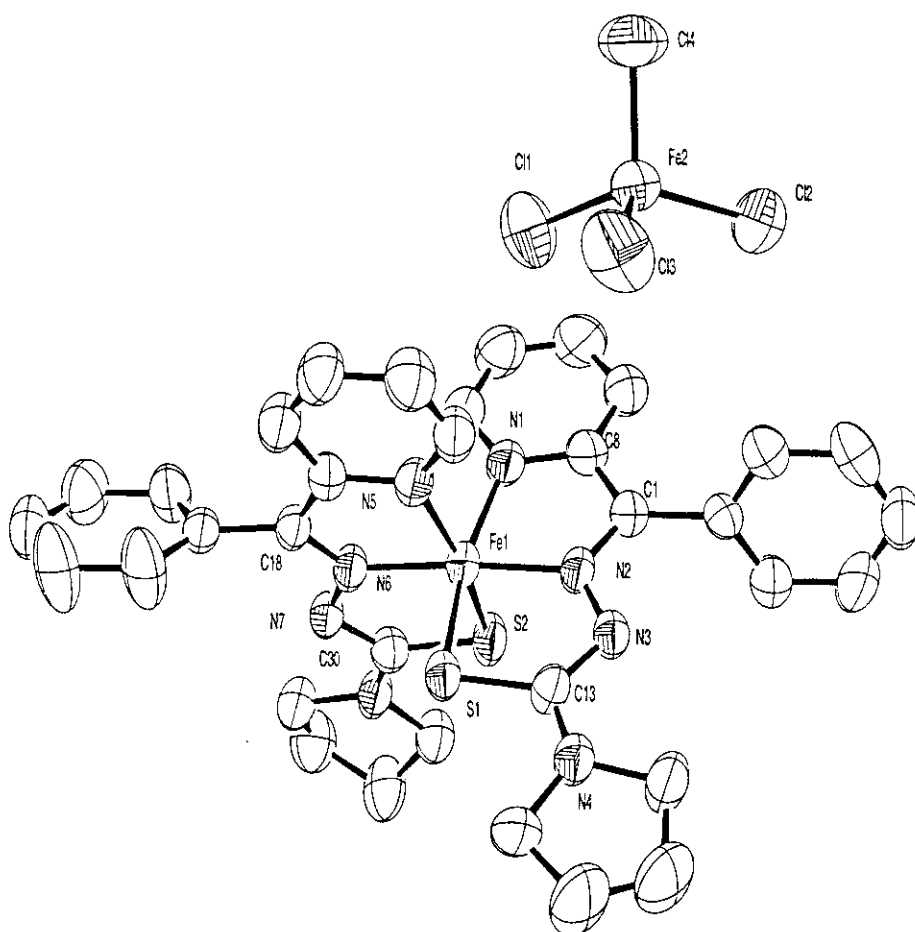


Figure 4.2. Packing of the compound 12, viewed along c axis

There is a slight shortening of the Fe-N(azomethine) bond distance compared to Fe-N(py) distances; this may be attributed to the fact that the azomethine nitrogen is a stronger base compared with the pyridyl nitrogen. The two azomethine nitrogen atoms are trans to each other, while the pyridyl nitrogen atoms and thiolato sulfate atoms are in cis positions. The ligands are orthogonal to the metal ion, with the NNS coordination in a meridional fashion. The chelate rings are almost planar. There exist strong C-H... π interactions between these metal containing chelate rings Cg(3) and Cg(2) with methyl protons and pyridyl ring protons. The tetrachloroferrate anion present in the molecule has a slightly distorted tetrahedral geometry with equal bond lengths ($\sim 2.187 \text{ \AA}$) and angles ($\sim 109.46^\circ$).

4.2.3. Molecular and crystal structure of compound 14

The compound $[\text{Fe}(\text{BpypTsc})_2]\text{FeCl}_4 \cdot 2\text{H}_2\text{O}$ (**14**) crystallizes into a triclinic lattice with P-1 space group symmetry with $[\text{Fe}(\text{BpypTsc})_2]$ cation and a tetrachloroferrate (FeCl_4^-) anion along with two molecules of lattice water. Table 4.4 presents the crystal data and structural refinement parameters and Table 4.5 presents the selected bond lengths and angles. Figure 4.3 shows the molecular structure of the compound along with atom numbering scheme. The iron(II) ion has a distorted octahedral coordination in the complex. The two molecules of monodeprotonated ligand, coordinate to iron via pyridyl nitrogens, azomethine nitrogens and thiolato sulfur atoms to form four five membered chelate rings. The FeCl_4 anion is having a tetrahedral structure.



*Figure 4.3. ORTEP diagram of the compound $\text{Fe}(\text{BpypTsc})_2\text{FeCl}_4 \cdot 2\text{H}_2\text{O}$ (**14**) with ellipsoids drawn at 54% probability level. Lattice water molecules and all hydrogen atoms are omitted for clarity.*

Table 4.4. Crystal data and refinement parameters of compound 14

Empirical formula	$C_{34}H_{38}Cl_4Fe_2N_8O_2S_2$
Formula weight	908.34
Temperature	293(2) K
Wavelength	0.70930 Å
Crystal system, space group	Triclinic, P -1
Unit cell dimensions	$a = 9.6430(7) \text{ \AA}$ $\alpha = 114.565(9)^\circ$ $b = 15.1480(15) \text{ \AA}$ $\beta = 93.789(7)^\circ$ $c = 16.2430(17) \text{ \AA}$ $\gamma = 101.760(7)^\circ$
Volume	$2082.1(3) \text{ \AA}^3$
Z, Calculated density	2, 1.449 Mg/m ³
F(000)	932
Crystal size	0.275 x 0.175 x 0.150 mm
Limiting indices	$0 \leq h \leq 11$, $-17 \leq k \leq 17$, $-19 \leq l \leq 19$
Reflections collected / unique	5912 / 5912 [R(int) = 0.0000]
Goodness-of-fit on F ²	1.134
Largest diff. peak and hole	1.287 and -0.405 e. Å ⁻³

Table 4.5. Selected bond lengths and angles of compound 14

Bond lengths (Å)		Bond angles (°)	
Fe(1)-N(2)	1.916(4)	N(2)-Fe(1)-N(6)	175.4(2)
Fe(1)-N(6)	1.928(5)	N(2)-Fe(1)-N(5)	102.2(2)
Fe(1)-N(5)	1.980(5)	N(6)-Fe(1)-N(5)	81.6(2)
Fe(1)-N(1)	1.984(5)	N(2)-Fe(1)-N(1)	81.1(2)
Fe(1)-S(2)	2.201(19)	N(6)-Fe(1)-N(1)	101.9(2)
Fe(1)-S(1)	2.225(19)	N(5)-Fe(1)-N(1)	86.8(2)
S(1)-C(13)	1.749(6)	N(2)-Fe(1)-S(2)	91.06(15)
N(2)-C(1)	1.309(7)	N(6)-Fe(1)-S(2)	85.55(16)
N(2)-N(3)	1.358(6)	N(5)-Fe(1)-S(2)	165.38(15)
Fe(2)-Cl(4)	2.156(2)	N(1)-Fe(1)-S(2)	89.13(16)
Fe(2)-Cl(3)	2.168(2)	N(2)-Fe(1)-S(1)	85.30(15)
Fe(2)-Cl(2)	2.171(2)	N(6)-Fe(1)-S(1)	92.03(15)
Fe(2)-Cl(1)	2.196(2)	N(5)-Fe(1)-S(1)	90.19(16)
C-H..... π	H.....Cg (Å)	X.....Cg (Å)	X-H.....Cg (°)
C12-H12.....Cg(4) ^a	2.7053	3.1962	113.95
C29-H29.....Cg(3) ^a	2.7790	3.1651	104.77
H-bonding interactions	H.....A (Å)	D.....A (Å)	D-H.....A (°)
O1-H102.....O2 ^b	0.94	2.0425	131
O2-H103.....O1 ^c	1.70	2.3247	128
O1-H104.....O2 ^d	1.65	2.3247	122
C14-H14A.....S2 ^e	2.78	3.6489	145
a = x, y, z; b = 2-x, 1-y, -z;		Cg(3) = Fe1, N1, C8, C1, N2	
c = 1+x, 1+y, z; d = 1-x, 1-y, -z		Cg(4) = Fe1, N5, C25, C18, N6	

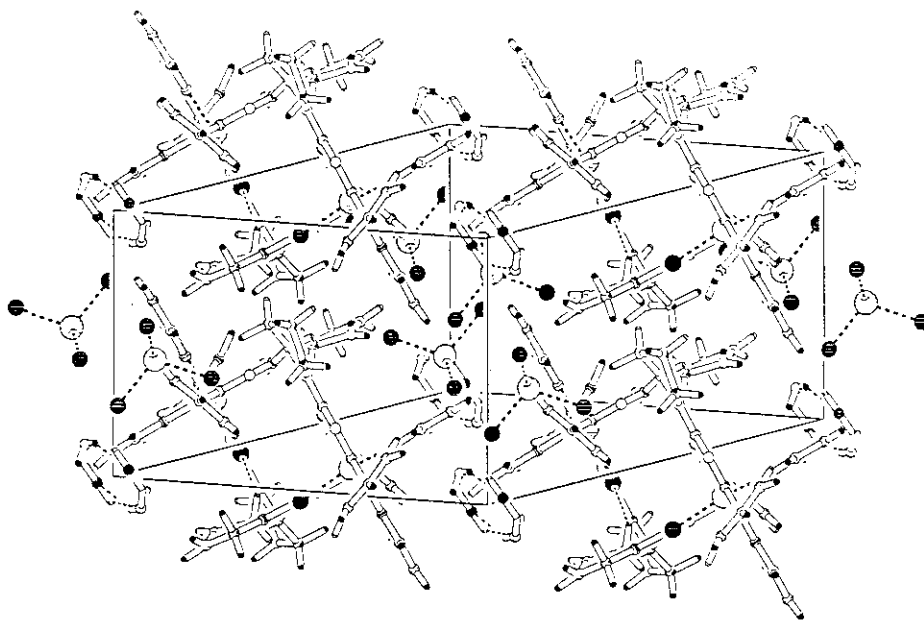


Figure 4.4. Packing diagram of the compound 14, view along a axis

Coordination lengthens the ligands C13-S1 and C1-N2 bonds to 1.749 and 1.309 Å respectively is an explicit indication of the deprotonation followed by the coordination of the ligand moiety. There is a slight shortening of the Fe-N(azomethine) bond distance compared to Fe-N(py) distances; this may be attributed to the fact that the azomethine nitrogen is a stronger base compared with the pyridyl nitrogen. The two azomethine nitrogen atoms are *trans* to each other, while the pyridyl nitrogen atoms and thiolato sulfur atoms are in *cis* positions. The ligands are orthogonal to the metal ion, with the NNS coordination in a meridional fashion. The chelate rings are almost planar. There exist strong C-H... π interactions between these metal containing chelate rings Cg(3) and Cg(4) with pyridyl ring protons. Figure 4.4. Shows the packing of the molecule in a unit cell. The tetrachloroferrate anion present in the molecule is slightly distorted tetrahedral with equal bond lengths (~ 2.187 Å) and angles ($\sim 109.46^\circ$). The compound packs in an offset fashion with alternate molecular sheets of the cation and anion forming molecular channels with an interesting nimbus of three water molecules bound together by strong H-bonding interactions around each corners of the triclinic lattice.

4.2.4. Infrared spectra

In Table 4.6 we have compiled the assignments of IR bands most useful for the establishment of the mode of coordination of thiosemicarbazone ligands in their iron(III) coordination. Figure 4.5 shows the IR spectrum of the compound 14. coordination of the azomethine nitrogen is indicated by the lowering of the band by 30-50 cm^{-1} . The band is not a pure vibrational band of C=N stretching, but it is a combination band of C=C vibrations of the pyridyl ring also⁷². Two bands ≈ 1250 and 840 cm^{-1} were assigned to the C-S stretching mode of vibrations. This band also finds in a lower energy compared to the ligand vibrations indicating the coordination of thiolato sulfur. Another band which is considered to be sensitive to coordination is $\nu(\text{N}=\text{N})$ which is raised in energy due to coordination because of the increased double bond character. The newly formed C=N bond due to the deprotonation of the ligands is also observed $\approx 1630 \text{ cm}^{-1}$. The spectra of the complexes showed in-plane and out-of-plane bending mode of vibrations $\rho \approx 440$ and 650 cm^{-1} .

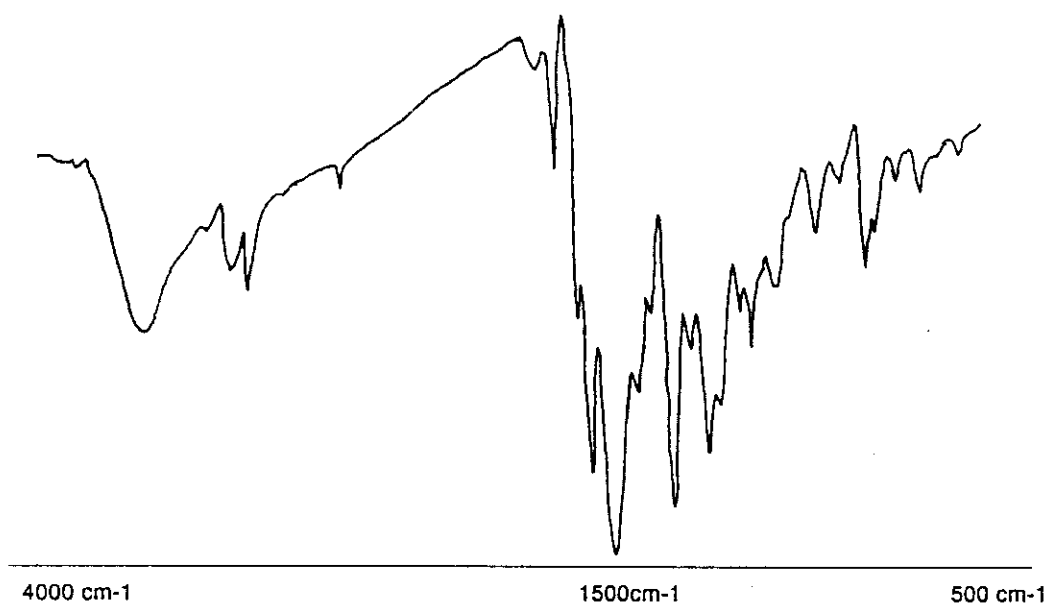


Figure 4.5. IR spectrum of the compound 14

Table 4.5. Ligand vibrations of the complexes

Compound	$\nu(\text{C}=\text{N})$	$\nu(\text{N}=\text{C})$	$\nu(\text{N}=\text{N})$	$\nu/\delta(\text{C}=\text{S})$
$\text{Fe}(\text{BpypTsc})_2\text{ClO}_4$ (11)	1594 s	1627 s	1163 s	1240 m, 843 w
$\text{Fe}(\text{PranThas})_2\text{FeCl}_4$ (12)	1597 s	1648 s	1193 s	1239 m, 839 w
$\text{Fe}(\text{BpypTsc})_2\text{NO}_3$ (13)	1594 s	1628 s	1108 s	1202 s, 839 w
$\text{Fe}(\text{BpypTsc})_2\text{FeCl}_4$ (14)	1595 m	1645 m	1111 s	1204 s, 844 w

All values are in cm^{-1}

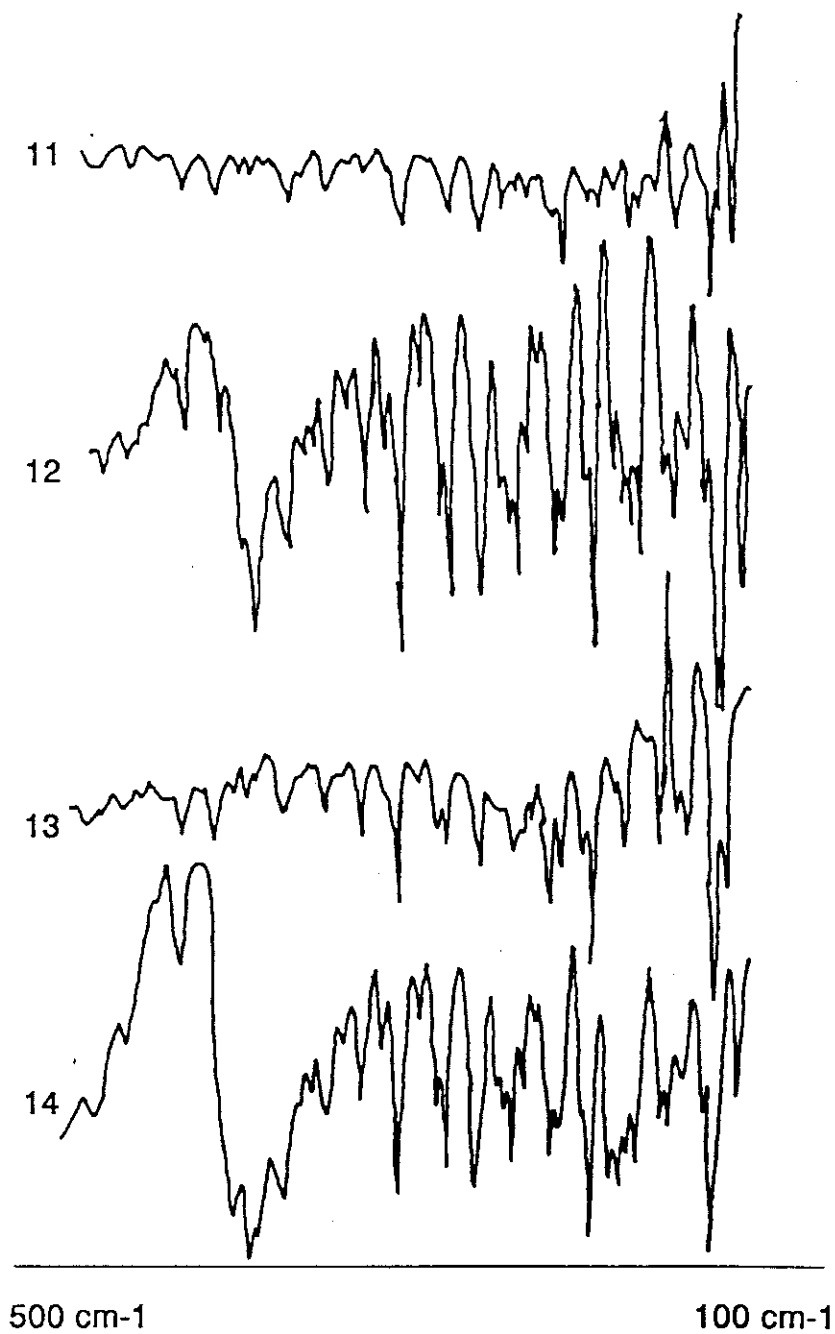


Figure 4.6. Far-IR spectra of the complexes

Table 4.7. M-L and anionic vibrational data of the complexes

Compound	$\nu(\text{Fe-N}_{\text{azo}})$	$\nu(\text{Fe-N}_{\text{pv}})$	$\nu(\text{Fe-S})$	$\nu(\text{X}^{\#})$
$\text{Fe}(\text{BpypTsc})_2\text{ClO}_4$ (11)	515 w	354 w	452 w	470 w, 1105s, 619w
$\text{Fe}(\text{PranThas})_2\text{FeCl}_4$ (12)	526 w	353 s	419 m	376 s, 325s, 123 s, 100 s
$\text{Fe}(\text{BpypTsc})_2\text{NO}_3$ (13)	585 w	364 w	450 w	698w, 839w, 1379 s, 1289s
$\text{Fe}(\text{BpypTsc})_2\text{FeCl}_4$ (14)	528 w	352 s	419 s	374 s, 320 s, 134 w, 110 s

All values are in cm^{-1} , # = ClO_4 , FeCl_4 , NO_3

Table 4.7 shows the polyatomic anion vibrations along with the M-L vibrations observed in the far-IR and IR regions. Figure 4.6 shows the far-IR spectra of the complexes. The spectra of compound **11** had broad split bands assignable to $\nu_3(\text{ClO}_4) \approx 1105 \text{ cm}^{-1}$, it is unlikely that the perchlorate ion is bound directly to iron(III) centre since there is no indication of splitting⁷³ of $\nu_4(\text{ClO}_4) \approx 619 \text{ cm}^{-1}$. This is also confirmed by the absence of $\nu_1(\text{ClO}_4) \approx 920 \text{ cm}^{-1}$. Besides these $\nu_2(\text{ClO}_4)$ is also observed $\approx 470 \text{ cm}^{-1}$. All these bands are split may be due to the strong H-bonding interactions in the molecule. A similar splitting occurs in the $\nu_3(\text{FeCl}_4)^{74} \approx 374 \text{ cm}^{-1}$ band in the spectra of the compounds **12** and **14**. This splitting may be due to the steric factors which reduce the symmetry from tetrahedral. Similarly the band corresponding to $\nu_4 \approx 134 \text{ cm}^{-1}$ is also found to be split due to site effects. The other two stretching modes ν_1 and ν_2 are found at approximately 330 and 114 cm^{-1} respectively in the spectrum of the compounds **12** and **14**. The spectrum of the compound **13** has two strong bands at 1389 and 1289 cm^{-1} corresponding to ν_1 and ν_4 of the nitrate group. The absence of a combination band $\approx 1740 \text{ cm}^{-1}$ assignable to $\nu_1 + \nu_4$ indicates the ionic nature of the group⁷⁵. Bands at ≈ 515 and 355 cm^{-1} were assigned to the Fe-N vibrations of the azomethine and pyridyl nitrogen coordination respectively. Fe-S bond stretching vibrations were found approximately at 420 cm^{-1} in the spectra of the complexes.

4.2.5. Electronic spectra

Table 4.8 shows the electronic spectral values in solid state DRS mode. Figure 4.7 shows the electronic spectrum of the compound **14**. The UV region is dominated by two intense intra ligand bands at 29850 cm^{-1} and 25300 cm^{-1} assigned to $\pi \rightarrow \pi^*$ and $n \rightarrow \pi^*$ transitions.

Table 4.8. Electronic spectral data of the complexes

Compound	$\pi \rightarrow \pi^*$	$n \rightarrow \pi^*$	LMCT	$d \rightarrow d$
Fe(BpypTsc) ₂ ClO ₄ (11)	365136	30487	26737, 15503	10362
Fe(PranThas) ₂ FeCl ₄ (12)	37037	29850	24213, 14992	10256
Fe(BpypTsc) ₂ NO ₃ (13)	36630	29585	24509, 15822	10373
Fe(BpypTsc) ₂ FeCl ₄ (14)	37037	30211	24390, 211416, 15974	10438

All values are in cm^{-1} , # = ClO₄, FeCl₄, NO₃

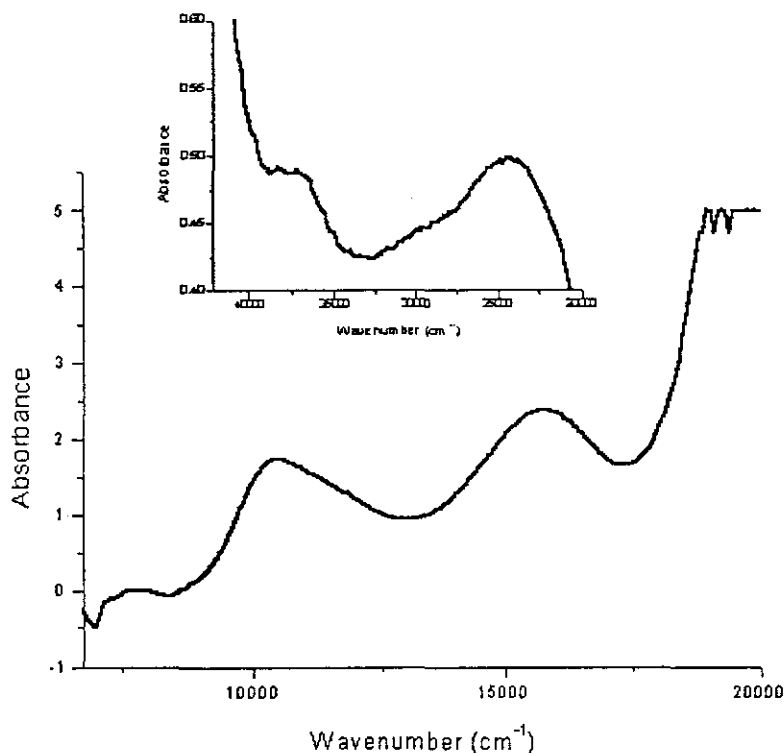


Figure 4.7. UV-Vis-NIR spectrum of the compound 14 (insight: UV region)

Usually $n \rightarrow \pi^*$ transitions involving N and S occur at a lower energy than $\pi \rightarrow \pi^*$. Bands which are between $36000\text{--}30000\text{ cm}^{-1}$ in the spectrum of the complexes having pyridyl ligands have assigned to $\pi \rightarrow \pi^*$ and $n \rightarrow \pi^*$ transitions and the bands between 15000 and 27000 cm^{-1} are assigned to $d \rightarrow \pi^*$ transitions. These transitions involve $S \rightarrow \text{Fe}$ and other ligand to metal charge transfer transitions. The bands below 15000 cm^{-1} is due to $d \rightarrow d$ transitions of the d^5 spin paired systems. A comparison of the spectra of **13** and **14** shows that there are no significant difference indicating the electronic spectra of the cations dominate the spectral properties⁷⁶. Therefore the spin forbidden transitions between $13700\text{--}16600\text{ cm}^{-1}$ of $[\text{FeCl}_4]^-$ are very weak to be observed. Similar observation is found in the spectra of the compounds **11** and **12** also. Unfortunately the electronic spectra of low-spin iron(III) compounds have not been adequately studied.

4.2.6. Electron paramagnetic resonance spectra

The EPR spectral parameters obtained for the iron(III) complexes are presented in Table 4.9. The Figures 4.8-4.11 shows the EPR spectra of the complexes. The EPR spectrum of d^5 iron(III) is expressed by the spin Hamiltonian⁷⁷,

$$H = D[S_z^2 - \frac{1}{3}S(S+1)] + E(S_x^2 - S_y^2) + g\beta HS \text{ with } S = \frac{1}{2} \text{ and } g = 2.00.$$

The polycrystalline EPR spectra of compounds **12** and **14** consist of a single broad line with a Δpk (peak to peak) value 190 and 270 G respectively. This is indicative of the presence of a high spin species in the system. The observed g value ≈ 2.0 and an isotropic spectrum indicate the spin-spin relaxation via dipole-dipole interactions. However the solid state spectrum of the other two compounds **11** and **13** are rhombic in nature with three g values. This type of feature is common for low spin octahedral complexes⁷⁸. The observed anisotropic character is due to rhombic distortion common for spin paired iron(III) complexes. The small variation of the g values from the free electron value is due to the presence of unpaired electron in the d_{xy} orbital.

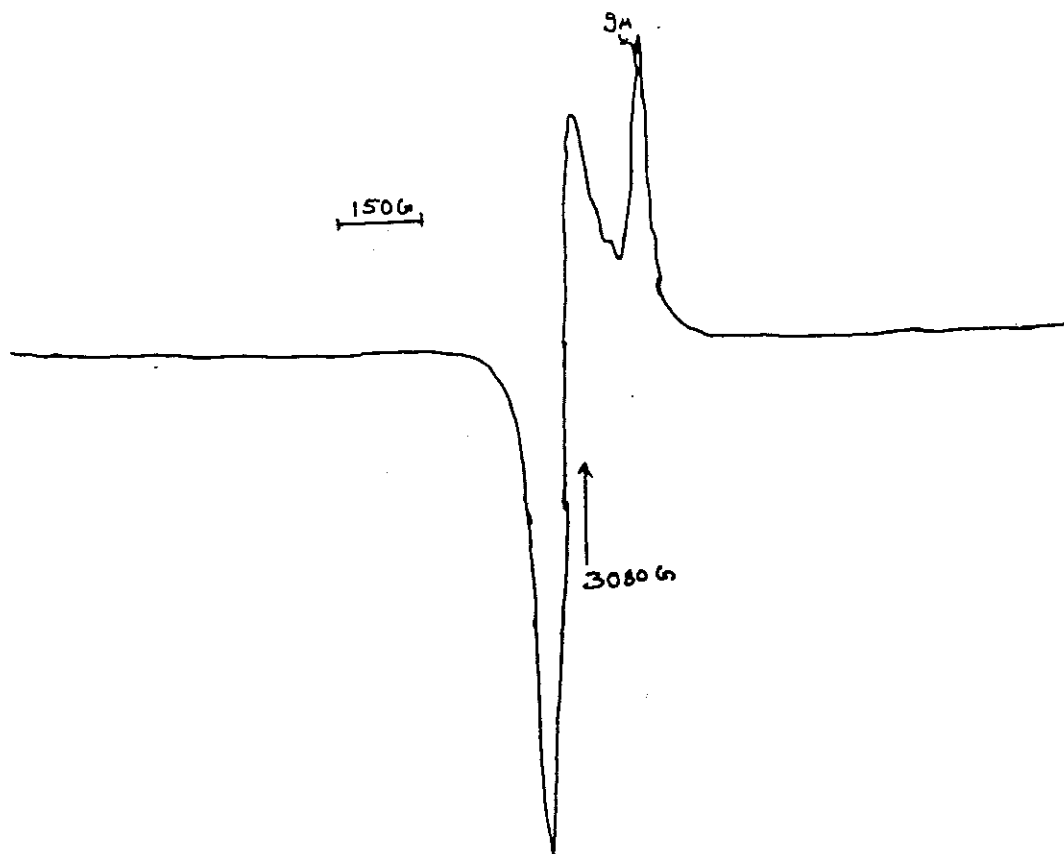


Figure 4.8. EPR spectrum of the compound **11** in polycrystalline state (298 K)

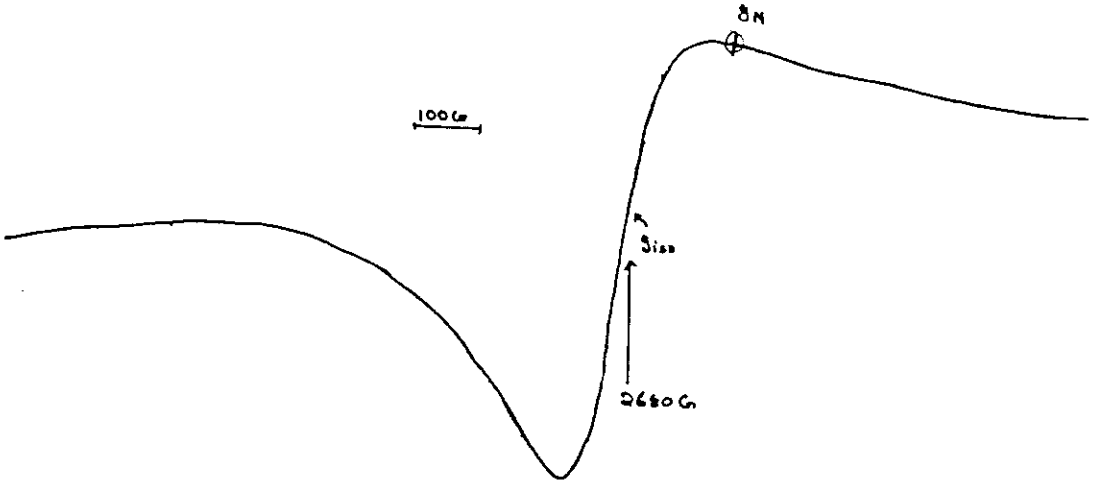


Figure 4.9. EPR spectrum of the compound 14 in polycrystalline state (298 K)

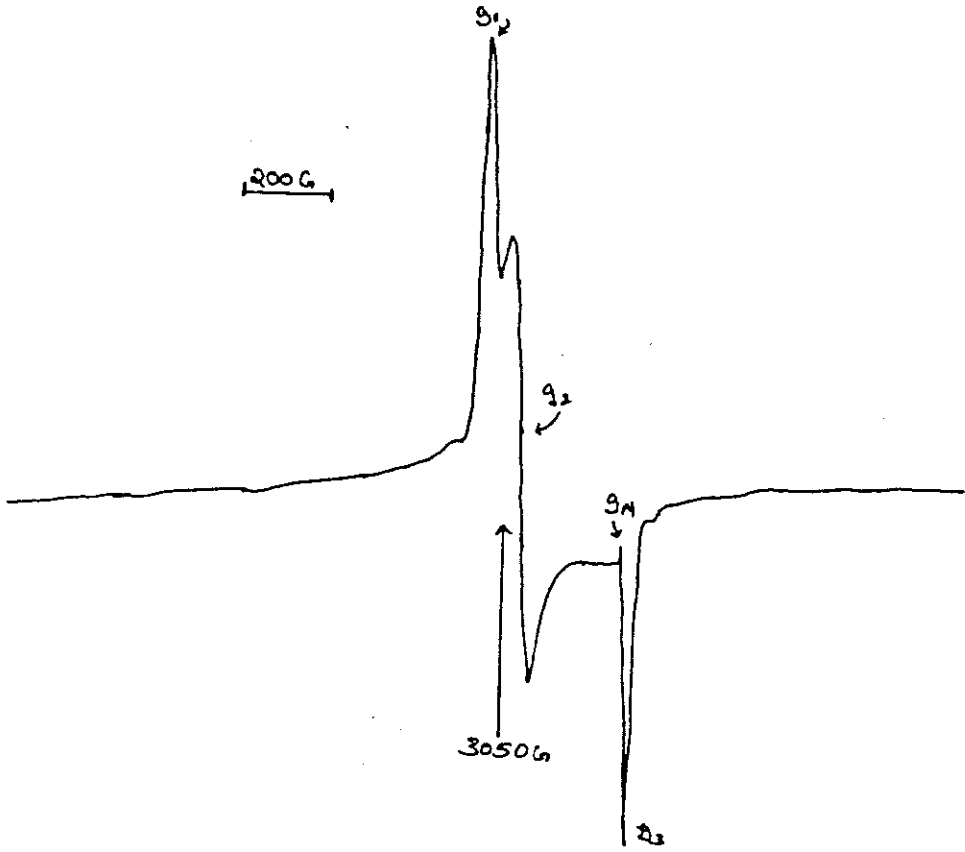


Figure 4.10. EPR spectrum of the compound 13 in DMF (77 K)

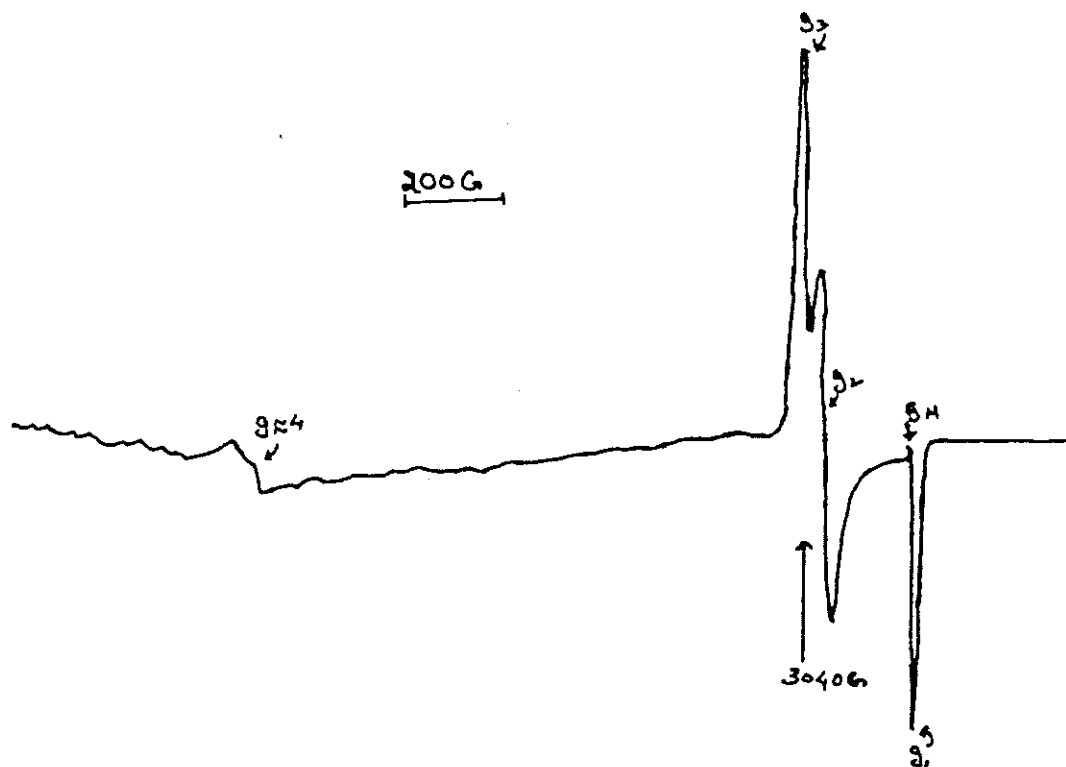


Figure 4.11. EPR spectrum of the compound 14 in DMF (77 K)

The isotropic spectra of the complexes 12 and 14 in polycrystalline state changes to rhombic spectra in frozen solution, since the g_{av} values obtained in both temperatures are similar, it is likely that lattice effects in the solid state may account for this change from isotropic to rhombic and it is common for spin paired iron(III) complexes. The small deviation of the anisotropic g values from 2.0 suggests that the unpaired electrons is in the d_{xy} orbital with a ground state configuration $d_{xz}^2 d_{yz}^2 d_{xy}^1$. It was interesting to note a sharp but small signal corresponding to $g=4.1$ indicating the presence of high spin species which was identified as $[\text{FeCl}_4]^-$ anion⁷⁹. The frozen solution spectra of the compounds 11 and 13 also show anisotropic rhombic spectra with three g values corresponding to low spin octahedral iron(III) system.

Table 4.9. EPR spectral data of the complexes

Compound	State	g_1	G_2	g_3/g_{av}	
Fe(BpypTsc) ₂ ClO ₄ (11)	Solid (RT)	1.995	2.038	2.120	$g_{av} = 2.051$
	CHCl ₃ , 77 K	1.990	2.134	2.178	$g_{av} = 2.101$
Fe(PranThas) ₂ FeCl ₄ (12)	Solid (RT)	-	-	2.023	$\Delta pk = 190 \text{ G}$
	CHCl ₃ , 77 K	1.984	2.082	2.101, 4.159	$g_{av} = 2.056$
Fe(BpypTsc) ₂ NO ₃ (13)	Solid (RT)	2.017	2.075	2.144	$g_{av} = 2.077$
	CHCl ₃ , 77 K	1.996	2.128	2.170	$g_{av} = 2.098$
Fe(BpypTsc) ₂ FeCl ₄ (14)	Solid (RT)	-	-	2.157	$\Delta pk = 270 \text{ G}$
	CHCl ₃ , 77 K	1.995	2.135	2.187, 4.186	$g_{av} = 2.105$

4.2.7. Mössbauer spectra

Mössbauer spectra of the complexes were recorded at 298 and 20 K in order to understand and confirm the spin behavior of the systems. The Mössbauer parameters calculated from the spectra are presented in Table 4.10, and Figures 4.12-15 shows the spectra of the complexes. All values were compared with α -iron as a standard. The positive δ^{is} values shows that the excited nucleus is not necessarily larger than the ground state.

Table 4.10. Mössbauer spectral data of the complexes

Compound	Temp	Spin	δ^{is} mm s ⁻¹	ΔE_q mm s ⁻¹
Fe(BpypTsc) ₂ ClO ₄ (11)	298 K	1/2	-0.17 (² T _{2g})	2.231 (² T _{2g})
Fe(PranThas) ₂ FeCl ₄ (12)	298 K	1/2	-0.13 (² T _{2g})	2.210 (² T _{2g})
	298 K	5/2	0.12 (⁶ A ₁)	0.675 (⁶ A ₁)
Fe(BpypTsc) ₂ NO ₃ (13)	298 K	1/2	-0.11 (² T _{2g})	2.351 (² T _{2g})
	20 K	1/2	-0.12 (² T _{2g})	2.352 (² T _{2g})
Fe(BpypTsc) ₂ FeCl ₄ (14)	298 K	1/2	-0.10 (² T _{2g})	2.110 (² T _{2g})
	20 K	1/2	-0.11 (² T _{2g})	2.241 (² T _{2g})
	298 K	5/2	0.17 (⁶ A ₁)	0.925 (⁶ A ₁)
	20 K	5/2	0.12 (² T _{2g})	0.625 (² T _{2g})

All values are relative to α -iron

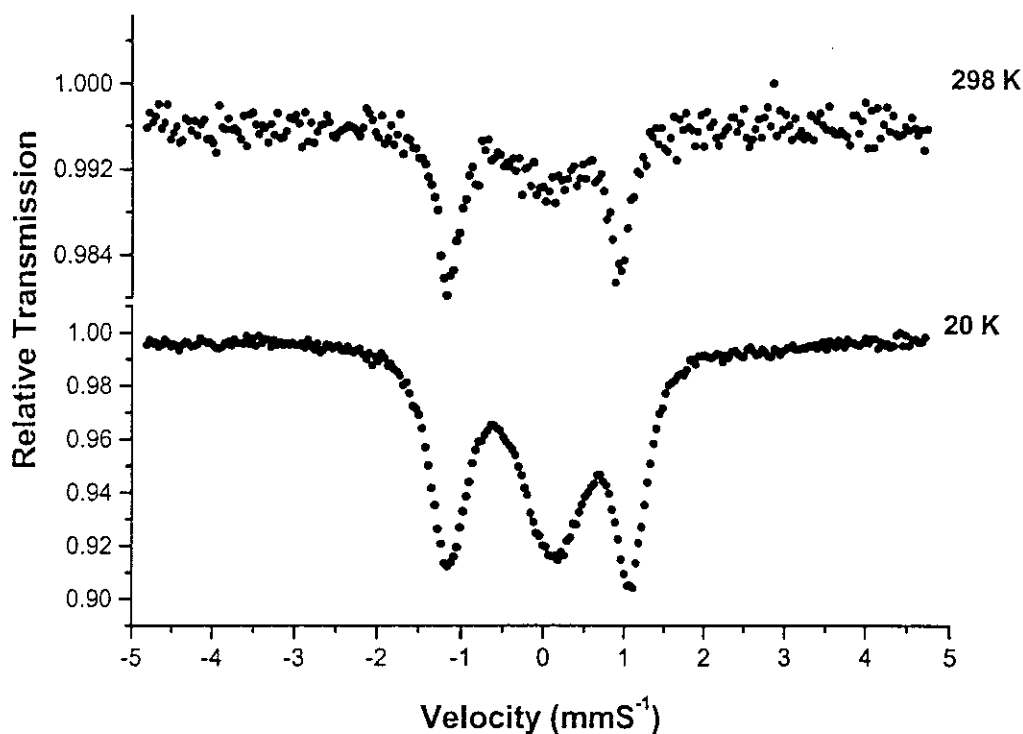


Figure 4.12. Mössbauer spectra of the compound 14 in different temperatures

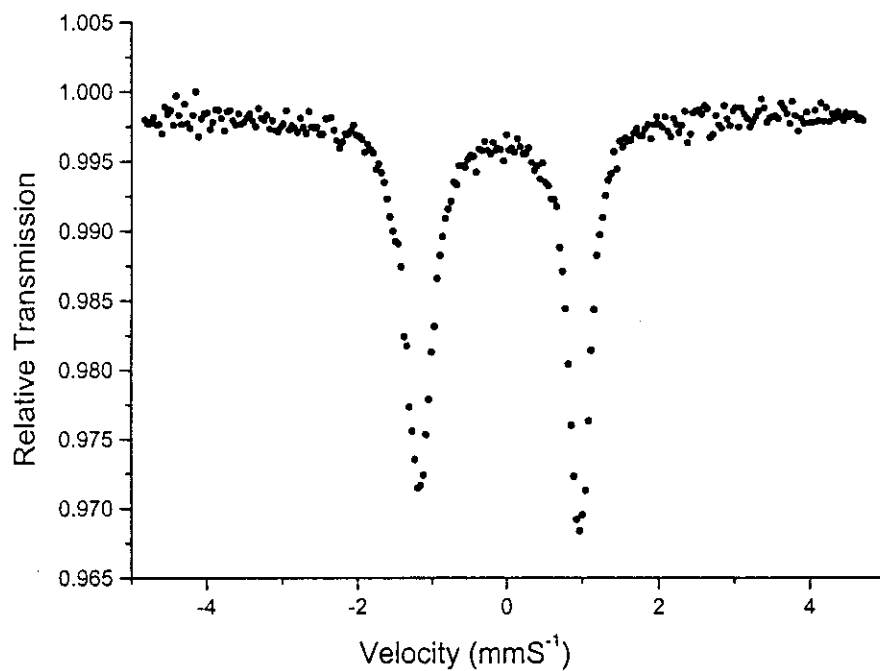


Figure 4.13. Mössbauer spectrum of the compound 11 (298 K)

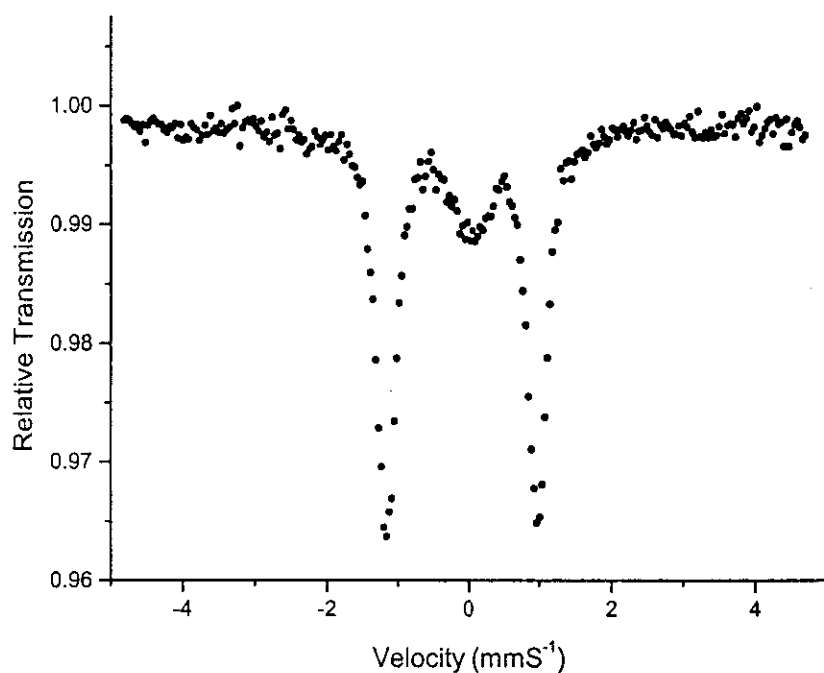


Figure 4.14. Mössbauer spectrum of the compound 12 (298 K)

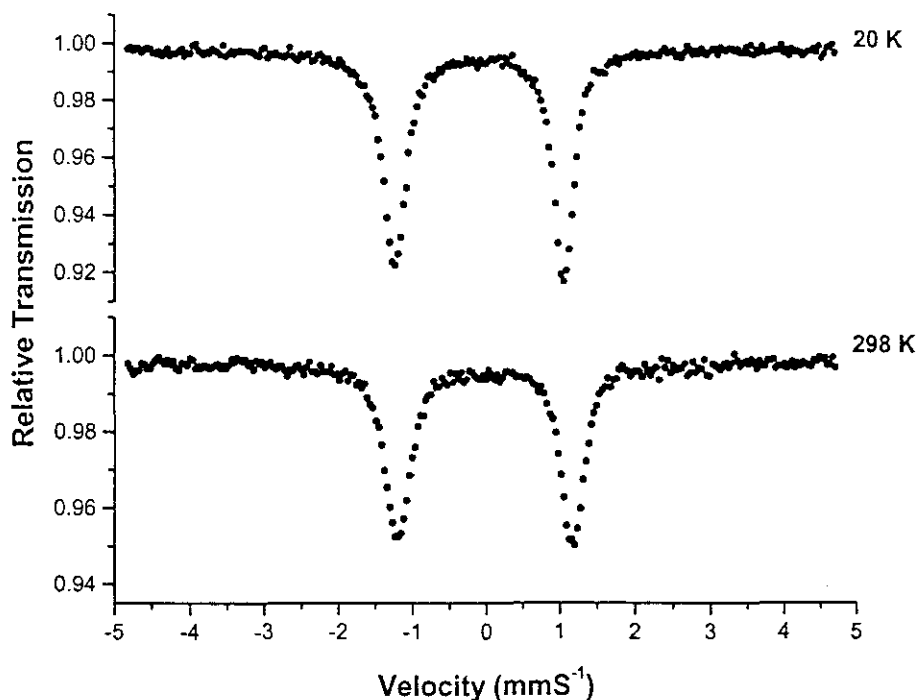


Figure 4.15. Mössbauer spectra of the compound 13 in different temperatures

The high intensity doublet in the spectra of all the complexes with an isomer shift approximately at -0.12 mmS^{-1} , characterized by a quadrupolar splitting $\Delta E_q \approx 2.1 \text{ mmS}^{-1}$, is ascribed to the low spin ${}^2T_{2g}$ ground state of low spin iron(III)⁸⁰. These values change a little when the temperature is lowered. The signals in the low temperature spectra were more intense but the 1:1 ratio between the quadrupole split spectra is not strictly observed in all cases. This is due to the anisotropic absorption known as Goldansky-Karyagin effect. The spectra of compounds 12 and 14 were unusually interesting with the presence of another broad signal corresponding to $\delta^{is} \approx 0.12 \text{ mm S}^{-1}$ $\Delta E_q \approx 0.67 \text{ mm S}^{-1}$ ascribed to tetrahedral high spin iron(III) FeCl_4 species⁸¹. The observation of the broad line with unresolved quadrupolar splitting is assumed to be due to much slower spin relaxation due to the orbital electrons of iron. The high spin signal is temperature dependent and in the 20 K spectrum of the compound 14 the signal was found to be shifted compared to 298 K spectrum, and was found to be more intensified. There are no changes between the 298 K and 20 K spectra showing a stable spin system without any magnetic interactions in the molecules⁸².

4.3. Antimicrobial studies

Details of the antimicrobial studies are described in detail in chapter 2. All compounds were screened against the microbial organisms and the results are tabulated in Table 4.11, and Figure 4.16 shows the zone of inhibition of the complexes for different pathogenic organisms. The compounds are less active compared to copper complexes and the parent thiosemicarbazone. And among them the perchlorate complex showed a moderate increase in the activity against *Vibrio cholerae* this may be due to the additional contribution from the perchlorate ion. The probable lowering of activity may be due to the completion of the coordination octahedra around the metal centre which makes the active centers of the compounds less exposed to the microbial organism for the necessary inhibitory activity.

Table 4.11. Microbial studies of the compounds

Compound	1 [#]	2 [#]	3 [#]	4 [#]
Fe(BpypTsc) ₂ ClO ₄ (11)	+ 8 mm	+ 8 mm	+ 8 mm	+ 9 mm
Fe(BpypTsc) ₂ NO ₃ (13)	+ 8 mm	+ 8 mm	+ 8 mm	+ 8 mm
Fe(BpypTsc) ₂ FeCl ₄ (14)	-	-	+ 8 mm	+ 8 mm

1) *Staphylococcus aureus*, 2) *Bacillus* sp (Gram positive);

3) *Salmonella paratyphi*, 4) *Vibrio cholerae* O1 (Gram negative)

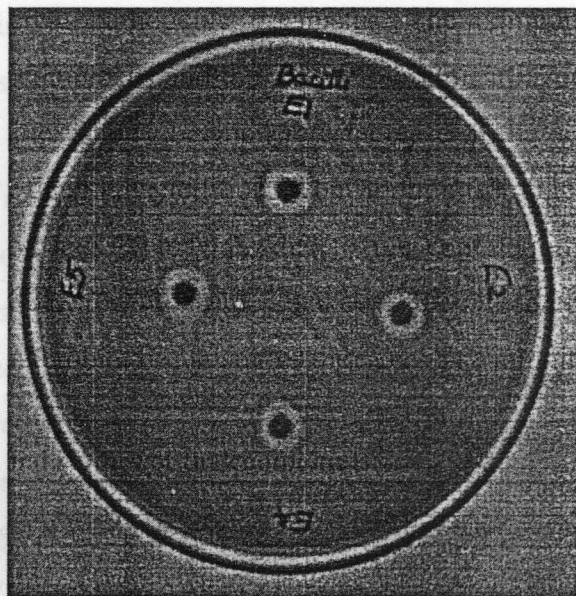


Figure 4.16. Microbial inhibition zones of the compounds 11, 12 and 14 against *Vibrio cholerae* O1

Chapter 5

Synthesis and studies of manganese(II) complexes

Manganese exhibits a wide variety of oxidation states from -3 to +7 and occurs widely in biological systems. The most well known of the manganese enzyme has a tetranuclear manganese(IV) system which is active in oxygen evolution step in photo system II. Among different oxidation states the more readily favored system is Mn(II). But this rarely occur in living systems. Excess levels of manganese leads to diseases like manganism similar to Parkinson's syndrome. Due to the absence of ligand field stabilization in high spin d^5 systems, like manganese has gained much interest in their spectroscopic properties. This chapter deals with the syntheses and spectral studies of two manganese(II) complexes of HBpypTsc and HDpkTsc.

5.1. Experimental

5.1.1. General

Manganese acetate (Merck) was used as received. The ligands HBpypTsc and HDpkTsc were synthesized as reported in Chapter 2. All solvents were distilled before use.

5.1.2. Synthesis of compound 15

A methanolic solution of manganese acetate (1 mmol) was added to a solution of HBpypTsc (2 mmol) in chloroform. The reaction mixture was refluxed for 20 minutes and cooled. Deep brown shining microcrystals of compound 15, was filtered, washed thoroughly with ether and dried over P_4O_{10} in vacuo. X-Ray quality single crystals were grown from a solution of chloroform in 6 days. Anal Found(Calcd) %: C 60.60 (60.61), H 5.05 (5.09), 16.64 (16.63).

5.1.3. Synthesis of compound 16

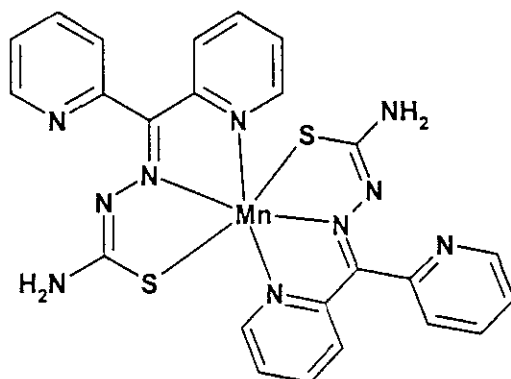
A methanolic solution of manganese acetate (1 mmol) was added to a solution of HDpkTsc (2 mmol) in chloroform. The reaction mixture was refluxed for 20 minutes and cooled. Deep brown shining microcrystals of compound 16, was

filtered, washed thoroughly with ether and dried over P_4O_{10} in vacuo. Anal % Found(Calcd): C 50.76 (50.79), H 3.56 (3.55), N 24.65 (24.68).

5.2. Results and discussions

5.2.1. Syntheses

Both compounds were readily formed from the reaction medium with the general stoichiometry $[MnL_2]$. Both compounds were nonconductors in DMF. Compound 15 was well soluble in polar organic solvents, while compound 16 was soluble only in DMF and DMSO. Magnetic susceptibility measurement in room temperature gave the values 6.01 and 5.91 respectively for compounds 15 and 16, which is attributed to the spin only values of d^5 high spin system with 6S ground state⁸³.



Formula of Mn(DpkTsc)₂ (16)

5.2.2. Electronic spectra

The electronic spectra were recorded in polycrystalline state in the diffused reflectance mode. The spectral data is presented in Table 5.1. The d-d transitions in the manganese(II) systems are doubly forbidden hence they don't register any characteristic bands in the visible region. However two broad bands ~ 25640 and 25000 cm^{-1} are typical charge transfer bands as expected for an octahedral Mn(II) complex⁸⁴. The Tanabe-Sugano diagram corresponding to such a system shows that the only high spin state Russell-Sanders term is 6S which in an octahedral geometry changes its notation to $^6A_{1g}$. Since there are no excited states with spin multiplicity with six, all electronic transitions are not only Laporte forbidden but are spin forbidden also⁸⁵. Consequently all electronic transitions have an extremely small molar extinction coefficients and it is very difficult to locate the bands.

The following transitions were assigned in terms of Racah parameters to the weak shoulders seen at $\approx 18100 \text{ cm}^{-1}$, ${}^6A_{1g} \rightarrow {}^4T_{1g}$ ($\epsilon = 0.01332 \text{ Lmol}^{-1}\text{cm}^{-1}$ [10B+5C]); 22400 cm^{-1} , ${}^6A_{1g} \rightarrow {}^4T_{2g}$ ($\epsilon = 0.009260 \text{ Lmol}^{-1}\text{cm}^{-1}$ [10B+5C]); 24600 cm^{-1} , ${}^6A_{1g} \rightarrow {}^4E_g$ ($\epsilon = 0.0323 \text{ Lmol}^{-1}\text{cm}^{-1}$ [17B+5C]); 25500 cm^{-1} , ${}^6A_{1g} \rightarrow {}^4A_{1g}$ ($\epsilon = 0.01425 \text{ Lmol}^{-1}\text{cm}^{-1}$ [7B+5C]). The energies of the last two transitions are independent of Dq, but dependent only on the values of Racah parameters B and C and hence the values were calculated from the Tanabe-Sugano diagram for d^5 systems⁸⁶. The values are characteristic of a tetragonally distorted octahedral environment. In the visible region the complexes show weak absorptions attributed to the forbidden nature of the spin doublets⁸⁷.

Table 5.1 Electronic and IR spectral data of the complexes

Compound	$n \rightarrow \pi^*$	${}^6A_{1g} \rightarrow {}^4T_{1g}$	${}^6A_{1g} \rightarrow {}^4T_{2g}$	${}^6A_{1g} \rightarrow {}^4E_g$	${}^6A_{1g} \rightarrow {}^4A_{1g}$	
Mn(BpypTsc) ₂ (15)	31545	18083	22471	25012	25316	
Mn(DpkTsc) ₂ (16)	31746	18110	22476	2522	25390	
	$\pi \rightarrow \pi^*$	B (cm ⁻¹)	B (B/B0)	Dq (cm ⁻¹)	C (cm ⁻¹)	
Mn(BpypTsc) ₂ (15)	36101	694	0.81	8584	2232	
Mn(DpkTsc) ₂ (16)	35842	688	0.80	8448	2256	
	$\nu(\text{C=N})$	$\nu(\text{N=C})$	$\nu/\delta(\text{C=S})$	$\nu(\text{Mn-N}_{\text{py}})$	$\nu(\text{Mn-N}_{\text{aza}})$	$\nu(\text{Mn-S})$
Mn(BpypTsc) ₂ (15)	1611 s	1476 s	1321 s, 785	318 w	521 m	416 w
Mn(DpkTsc) ₂ (16)	1586 s	1417 s	1267s, 788	314 w	522 m	418 w

All values are reported in cm⁻¹

5.2.3. IR spectra

The significant IR bands and their tentative assignments are also presented in Table 5.1. Figure 5.1 shows the IR spectrum of the compound 15. As with NNS donors the coordination is expected *via* thiolate sulfur, pyridyl nitrogen and azomethine nitrogen. On coordination the azomethine nitrogen $\nu(\text{C=N})$ was found to be lowed by 25 cm^{-1} at $\approx 1600 \text{ cm}^{-1}$, the appearance of a new band $\approx 1450 \text{ cm}^{-1}$ due to the newly formed $\nu(\text{N=C})$ supports the above observation. $\nu(\text{N=N})$ also appears at a higher frequency around 1116 cm^{-1} in the spectrum of the complexes. The mode of coordination *via* sulfur atom is expected through deprotonated thiolate sulfur indicated by a band $\approx 1320 \text{ cm}^{-1}$. Besides these the lower wavenumber regions show bands around 520, 416 and 361 cm^{-1} , assignable to Mn-N_{py}, Mn-N_{azomethine} and Mn-S stretching respectively⁸⁸. In-plane and out-of-plane bending vibrations of thiosemicarbazone moiety were observed near 410 and 640 cm^{-1} .

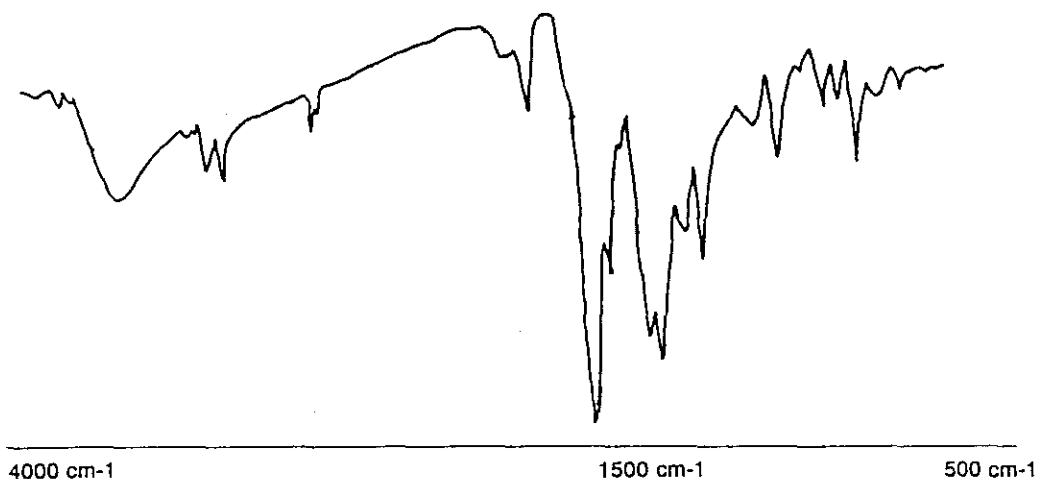


Figure 5.1. IR spectrum of the compound $Mn(BpypTsc)_2$ (16)

5.2.4. Electron paramagnetic resonance spectra

The spin Hamiltonian used to represent the EPR spectra of Mn(II) is given by⁸⁹

$$H = g\beta H_s + D[S_z^2 - \frac{1}{3}S(S+1)] + E(S_x^2 - S_y^2)$$

Where H is the magnetic field vector,

D is the axial zero field splitting term and E is the rhombic zero field splitting parameter. If D and E are very small compared to $g\beta H_s$, five EPR transitions are expected with a g value ~ 2.0 given by the Bra-Ket notations $|+5/2\rangle \leftrightarrow |+3/2\rangle$, $|+3/2\rangle \leftrightarrow |+1/2\rangle$, $|+1/2\rangle \leftrightarrow |-1/2\rangle$, $|-1/2\rangle \leftrightarrow |-3/2\rangle$ and $|-3/2\rangle \leftrightarrow |-5/2\rangle$. If D is large, then only one transition between $|+1/2\rangle \leftrightarrow |-1/2\rangle$ will be observed. If D or E is very large, the lowest doublet has effective g value $g_{\parallel} \sim 2.0$, $g_{\perp} \sim 6.0$. for $D \neq 0$ and $E = 0$. but for $D = 0$ and $E \neq 0$, middle Kramer's doublet has anisotropic g value of 4.29. Depending upon the values of A and D, the number of lines appear in the spectra are 6, 24 or 30. Figure 5.2. Shows the EPR spectrum of the compound 15 recorded in DMF solution at 77 K.

The spectra of both compound were almost similar exhibiting a six line manganese hyperfine pattern centered at $g = 2.015$ and 2.097 with hyperfine coupling constant $A = 96$ and 56 G, respectively for compounds 15 and 16. Which is expected for an odd unpaired electron system with $S = \pm 5/2$, $M_s = \pm 5/2, \pm 3/2, \pm 1/2$ and $I = \pm 5/2$, $M_I = \pm 5/2, \pm 3/2, \pm 1/2$ with g and A tensors isotropic, resulting from allowed transitions ($\Delta M_s = \pm 1, \Delta M_I = 0$). The observed g values are very close to the free electron spin value of 2.0023 which is consistent with the typical manganese(II) and also suggestive of the absence of spin orbit coupling in the ground 6A_1 state. Every

adjacent pair of the six hyperfine lines, there is a pair of relatively weak forbidden lines of ($\Delta M_s = \pm 2$, $\Delta M_I = 0$) transition. This is due to the mixing of nuclear hyperfine levels by the zero field-splitting factor of the Hamiltonian. The average separation of the forbidden hyperfine doublets is 23.5 G. The hyperfine values are lower than that obtained for ionic compounds indicating considerable amount of covalency in the M-L bonds⁹⁰⁻⁹².

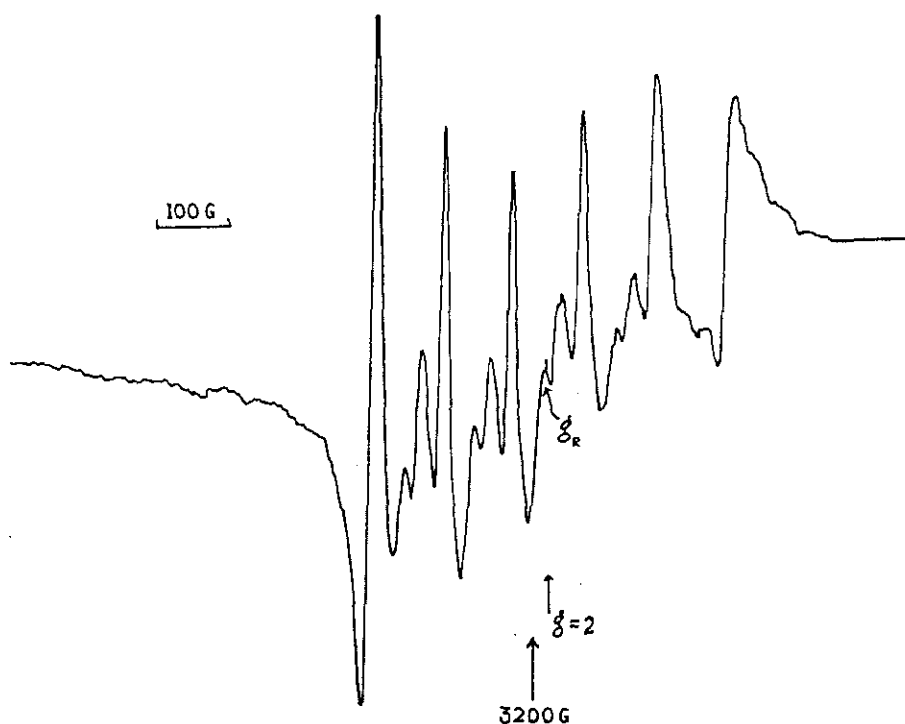


Figure 5.2. EPR spectrum of the compound 15, in DMF (77 K)

5.2.5. Molecular and crystal structure of compound 15

The compound crystallizes in to a monoclinic lattice with P21/c space group symmetry. The crystal refinement parameters are listed in Table 5.2, selected bond lengths and angles are listed in Table 5.3. Figure 5.2 shows the molecular structure of the compound along with atom numbering scheme and figure 5.3 shows the packing of the molecule in a unit cell. The one half of the molecule is related to the other half by a two fold axis passing through manganese atom is six coordinated in an octahedral geometry, by azomethine N, the pyridyl N and thiolate S atom of two planar BpypTsc moiety.

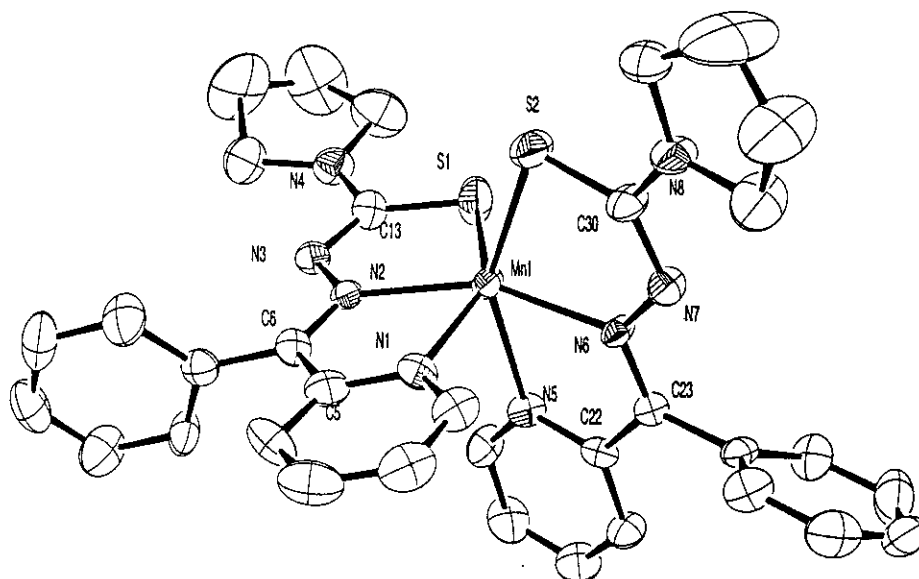


Figure 5.2. ORTEP diagram for the compound $Mn(BpypTsc)_2$ (15) in 54 % probability ellipsoids. Hydrogen atoms are removed for clarity.

The perspective view of the complex shows that the ligand BpypTsc is coordinated in a meridional arrangement⁹³. As observed one ligand and azomethine nitrogen of the other ligand are approximately on the same plane. The apical positions of the octahedron are occupied by one of the nitrogen N4 of the pyridyl ring and S1 of the same ligands. From the bond angles it is observed that the coordination geometry is quiet far from a perfect octahedron. Coordination lengthens the thiosemicarbazone moiety's C-S bond lengths to 1.750 Å. Comparatively larger bond lengths in the M-L bonds, are indicative of weak bonding of the metal to the ligand. The packing is stabilized by the intermolecular π - π interactions and C-H... π interactions in the metal containing chelate ring showing considerable amount of π -electron delocalization in the molecules.

Table 5.2. Crystal refinement parameters of compound 15

Empirical formula	$C_{34}H_{34}MnN_8S_2$
Formula weight	673.75
Crystal system, space group	Monoclinic, P21/c
Unit cell dimensions	$a = 10.7790(7) \text{ \AA}$, $\alpha = 90^\circ$ $b = 20.4342(13) \text{ \AA}$, $\beta = 94.895^\circ$ $c = 14.9354(9) \text{ \AA}$, $\gamma = 90^\circ$
Volume	$3277.7(4) \text{ \AA}^3$
Z, Calculated density	4, 1.365 Mgm^3
Crystal size	0.40 x 0.32 x 0.10 mm
Limiting indices	$-12 \leq h \leq 12$, $-16 \leq k \leq 24$, $-17 \leq l \leq 14$
Goodness-of-fit on F^2	1.057

Table 5.3. Selected bond lengths and angles of the compound 15

Bond lengths (Å)		Bond angles (°)	
Mn(1)-N(2)	2.227(6)	N(2)-Mn(1)-N(6)	155.5(2)
Mn(1)-N(1)	2.307(6)	N(2)-Mn(1)-N(5)	95.2(2)
Mn(1)-S(2)	2.499(2)	N(6)-Mn(1)-N(5)	71.9(2)
Mn(1)-S(1)	2.523(2)	N(2)-Mn(1)-N(1)	71.9(2)
S(1)-C(13)	1.705(8)	N(2)-Mn(1)-S(2)	116.42(16)
N(2)-C(6)	1.296(9)	N(6)-Mn(1)-S(2)	76.92(16)
N(2)-N(3)	1.358(8)	N(5)-Mn(1)-S(2)	148.02(17)
π - π interactions		α (°)	
Cg(4).....Cg(3) ^a	3.1706	88.54	57.99
C-H..... π interactions		β (°)	
C1-H1A.....Cg(2) ^a	2.7534	X.....Cg (°)	H.....X.....Cg (°)
C2-H2A.....Cg(1) ^b	2.667	3.2378	113.34
C18-H18.....Cg(1) ^a	2.8672	3.4235	138.98
		3.3860	116.50
Equivalent position code: a = x, y, z; b = x, 1/2-y, 1/2+z			
Cg(1) = Mn(1), S(1), C(13), N(3), N(2), Cg(2) = Mn(1), S(2), C(30), N(7), N(6)			
Cg(3) = Mn(1), N(1), C(5), C(6), N(2)			

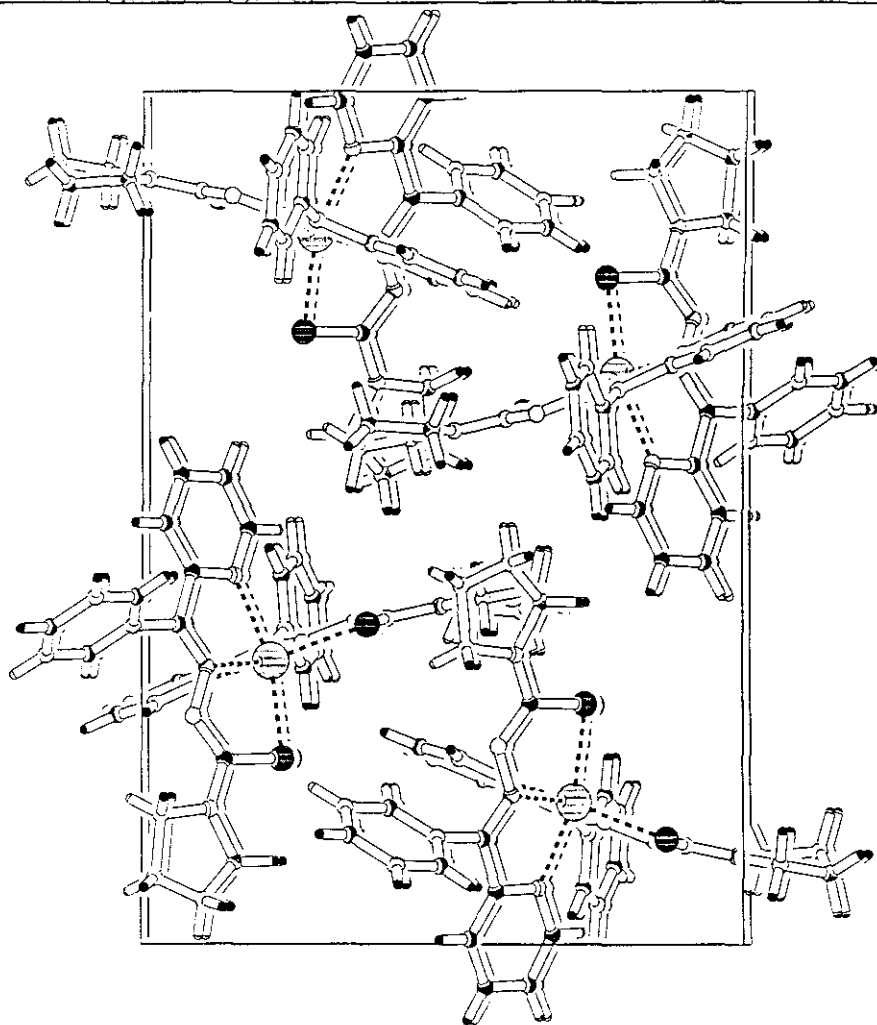


Figure 5.4 Packing diagram of the compound 15

Chapter 6

Synthesis and studies of a gold complex

The chemistry of gold has increased considerably in recent years because the theoretical interest of the relativistic and correlation effects which are especially important in this metal and the applications found for new and old gold complexes. There fore many chemists have focused their work in this golden direction and the number and types of new gold complexes have grown up steadily. Oxidation states which not long ago were denoted as unusual in the chemistry of gold, nowadays are represented by a great variety of structures and stoichiometries. Square planar gold(III) complexes were known for years but their number is less compared to the any other metal complexes. Though there are some recent reports of thiosemicarbazones reacting with organometallic compounds of gold(III) giving ligand displacement reactions to yield thiosemicarbazonate complexes of gold(III)⁹⁴ an attempt was never made on a direct reaction of a simple reaction. The work embodied in this chapter stemmed out of our interest in studying a paramagnetic gold complex but from there we accidentally ended up with a diamagnetic complex with ionic Au(III)/Au(I) centers.

6.1. Experimental

6.1.1. General

Gold(III) chloride (Aldrich) was used as received. The ligand HBpypTsc was synthesized as discussed in Chapter 2. All solvents were purified before use.

6.1.2. Synthesis of compound 17

A methanolic solution of gold(III)chloride (1 mmol) was added to a solution of HBpypTsc (1 mmol) in chloroform. The resultant wine red solution was stirred for 2 h in a magnetic stirred. The reaction was carried out in a 100 mL RB flask in an open atmosphere. After 2 h of stirring reddish brown microcrystalline powders of the compound 17, was separated was filtered washed thoroughly with diethyl ether and dried over P₄O₁₀ *in vacuo*. X-Ray quality single crystals were grown by slowly evaporating the methanolic solution of the compound in 7 days.

6.2. Results and discussions

6.2.1. Synthesis

Though there are some reports of thiosemicarbazone as well as dithiolate complexes of gold(III)⁹⁵, and their structures were well established the reaction which we have performed was first of its kind to the best of our knowledge. Literature does not provide any data of a direct reaction of the metal salt with the ligand. During reaction we have expected the formation of an octahedral complex where the two unpaired electrons will occupy e_g orbitals and will lead to a paramagnetic complex. But after elemental analysis the compound 17 was having a stoichiometry $\text{Au}_2\text{BpypTscCl}_2$. The molar conductivity measurement in DMF solution gave a value of $95 \Omega^{-1}\text{cm}^2\text{mol}^{-1}(10^{-3} \text{ M})$ which indicated that the complex could be a 1:1 electrolyte⁶⁹. However a room temperature magnetic susceptibility measurements pointer out that the complex is diamagnetic. The complex does not gave any EPR signal both in polycrystalline state at 298 K as well as in a solution at 77K. Based on the above observations we have arrived at a square planar gold(III) structure for the cationic part containing BpypTsc moiety (Figure 6.1). But, How to account for the remaining one gold and two chlorine atoms?. Will it be a linear $[\text{AuCl}_2]^-$ anion formed?. Or Will there be any other structures in the complex?. IR and X-Ray diffraction studies gave us the right answer.

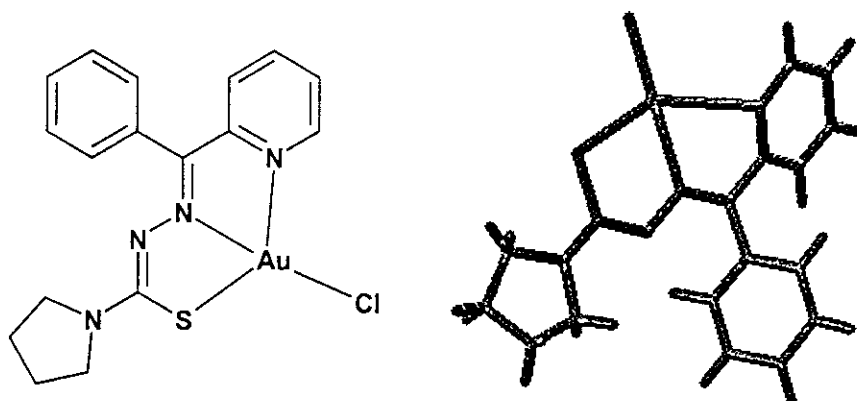


Figure 6.1. Structure formulae of the cationic part of compound 17

6.2.3. IR spectra of compound 17

IR spectra of the compound 17 was recorded in the 50-4000 cm^{-1} region gave a tentative idea of the coordination sphere as well as the structure of the compound. On coordination of the azomethine nitrogen $\nu(\text{C}=\text{N})$ shifts to lower wave numbers from 1630 cm^{-1} to 1556 cm^{-1} . The occurrence of $\nu(\text{NN})$ at a higher wave numbers around 1164 cm^{-1} in the spectrum of the complex compared to that of the ligand (1118 cm^{-1}) confirm the coordination of azomethine nitrogen. IR spectra of the complex show a new sharp band at $\approx 1636 \text{ cm}^{-1}$ is assigned to the newly formed $\nu(\text{N}=\text{C})$ after the coordination. This indicates that the ligand enolizes and coordinates in the thiolate form. Coordination *via* thiolate sulfur is also indicated by the ν/δ (C-S) bands found at ≈ 1311 and 775 cm^{-1} . Besides the in-plane and out-of-plane bending frequencies of the thiosemicarbazone moiety is observed at 649 and 474 cm^{-1} respectively. The spectra was rich in peaks assignable the phenyl ring deformations and pyridyl ring breathing vibrations in the region below 1400 cm^{-1} .

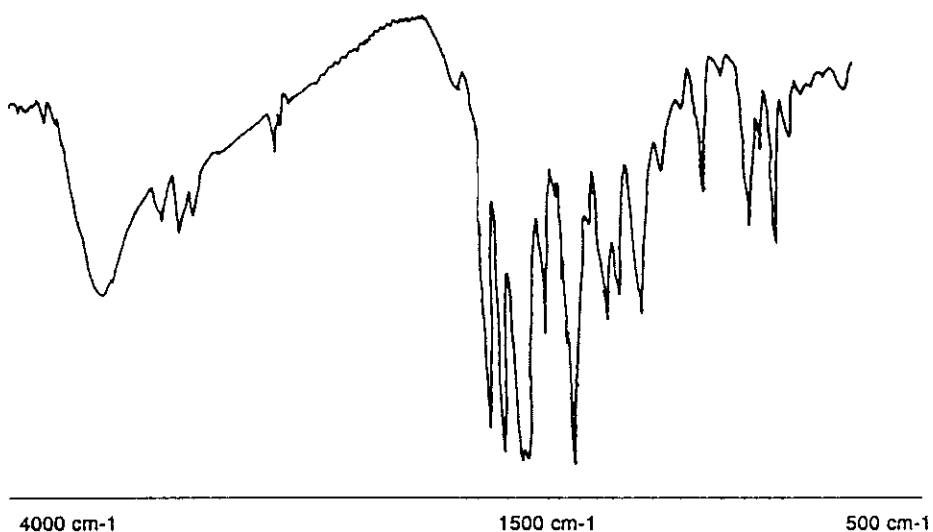


Figure 6.2. IR spectrum of the compound 17 (500-4000 cm^{-1})

Besides these bands the far-IR (Figure 6.3) spectrum showed bands corresponding to the different Au-L stretching frequencies. The $\nu(\text{Au-N})$ stretching frequency for azomethine nitrogen is observed around 474 cm^{-1} and the $\nu(\text{Au-N})$ for the pyridyl nitrogen is observed at 419 cm^{-1} . The presence of a band at 281 cm^{-1} which is assignable to $\nu(\text{Au-S})$ is another indication of involvement of sulfur coordination. A sharp absorption band at 235 cm^{-1} was assigned to the stretching frequency of the coordinated Au-Cl bond in the cationic part^{96,97}. These assignments completes the coordination sphere of the complex with a terdentate coordination of the thiosemicarbazone and a coordinated chloride. We were able to observe three unique vibrational frequencies assigned as ν_1 , ν_2 , ν_3 of a linear $[\text{Cl-Au-Cl}]^-$ structure⁹⁸. The frequencies were assigned as ν_1 at 330 cm^{-1} , ν_2 at 123, 104 and ν_3 at 357 cm^{-1} in the far IR spectrum. The linear AuCl_2^- anion is having a C_{2v} symmetry and all the three modes of vibrations are both IR and Raman active. The spectra follows the general observation of $\nu_3 > \nu_1$. These observations pointed to the presence of a linear $[\text{AuCl}_2]$ species in the complex. Considering the IR spectral inferences an approximate $[\text{AuBpypTscCl}][\text{AuCl}_2]$ structure was assigned to the compound 17.

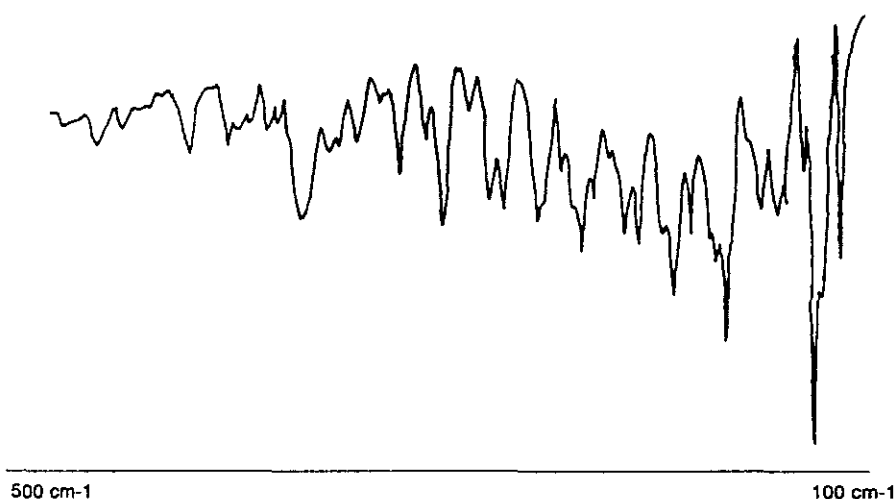


Figure 6.3. Far-IR spectrum of the compound 17

6.2.3. Molecular and crystal structure of compound 17

The compound 17 crystallized in to a monoclinic lattice with P21/c space group symmetry. Table 6.1 presents the structural refinement parameters of the compound 17. Table 6.2 lists the selected bond lengths and angles. The complex had a square planar geometry with Au(III) lying in an approximate plane with four coordinated N(4)-N(3)-S(1)-Cl(1) atoms. It was interesting to note the presence of $[\text{AuCl}_2]^-$ anion which is linear in the crystal structure. The molecular structure along with atomic numbering scheme is presented in Figure 6.4. The BpypTsc is present in the thiolate form and coordinated to gold via the azomethine nitrogen N3, the mercapto sulfur S1, and pyridyl nitrogen N4 and chloride Cl1. Due to the conjugated π -electron system in the thiosemicarbazone moiety they are coplanar with the coordination sphere around gold⁹⁹.

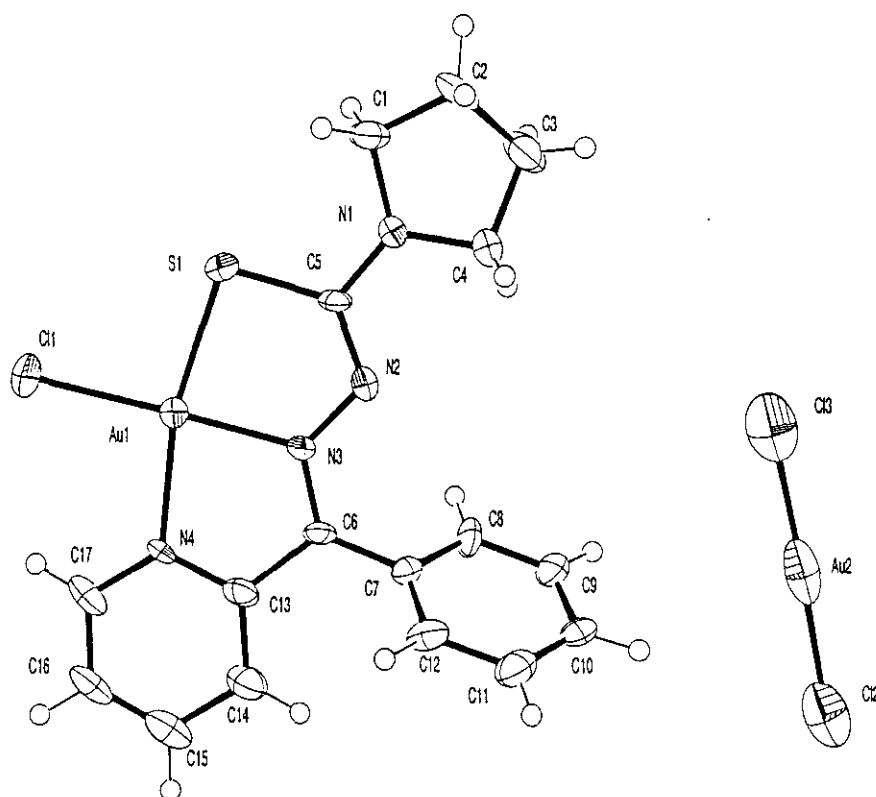


Figure 6.4. ORTEP diagram showing the compound $[\text{AuBpypTsc}]\text{AuCl}_2$ (17) in 56% probability. All hydrogen atoms are arbitrarily assigned as spheres of smaller radii.

Table 6.1. Structural refinement parameters of compound 17

Empirical formula	C ₁₇ H ₁₇ Au ₂ Cl ₃ N ₄ S
Formula weight	809.69
Temperature	293(2) K
Wavelength	0.71073 Å
Crystal system, space group	Monoclinic, P21/c
Unit cell dimensions	a = 17.3491(10) Å, α = 90° b = 15.0670(9) Å, β = 92.632(1)° c = 8.0506(5) Å γ = 90°
Volume	2102.2(2) Å ³
Z, Calculated density	4, 2.558 Mg m ⁻³
Absorption coefficient	14.433 mm ⁻¹
F(000)	1488
Crystal size	0.40 x 0.32 x 0.10 mm
Theta range for data collection	2.70 to 28.28 deg.
Limiting indices	-23 ≤ h ≤ 22, -20 ≤ k ≤ 11, -10 ≤ l ≤ 10
Reflections collected / unique	11841 / 5087 [R(int) = 0.0654]
Completeness to 2θ	28.28 97.4 %
Max. and min. transmission	0.3263 and 0.0686
Data / restraints / parameters	5087 / 0 / 244
Goodness-of-fit on F ²	1.026
Final R indices [I > 2σ(I)]	R1 = 0.0659, wR2 = 0.1686
R indices (all data)	R1 = 0.0877, wR2 = 0.1924
Largest diff. peak and hole	3.718 and -5.134 e. Å ³

Table 6.2. Selected bond lengths and angles of the compound 17

Bond lengths (Å)		Bond angles (°)	
Au(1)-N(3)	1.985(9)	N(3)-Au(1)-N(4)	80.9(4)
Au(1)-N(4)	2.083(10)	N(3)-Au(1)-S(1)	86.1(3)
Au(1)-S(1)	2.257(3)	N(4)-Au(1)-S(1)	167.1(2)
Au(1)-Cl(1)	2.267(3)	N(3)-Au(1)-Cl(1)	178.7(3)
Au(2)-Cl(2)	2.274(6)	N(4)-Au(1)-Cl(1)	97.8(3)
Au(2)-Cl(3)	2.275(7)	S(1)-Au(1)-Cl(1)	95.08(12)
S(1)-C(5)	1.772(11)	Cl(2)-Au(2)-Cl(3)	177.28(18)
N(2)-C(5)	1.305(14)	C(5)-S(1)-Au(1)	93.4(3)
N(2)-N(3)	1.367(12)	C(6)-N(3)-Au(1)	117.5(8)
N(3)-C(6)	1.293(14)	N(2)-N(3)-Au(1)	120.7(7)
Ring-metal interactions			
Cg(I)...Me(J)	Cg(I)...Me(J) (Å)	β(°)	α(°)
Cg(1).....Au(2) ^a	3.405	3.398	3.66
Cg(2).....Au(2) ^a	3.925	3.411	29.67
Cg(4)...Au(2) ^b	3.474	3.446	7.33
a = x, 1/2-y, -1/2+z	Cg(1) = Au(1), S(1), C(5), N(2), N(3)		
b = x, 1/2-y, -3/2+z	Cg(2) = Au(1), N(3), C(6), C(13), N(4)		
	Cg(4) = N(4), C(13), C(14), C(15), C(16), C(17)		
C-H.....π interactions			
X-H...Cg(I)	H---Cg(I) (Å)	X...Cg(I) (Å)	X-H...Cg(I) (°)
C(1)-H(1B)...Cg(1) ^c	3.2194	4.1757	169.01
C = -x, -y, -z			

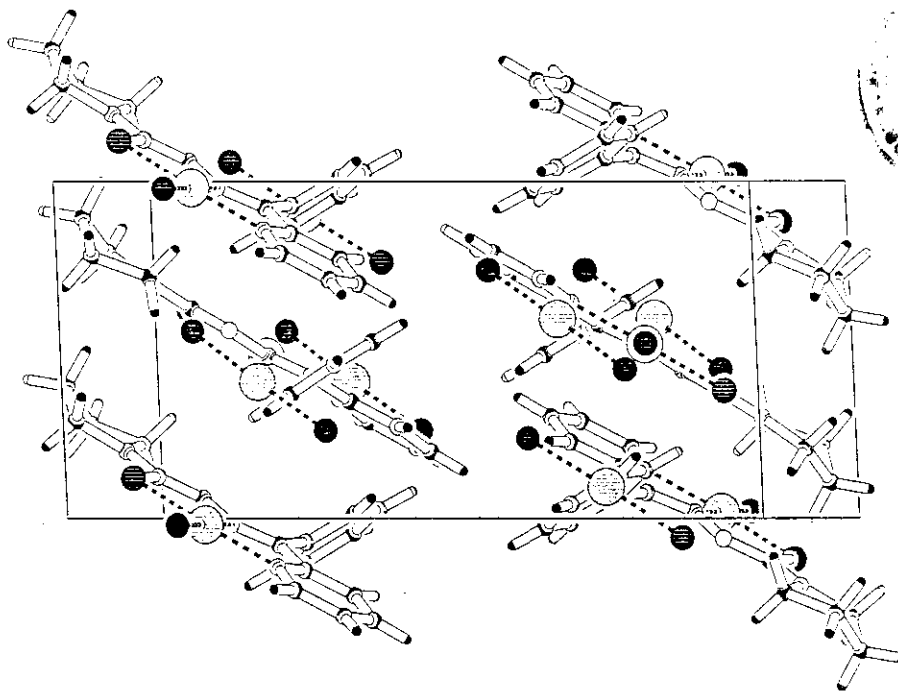


Figure 6.4. Packing of the compound 17 view along a axis.

Gold atom is atom is in the same plane with the coordinating Cl(1), azomethine nitrogen N(3), pyridyl nitrogen N(4), and thiolate sulfur S(1) indicated by the bond angles N(4)-Au(1)-N(3) (80.4°), N(3)-Au(1)-Cl(1) (178.3°), N(4)-Au(1)-Cl(1) (97.8°). The Au-Cl bond lengths are similar $\sim 2.27 \text{ \AA}$ in both species. Figure 6.4 shows the packing of the molecule in a unit cell. The molecule packs into a face-to-face fashion with alternative channels of the cationic and anionic moieties stacked in to molecular columns. A PLATON analysis short ring interactions did not show any π - π interactions in the molecule, but there are moderately strong metal-ring interaction in the compound. The gold atom in the anionic species interacts with the metal containing chelate rings of the cationic moiety. This is a type of interaction between charged atoms can be a dipole-induced dipole type interaction. But the packing stability is poor since this is a π -rich- π -rich type interaction which is least favored. There are no hydrogen bonding network to stabilize the packing, except a weak C-H... π interaction between Cg(1) and Cl-H1.

G18634

Chapter 7

Synthesis and studies of vanadium complexes

Vanadium is an essential element found in different organisms. The study of chemistry of vanadium has been driven by its presence in biological systems. oxovanadium(IV) and vanadate(V) are the main species present in solution under physiological conditions. The coordination chemistry of vanadium has received considerable attention since the discovery of *vanadyl bromoperoxidase*, from marine brown algae *Ascophyllum nodosum*. Since then several vanadium containing enzymes were isolated and characterized. Thus vanadium has gained importance as an important element by catalyzing both peroxidase and nitrogenase processes in biological systems. In recent years it has been established that vanadium compounds have insulin-mimetic properties. A compound bis(picolinato)oxovanadium(IV) has proved to be an orally active and long acting insulin-mimetic compound with which insulin-dependent Diabetes mellitus may be treated in rats¹⁰⁰. This chapter attempts to synthesize such a model complex of vanadium which resulted in a μ -oxo bridged molecule.

7.1. Experimental

7.1.1. General

Vanadyl acetylacetonate (Aldrich) was used as received. The ligand HBpypTsc was synthesized by the procedure discussed in chapter 2. All solvents were distilled before use.

7.1.2. Synthesis of compound 18 and 19

A stirred solution of the ligand HBpypTsc (1 mmol) in chloroform as added a solution of vanadylacetyl acetate (1 mmol) and stirred for 10 minutes. To this was added a methanolic solution of NaN_3 (1 mmol). Stirring was continued for 30 minutes. After 1 h the solution turned orange with a green colored precipitate of compound 18. The solution was filtered washed with ether. The filtrate was allowed to stand for 6 days gave X-ray quality single crystals of compound 19. Anal.% Calcd (Found) for 18: C 48.9 (48.8), 4.05 (4.10), 23.45 (23.44) and for 19: C, 52.10 (52.04), H, 4.32 (4.37), N 14.27 (14.28).

7.2. Results and Discussions

7.2.1. Synthesis

Both compounds **18** and **19** were obtained from the same reaction medium. The results of the partial elemental analysis of compound **18** gave an approximate stoichiometry of VOBpypTscN_3 where the compound **19** was formed to be $\text{V}_2\text{O}_4(\text{BpypTsc})_2$. Magnetic susceptibility measurement was carried out at room temperature for both compounds. The magnetic moment of the compound **18** was found to be 1.76 BM while compound **19** was diamagnetic¹⁰¹. The value of magnetic moment is consistent with the spin only values for mononuclear complexes having d^1 configuration. Figure 7.1 shows the expected structure of compound **18**.

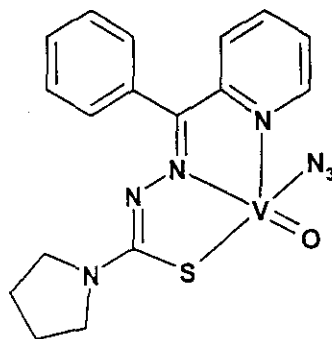


Figure 7.1. Structural formula of compound **18**

7.2.2. Electronic spectra

Both complexes showed three bands at ≈ 40300 , 36200 and 29750 cm^{-1} corresponding to the $\pi \rightarrow \pi^*$ and $n \rightarrow \pi^*$ transitions of the ligand moiety. The compound **18** showed the characteristic absorption bands for five coordinate VO(IV) species. Three transitions were possible viz., ${}^2\text{B}_2 \rightarrow {}^2\text{E}$ ($d_{xy} \rightarrow d_{xz}, d_{yz}$) which was found at 12180 cm^{-1} , and a broad band at 17953 cm^{-1} was assigned ${}^2\text{B}_2 \rightarrow {}^2\text{A}_1$ ($d_{xy} \rightarrow d_{z^2}$), ${}^2\text{B}_2 \rightarrow {}^2\text{B}_1$ ($d_{xy} \rightarrow d_{x^2-y^2}$) transitions¹⁰². These closely lying states are indicative of small tetragonal distortion to the vanadyl environment. Intraligand charge transfer transitions were observed at 22573 cm^{-1} . The spectrum of compound **19** is a d^0 species and no d-d transitions were observed. The spectra did not showed

intense CT bands but the $\pi \rightarrow \pi^*$ and $n \rightarrow \pi^*$ transitions of the ligand moiety were observed with out much shift of reduction in intensity.

7.2.3. IR spectra

Figure 7.2 shows the IR spectrum of the compound 19. The coordination of azomethine nitrogen was indicated by shifting of azomethine stretching frequency by 25-50 cm^{-1} . The $\nu(\text{C}=\text{N})$ was found at 1538 cm^{-1} . The observation of the newly formed at a higher frequency at, $\nu(\text{N}=\text{C})$ at 1595 cm^{-1} , and the occurrence of $\nu(\text{N}=\text{N})$ at a higher frequency at 1116 cm^{-1} also indicate the coordination of the ligand after coordination. The coordination of thiolate sulfur is indicated by the bands at 1387 and 786 cm^{-1} assigned to ν/δ (C-S). The coordination of azomethine nitrogen is indicated by a weak band at 509 cm^{-1} . A strong band at 847 cm^{-1} is an evidence of presence of V=O bond in the compound¹⁰³. A single sharp absorption at 929 cm^{-1} indicates the presence of V-O-V stretching frequency. Besides these bands the spectrum of the compound showed in-plane and out of plane modes of vibrations of thiosemicarbazone moiety at 485 and 696 cm^{-1} .

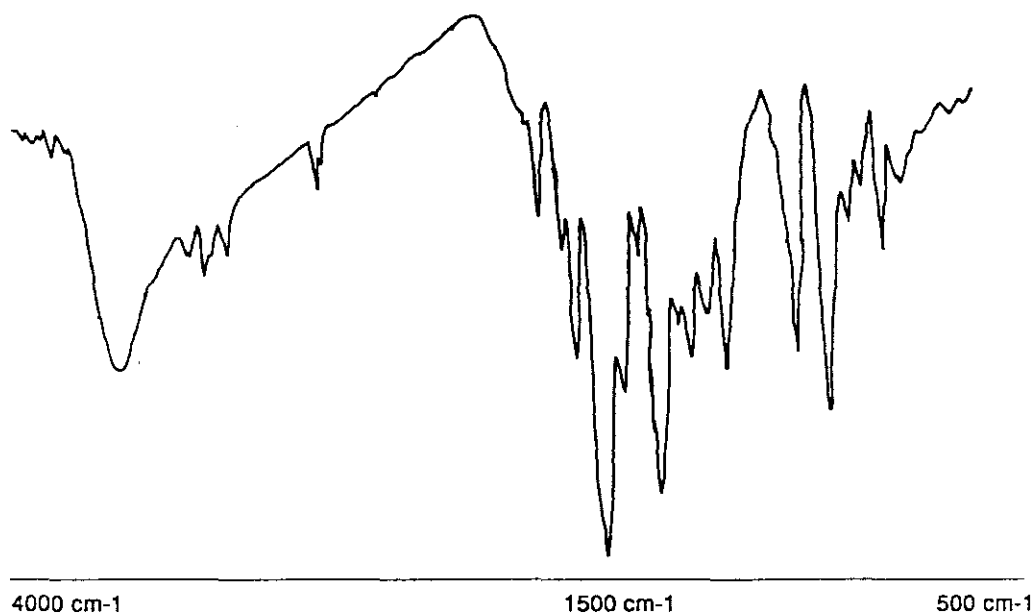


Figure 7.2. IR spectrum of the compound 19

7.2.4. Electron paramagnetic resonance spectra

The spin Hamiltonian representing the EPR of vanadyl species is given by¹⁰⁴

$$H = \beta [g_{\parallel} H_x S_x + g_{\perp} (H_x S_x + H_y S_y)] + A I_x S_x + B (I_x S_x + I_y S_y)$$

Where β is the Bohr magneton, and A and B are the vanadium nuclear hyperfine constants. The EPR spectrum of the compound **18** was obtained in the polycrystalline state at 298 K and in DMF solution at 298 K and 77 K. the spectrum in polycrystalline state gave a broad isotropic signal with $g_0 = 1.99$ due to enhances spin-lattice relaxation. The solution spectrum in DMF solution showed typical eight line spectra with $g_{\text{iso}} = 1.866$ and $A_{\text{iso}} = 85.75$ G, characteristic of mononuclear oxovanadium(IV) containing an unpaired electron being coupled to the vanadium nuclear spin (^{51}V , $I=7/2$)¹⁰⁵. The glassy spectrum at 77 K is well resolved in to two sets of eight line patterns which are typical of five coordinate vanadyl complexes with $g_{\parallel} = 1.934$ and $g_{\perp}=1.990$. Figure 7.3 shows the EPR spectrum of the compound **18**. The g and A values are sensitive to vanadium coordination environment which was used to distinguish between species with different coordination environment¹⁰⁶.

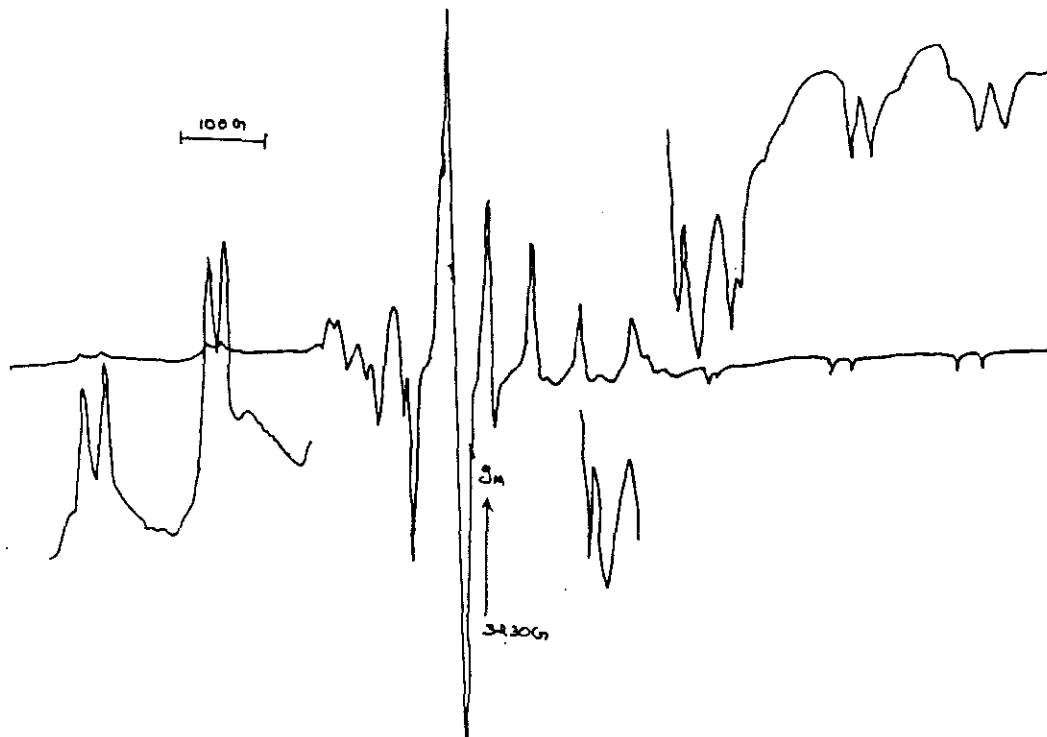


Figure 7.3. EPR spectrum of the compound **18**, in DMF (77 K)

The spectra showed typical eight line pattern indicating that a single vanadium species exists in the molecule with $A_{\parallel} = 162.75$, $A_{\perp} = 92.97$. The absence of any ligand nuclear superhyperfine lines in the g_{\parallel} features indicate that the unpaired electron stays in the d_{xy} (2B_2) ground state. The molecular orbital coefficients α^2 and β^2 are calculated by making use of the equations

$$\alpha^2 = (2.0023 - g_{\parallel})E / 8\lambda\beta^2 \text{ and}$$

$$\beta^2 = [7/6(-A_{\parallel}/P + A_{\perp}/P + g_{\parallel} - 5g_{\perp}/12 - 9g_c/14)]$$

where $P = 128 \times 10^{-4} \text{ cm}^{-1}$, $\lambda = 170 \text{ cm}^{-1}$, and E is the electronic transition energy of ${}^2B_2 \rightarrow {}^2E_2$. The values calculated were 1.028 and 0.6899 respectively indicate that in-plane σ -bonding is more than in-plane π -bonding¹⁰⁷. Based on the EPR parameters a distorted square pyramidal structure was suggested for compound 18.

7.2.5. Molecular and crystal structure of compound 19

The compound 19 crystallizes in to a monoclinic lattice with P21/n space group symmetry. The crystal data and structural refinement parameters are presented in Table 7.1., selected bond lengths and angles are listed in Table 7.2. Figure 7.4 shows the molecular structure of the compound 19.

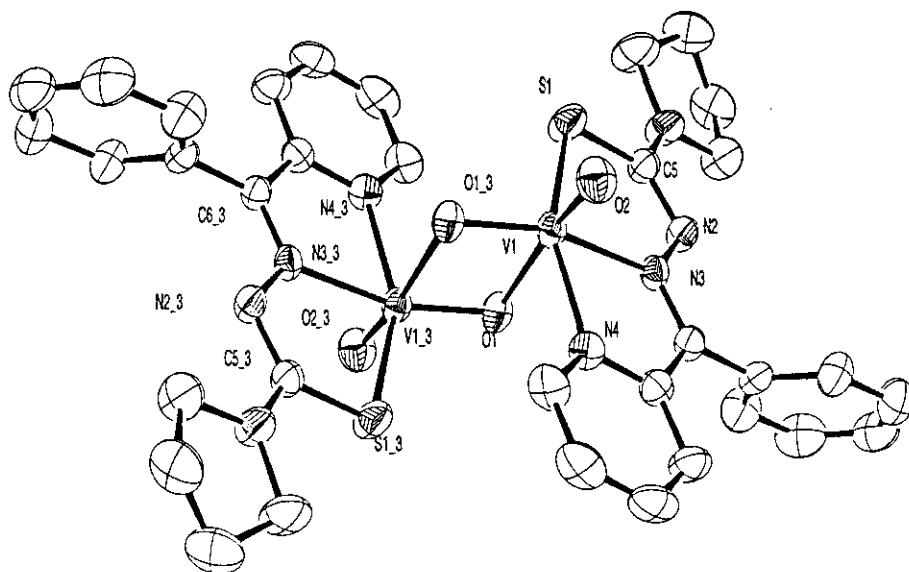


Figure 7.2. ORTEP diagram of the compound 19 with 54% probability. All hydrogen atoms were removed for clarity.

Table 7.1. Crystal data and refinement parameters of compound 19

Empirical formula	$C_{34}H_{34}N_8O_4 S_2V_2$
Formula weight	784.69
Temperature	293(2) K
Wavelength	0.71073 Å
Crystal system, space group	Monoclinic, P21/n
Unit cell dimensions	$a = 10.3912(8) \text{ \AA}$ $\alpha = 90^\circ$ $b = 17.4103(14) \text{ \AA}$ $\beta = 117.385(1)^\circ$ $c = 10.9419(9) \text{ \AA}$ $\gamma = 90^\circ$
Volume	$1757.7(2) \text{ \AA}^3$
Z, Calculated density	2, 1.483 Mg/m ³
Absorption coefficient	0.701 mm^{-1}
F(000)	808
Crystal size	0.52 x 0.44 x 0.18 mm
Theta range for data collection	2.40 to 28.29 deg.
Limiting indices	$-13 \leq h \leq 11$, $-14 \leq k \leq 23$, $-14 \leq l \leq 14$
Reflections collected / unique	10722 / 4286 [R(int) = 0.0272]
Completeness to θ	28.29, 98.0 %
Max. and min. transmission	0.8842 and 0.7119
Data / restraints / parameters	4286 / 0 / 226
Goodness-of-fit on F^2	1.156
Final R indices [I > 2 σ (I)]	R1 = 0.0569, wR2 = 0.1242
R indices (all data)	R1 = 0.0732, wR2 = 0.1311
Largest diff. peak and hole	0.472 and -0.332 e. Å ⁻³

Table 7.2. Selected Bond lengths and angles of the compound 19

Bond lengths (Å)		Bond angles (°)	
V(1)-O(2)	1.614(2)	O(2)-V(1)-N(4)	90.23(11)
V(1)-N(4)	2.117(2)	O(2)-V(1)-N(3)	102.38(10)
V(1)-N(3)	2.185(2)	N(4)-V(1)-N(3)	73.91(8)
V(1)-O(1)	2.354(2)	O(2)-V(1)-O(1)	172.82(10)
V(1)-S(1)	2.3902(9)	N(4)-V(1)-O(1)	82.75(8)
S(1)-C(5)	1.741(3)	N(3)-V(1)-O(1)	74.28(7)
N(2)-N(3)	1.365(3)	O(2)-V(1)-S(1)	96.26(9)
N(3)-C(6)	1.308(3)	O(1)-V(1)-S(1)	89.24(6)
π-π interactions			
C(g).....Cg(J)	Cg(I).....Cg(J) Å	α°	β°
Cg(1).....Cg(5) ^a	3.9650	1.260	3.289
Cg(2).....Cg(1) ^a	2.7646	1.204	1.559
Cg(3).....Cg(1) ^a	2.6828	1.032	1.500
Ring metal interactions			
Cg(3).....V(1) ^b	3.995	3.022	40.85
C-H.....π interactions			
C(8)-H(8A).....Cg(5) ^c	2.9149	3.6728	139.58
C(15)-H(15A).....Cg(2) ^c	2.9883	3.6963	134.10
H-bonding interactions			
H.....A (Å)	D.....A (Å)	D-H.....A(°)	
C(10)-H(10A).. O(2) ^d	2.44	3.2772	149
1 C(15) -- H(15A).. O(2) ^e	2.44	3.3003	154
Equivalent position code: a = x, y, z; b = 1-x, -y, 1-z; c = -1/2 + x, 1/2 - y, -1/2 + z; d = 1/2 + x, 1/2 - y, 1/2 + z; e = 1/2 + x, 1/2 - y, -1/2 + z			
Cg(1) = V(1), O(1), V(1)a, O(1)a; Cg(2) = V(1), S(1), C(5), N(2), N(3)			
Cg(3) = V(1), N(3), C(6), C(13), N(4); Cg(5) = N(4), C(13), C(14), C(15), C(16), C(17)			

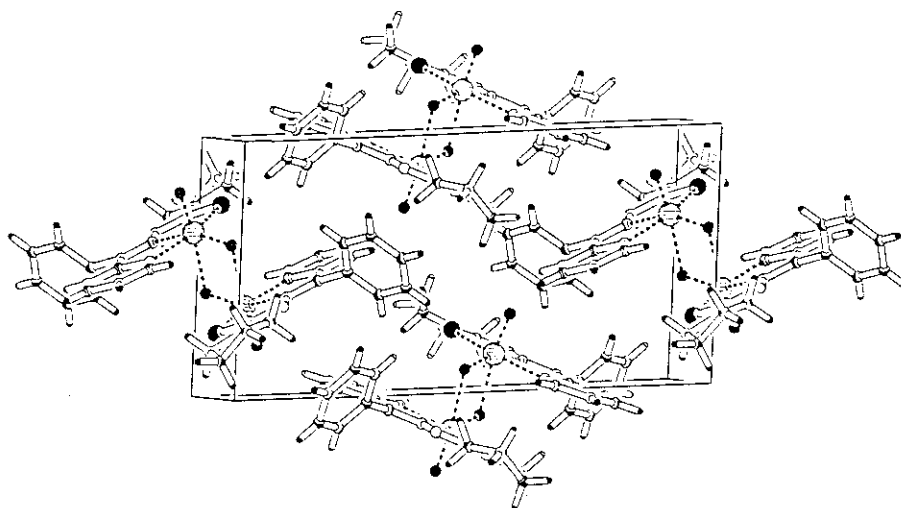


Figure 7.5. Packing of the compound 19 view along a axis.

Bonding lengthens the thiosemicarbazones moieties C-S, and C-N bond lengths to 1.741 and 1.308 Å respectively. This is an indication of coordination via deprotonated thiosemicarbazone¹⁰⁸. The bond lengths V1-O1 (2.354) is larger than V1-O2 (1.614) indicate that V1-O1 is a single bond while the latter is a double bond. The coordination geometry round each vanadium atom is pseudo octahedral bridged by μ_2 -oxo bridges. Bridging oxygen atoms are slightly below the plane of the thiosemicarbazone moiety indicated by the bond angle O2-V1-O1 (106.02).

The compound packs in to an offset fashion with considerable stacking interactions which are stabilized by an extensive 3-D network of H- bonding with the axial oxygen atom O2. There are strong induced dipole-induced dipole type of interactions with the vanadium atom and the neighboring metal containing chelate ring Cg(3). These interactions stabilize the V1-O1-V1-O1 four membered chelate ring, with considerable amount of electron delocalization in the ring. This is indicated by the strong π - π interactions between the ring Cg(1) with near by chelate ring and the pyridyl ring of the BpypTsc moiety. There exist strong C-H... π interactions between the protons to thiosemicarbazones with the ring Cg(2) indicating electron delocalization in the chelate rings also.

Summary and conclusion

The thesis deals with the synthesis, structural characterization and biological studies of three thiosemicarbazones of 2-benzoylpyridine, 2-acetylpyridine and di-2-pyridyl ketone and their transition metal complexes. The entire thesis is divided into seven chapters.

Chapter 1 reviews the structure, bonding and stereochemistry of thiosemicarbazone ligands and their metal complexes. The different analytical and spectroscopic techniques employed for the analysis of the ligands and their complexes are discussed.

Chapter 2 describes the detailed synthesis of the thiosemicarbazones HBpypTsc, HPranThas and HDpkTsc. Crystal and molecular structures of the compounds HBpypTsc, HDpkTsc and HPranThas are discussed in detail. Thiosemicarbazones are synthesized by adopting and modifying a multi stepped synthesis reported elsewhere. The newly synthesized compound HBpypTsc is characterized by means of NMR and IR spectroscopy. The compound HBpypTsc exist as E isomer in the crystal lattice indicated by the low frequency singlet near $\delta = 14.3$ ppm in the $^1\text{H-NMR}$ spectrum of the compound. Electronic transitions were assigned on the basis of UV-Vis spectra. The compound HBpypTsc and its synthetic precursors are screened against five pathogenic organisms viz. *Bacillus Sp*, *Staphylococcus aureus*, *Salmonella paratyphi*, *Escherichia Coli* and *Vibrio Cholerae O1*. None of the precursors were active but surprisingly the ligand HBpypTsc was active against all organisms except *E. Coli*. This leads to the conjecture that the azomethine bond formation could be regarded as a key step in the structure to activity relationship. However the compound HBpypTsc was less active compared to the previously studied HPranThas which may be due to the steric factor imposed by the phenyl ring of the 2-benzoylpyridine moiety.

Chapter 3 discusses the synthesis of ten copper(II) complexes of HBpypTsc. All compounds were characterized by means of UV-Vis and IR spectroscopies. The spin Hamiltonian and bonding parameters were calculated from EPR spectra. Crystal and molecular structure of the compounds 2, 6, 7, 9 and 10 were found out by single crystal X-Ray diffraction. Analysis of short ring interaction shows the metal

containing chelate rings has considerable electron delocalization. Two compounds **2** and **9** were μ -bridged with chlorine and sulfur respectively. The chapter reports the synthesis of the first mercapto coordinated square planar complex of copper(II). All compounds were screened against clinical pathogens. All compounds showed more inhibitory activity compared to the ligands. The increased activity is thought to be due to the square planar coordination and easy removal of the coordinated gegenions while reacting with the microbial cell structures. None of the complexes were active against *E. Coil*. The complexes of chloride, nitrate and perchlorate were most active among the series and they were inhibitorier against *Salmonella paratyphi* and *Vibrio Cholerae O1*

Chapter 4 discusses the synthesis of four low spin iron(III) complexes of HBpypTsc and HPranThas containing uncoordinated polyatomic anions. Two complexes **12** and **14** had two iron centers as observed from single crystal X-Ray diffraction studies. The coordination environment is clearly sketched from the IR spectral analysis. All compounds have an octahedral geometry around low spin iron(III) centre. The spin Hamiltonian parameters necessary to understand the electronic states were found out from the EPR spectra of the complexes. Mössbauer spectral experiments aided the assignment of the spin states of the complexes. All complexes were screened against biological organisms. They were found to be less active compared to copper complexes as well as the ligands. This lower activity is attributed to the completion of the coordination sphere with the ligands. This indicates that the ligand displacement reactions have a vital role in the biological activities of these types of compounds.

Chapter 5 describes the synthesis of two manganese(II) complexes of HBpypTsc and HDpkTsc. The structure of the compound $Mn(BpypTsc)_2$ (**15**) was solved by single crystal X-Ray diffraction and is found to be distorted octahedral. The parameters of molecular stacking and interactions were calculated and described. All electronic transitions were assigned by making use of electronic spectroscopy, and the coordination behavior was assessed by IR spectroscopy. EPR spectra of the complexes showed a six line hyperfine splitting with forbidden transitions. The g and A values calculated from the spectra clearly shows the electronic environment around manganese atom is slightly distorted.

Chapter 6 discusses the synthesis of a gold(III) complex of HBpypTsc. The molecular and crystal structure was found out by single crystal X-Ray diffraction. The compound has a very interesting structure with a gold(III) cation in square planar environment with the BpypTsc and chloride gegenion where the anion is $[\text{AuCl}_2]^-$, IR spectrum of the complex clearly showed the presence of the anionic vibrations. The coordination sphere is assessed by the analysis of IR spectrum. The self assembling aspect of the compound is also discussed. The compound possesses interesting ring-metal interactions which are of the type dipole-induced dipole interactions.

Chapter 7 deals with the synthesis of an oxovanadium(IV) complex and its oxidized product a vanadate(V) complex with μ -oxo bridges. EPR studies and electronic spectra of the oxovanadium(IV) complex clearly shows the complex could be square pyramidal in structure. The oxidized product obtained from the same reaction medium showed the presence of two octahedral vanadium centers bridged via oxygen atoms. Analysis of short ring interactions showed considerable amount of electron delocalization in the four membered chelate ring formed by the oxygen bridging.

The real impetus towards commissioning the present study was to understand the self assembling aspects of the transition metal complexes of thiosemicarbazone ligands. And without doubt the most interesting observation is that all the compounds exhibit intramolecular stacking parameters which are appropriate enough to consider that effective metal chelate ring-aromatic ring-metal center $\pi \dots \pi$ interactions are operative. To our knowledge these weak intra molecular interactions- $\pi \dots \pi$, C-H... π or chelate ring...metal interactions- involving metal chelate rings can be evidenced for metalloaromaticity - a classic concept which is of considerable interest in inorganic chemistry quite recently. Interestingly the referred intra - and intermolecular $\pi \dots \pi$ stacking interactions coexist with an extensive 3-D hydrogen bonding network. Our secondary aim was to investigate the antimicrobial activities of the metal complexes compared to their ligands. We have screened the ligands, its synthetic precursors and their copper(II) and iron(III) against clinical pathogens and are found to be moderately active against them.

References

- [1] M. A. Ali, S. E. Livingstone, *Coord. Chem. Rev.*, 13 (1974) 101.
- [2] M. J. M. Campbell, *Coord. Chem. Rev.*, 15 (1975) 279.
- [3] S. Padhye, G. B. Kauffman, *Coord. Chem. Rev.*, 63 (1985) 127.
- [4] C. A. Brown, W. Kaminsky, K. A. Claborn, K. I. Goldberg, D. X. West, *J. Brazilian Chem. Soc.*, 13 (2002) 10.
- [5] R. Panico, W. H. Powell, J. C. Richer (Eds), *IUPAC Nomenclature of Organic Compounds*, Blackwell, London, (1993) 105.
- [6] D. X. West, S. B. Padhye, P. B. Sonawane, *Structure and Bonding*, 76 (1991) 1.
- [7] R. B. Singh, H. Ishii, *Crit. Rev. Anal. Chem.*, 22 (1991) 381.; R.K. Mahajan, I. Kaur, T.S. Lobana, *Talanta* 59 (2003) 101.
- [8] S. N. Padeya, J. R. Dimmock, *Pharmazie*, 48 (1993) 659.
- [9] D. Chattopadhyay, S. K. Mazumdar, T. Banerjee, W. S. Sheldrick, *Acta Crystallogr. C Cryst. Struc. Commun.*, 45 (1989) 314.
- [10] G. J. Palenik, D. F. Rendle, W. S. Carter, *Acta. Crystallogr. B*, 30 (1974) 2390.
- [11] P. Domiano, G. G. Fava, M. Nardelli, P. Sagarabotto, *Acta. Crystallogr. B*, 25 (1968) 343.
- [12] D. L. Klayman, J. F. Bartoserich, T. S. Griffin, C. J. Manson, J. P. Scovill, *J. Med. Chem.*, 22 (1979) 885.
- [13] D. X. West, A. E. Liberta, S. B. Padhye, R. C. Chikate, P. B. Sonavane, A. S. Kumbhar, R. G. Yerande, *Coord. Chem. Rev.*, 123 (1993) 49.
- [14] A. E. Liberta, D. X. West, *Biometals*, 5 (1992) 121.
- [15] L. A. Saryan, E. Ankel, C. Krishnamoorthi, D. H. Petering, H. Elford, *J. Med. Chem.*, 22(1979) 1218.
- [16] M. Bochmann, K. J. Webb, M. B. Hursthouse, M. Mazid, *J. Chem. Soc., Dalton Transactions*, (1991) 2317.
- [17] N. C. Kasuga, K. Sekino, C. Koumo, N. Shimada, M. Ishikawa, K. Nomiya, *J. Inorg. Biochem.*, 84 (2001) 55.
- [18] F. A. French, E. J. Blanz Jr, Do. J. R. Amaral, D. A. French, *J. Med. Chem.*, 13 (1970) 1117.
- [19] E. Hogarth, A. Martin, M. Storey, E. Young, *Br. J. Pharmacol.*, 4 (1949) 248.
- [20] R. W. Bymes, M. Mohan, W. E. Antholine, R. X. Xu, D. H. Petering, *Biochemistry*, 29 (1990) 7046.
- [21] Ah. Altun, M. Kumaru, A. Dimoglo, *J. Mol. Struc. Theochem*, 535 (2001) 235.
- [22] P. Ren, T. Liu, J. Qin, C. Chen, *Spectrochim Acta*, 59 A (2003) 1095; Y. P. Tian, W. T. Yu, C Y. Zhao, M. H. Jiang, Z. G. Cai, H. K. Fun, *Polyhedron*, 21 (2002) 1217.
- [23] P. Pelagatti, A. Venturini, A. Leporati, M. Carcelli, M. Costa, A. Bacchi, G. Pelizzi, C. Pelizzi, *J. Chem. Soc., Dalton Transactions*, (1998) 2715.
- [24] J. S. Casas, M. V. Castano, E. E. Castellano, J. Ellena, M. S. Garca-Tasende, A. Gatto, A. Sanchez, L. M. Sanjuan, J. Sordo, *Inorg. Chem.*, 41 (2002) 1150.
- [25] M. Maji, M. Chatterjee, S. Ghosh, S. K. Chattopadhyay, B. M. Wu, T. C. W. Mak, *J. Chem. Soc., Dalton Transactions*, (1999) 135.; F. Basuli, S. M. Peng, S. Bhattacharya, *Inorg. Chem.*, 39 (2000) 1120.

- [26] P. Gomas-Saiz, J. Garcia-Tojal, M. A. Mastero, F. J. Arnaiz, T. Rojo, *Inorg. Chem.*, 41 (2002) 1345.; D. V. Garcia, A. Fernandez, J. J. Fernandez, M. Lopez-Torres, A. Suarez, J. M. Ortiguera, J. M. Vila, H. Adams, *J. Organometallic Chem.*, 595 (2000) 199.
- [27] A. R. Cowley, J. R. Dilworth, P. S. Donnelly, E. Labisbal, A. Sousa, *J. Amer. Chem. Soc.*, 124 (2002) 5270.
- [28] A. G. Quiroga, J. M. Perez, E. I. Montero, D. X. West, C. Alonso, C. N. Runniger, *J. Inorg. Biochem.*, 75 (1999) 293.
- [29] J. S. Casas, M. S. Garcia-Tasende, J. Sordo, *Coord. Chem. Rev.*, 209 (2000) 197.
- [30] G. M. Sheldrick, SHELXL 97, Program for the Solution of Crystal Structures, University of Göttingen: Göttingen, Germany, 1997.
- [31] G. M. Sheldrick, SHELXS 97, Program for the Solution of Crystal Structures, University of Göttingen: Göttingen, Germany, 1997.
- [32] Siemens, SMART and SAINT. Versions 4.0. Siemens Analytical X-ray Instruments Inc., (1996). Madison, Wisconsin, USA.
- [33] A. L. Spek, *Acta Crystallogr. A*, 6 (1990) c34.
- [34] J. P. Scovill, *Phosphorous Sulfur Silicon Relat. Elem.*, 60 (1991) 15.
- [35] H. H. Allen, O. Kennard, D. G. Watson, L. Brammer, A. G. Orpen, R. Taylor, *J. Chem. Soc. Perkin Transactions*, (1987) S1.; A. Usman, I. A. Razak, S. Chantpromma, H. K. Fun, V. Philip, A. Sreekanth, M. R. P. Kurup, *Acta Crystallogr. C Cryst. Struc. Commun.*, 58 (2002) o652.; C. Y. Duan, B. M. Wu, T. C. W. Mak, *J. Chem. Soc. Dalton Transactions* (1996) 3485.
- [36] R. M. Silverstein, F. X. Webster, *Spectrometric Identification of Organic Compounds*, 6th Edn, John Wiley & Sons, (1998) NY.
- [37] I. C. Mendes, L.R. Teixeira, R. Lima, H. Beraldo, N.L. Speziali, D.X. West, *J. Mol. Struct.* 559 (2001) 355.
- [38] D. X. West, A.M. Stark, G.A. Bain, A.E. Liberta, *Transition Met. Chem.* 21 (1996) 289.
- [39] L. H. Hall, K. G. Rajendran, D. X. West, A. E. Liberta, *Anticancer Drugs*, 4 (1993) 2.
- [40] S. E. Livingstone, K. Veda, J. Mortia, J. Komano, *J. Antibiotics*, 34 (1981) 317.
- [41] S. Sivakumar, *Structural Spectral Biological and Electrochemical Studies of Some 3d Transition Metal Complexes of ONS and NNS Donor Ligands*, Ph. D. Thesis, Cochin University of Science and Technology, Kochi-682 022, May (2003).
- [42] B. S. Garg, M. R. P. Kurup, S. K. Jain, Y. K. Bhoon, *Transition Met. Chem.*, 13 (1988) 309.
- [43] J. R. Anacona, M. Azocar, O. Nusetti, C. R. Barbarin, *Transition Met. Chem.*, 28 (2003) 24.
- [44] A. B. P. Lever, *Inorganic Electronic Spectroscopy*, 2nd Edn, Elsevier, (1984). Amsterdam.
- [45] P. Bindu, M. R. P. Kurup, *Transition Met. Chem.*, 25 (1997) 578., Y. K. Bhoon, J. P. Scovill, D. L. Klayman, *Spectrochim. Acta, Part A*, 41 (1985) 407.
- [46] K. Nakamoto, *Infrared and Raman Spectra of Inorganic and Coordination Compounds Vol 1&2*, 5th Edn, John Wiley & Sons, (1997) NY.
- [47] A. B. P. Lever, E. Mantovani, B. S. Ramaswami, *Canadian J. Chem.*, 49 (1971) 1957.
- [48] B. J. Hathaway, A. E. Underhill, *J. Chem. Soc. A.* (1961) 3091.
- [49] D. Kivelson, R. Nieman, *J. Chem. Phys.*, 35 (1961) 149.

- [50] B. J. Hathaway, D. E. Billing, *Coord. Chem. Rev.*, 5 (1970) 149.
- [51] S. K. Jain, B. S. Garg, Y. K. Bhoon, *Spectrochim Acta, Part A*, 42 (1986) 959.
- [52] J. Casabo, M. Izaquierdo, J. Ribas, C. Diaz, *Transition Met. Chem.*, 8 (1983) 110.
- [53] V. M. Massacesi, A. W. Addison, *J. Chem. Soc., Dalton Transactions*, (1979) 600.
- [54] A. H. Maki, B. R. McGarvey, *J. Chem. Phys.*, 29 (1958) 35.
- [55] J. R. Wasson, C. Trapp, *J. Chem. Phys.*, 73 (1969) 3763.
- [56] M. J. Bew, B. J. Hathaway, R. R. Faraday, *J. Chem. Soc., Dalton Transactions*, (1972) 1229.
- [57] D. Kivelson, R. Neiman, *J. Chem. Soc., Dalton Transactions*, (1961) 149.
- [58] D. X. West, *J. Inorg. Nucl. Chem.*, 43 (1984) 3169.
- [59] J. R. Pilbrow, T. D. Smith, A. D. Toy, *Australian J. Chem.*, 23 (1970) 2287.
- [60] B. J. Hathaway, In G. Wilkinson, R. D. Gillard, J. A. McCleverty (Eds) *Comprehensive Coordination Chemistry II, Vol 5* (1987) 533, Pergamon, Oxford.
- [61] B. J. Hathaway, *Structure and Bonding, Vol. 14* (1973) 60, Springer, Verlag, Heidelberg.
- [62] P. Bindu, M. R. P. Kurup, T. R. Satyakeerthy, *Polyhedron*, 18 (1999) 321.
- [63] R. S. Giordano, R. D. Bereman, *J. Amer. Chem. Soc.*, 96 (1974) 5064.; R. S. Giordano, R. D. Bereman, *Inorg. Nucl. Chem. Letters*, 10 (1974) 203.; R. Pogni, M. C. Barato, A. Diaz, R. Basosi, *J. Inorg. Biochem.*, 79 (2000) 333.
- [64] R. P. John, A. Sreekanth, M. R. P. Kurup, A. Usman, A. R. Ibrahim, H. K. Fun, *Spectrochim. Acta, Part A*, 59 (2003) 1349.
- [65] C. Janiak, *J. Chem. Soc. Dalton Transactions* (2000) 3885.
- [66] H. Masui, *Coord. Chem. Rev.*, 219-221 (2001) 957.
- [67] Y. Teitz, D. Ronen, A. Vansover, T. Stematsky, J. L. Riggs, *Antiviral Research* 24 (1994) 305.
- [68] Y. K. Bhoon, J. P. Scovill, D. L. Klayman, *Transition Met. Chem.* 7(1982) 264.
- [69] W. J. Geary, *Coord. Chem. Rev.*, 7 (1971) 81.
- [70] S. Vasudevan, H. N. Vasan, C. N. R. Rao, *Chem. Phys. Lett*, 65 (1979) 444.
- [71] N. C. Saha, R. J. Butcher, S. Chaudhari, N. Saha, *Polyhedron*, 22 (2003) 375.
- [72] D. X. West, P. M. Ahrweiler, G. Ertem, J. P. Scovill, D. L. Klayman, J. L. F. Anderson, R. Gilardi, C. George, L. K. Pannel, *Transition Met. Chem.*, 10 (1985) 264.
- [73] H. Siebert, *Z. Anorg. Allg. Chem.*, 275 (1954) 225.
- [74] J. S. Avery, C. D. Burbridge, D. M. L. Goodgame, *Spectrochim. Acta, Part A*, 24 (1968) 1721.
- [75] I. Nakagwa, J. L. Walter, *J. Chem. Phys.*, 51 (1969) 1389.
- [76] E. Konig, K. Madeja, *Spectrochim. Acta, Part A*, 23 (267) 45.
- [77] R. D. Dowsing, J. F. Gibson, *J. Chem. Phys.*, 50 (1969) 294.
- [78] B. S. Garg, M. R. P. Kurup, S. K. Jain, Y. K. Bhoon, *Transition Met. Chem.*, 13 (1988) 247.
- [79] B. S. Garg, M. R. P. Kurup, S. K. Jain, Y. K. Bhoon, *Synth. Rect. Inorg. Met.-Org. Chem.*, 28 (1998) 1415.
- [80] S. Floquet, M. L. Boillot, E. Riviere, F. Varret, K. Boukheddaden, D. Morineau, P. Negrier, *New. J. Chem.*, 27 (2003) 341.
- [81] N. A. Bell, J. S. Brooks, J. K. Robinson, S. C. Thrope, *J. Chem. Soc., Faraday Transactions*, 94 (1998) 3155.
- [82] A. G. Maddock, *Mössbauer Spectroscopy, Principles and Applications of the Techniques*, (1997) Horwood Pub. UK.

- [83] B. N. Figgis, J. Lewis, *Prog. Inorg. Chem.*, 6 (1964) 37.
- [84] J. R. Hartman, B. m. Foxman, S. R. Cooper, *Inorg. Chem.*, 23 (1984) 1381.
- [85] W. Linert, F. Renz, R. Boca, *J. Coord. Chem.*, 40 (1996) 293.
- [86] B. A. Gingras, A. F. Sirianni, *Canadian J. Chem.*, 42 (1964) 17.
- [87] S. Purohit, A. P. Koley, L. S. Prasad, P. T. Manoharan, S. Ghosh, *Inorg. Chem.*, 28 (1989) 3735.
- [88] B. S. Garg, M. R. P. Kurup, S. K. Jain, Y. K. Bhoon, *Transition Met. Chem.*, 13 (1988) 92.
- [89] D. J. E. Ingram, *Spectroscopy at Radio and Microwave Frequencies*, 2nd Edn, Butterworth (1967) UK.
- [90] A. Carington, A. D. Mchachlan, *Introduction to Magnetic Resonance*, Harper & Row, (1969) p 173, NY.
- [91] B. Bleny, R. S. Rubins, *Proc. Phys. Soc. London*, 77 (1961) 103.
- [92] R. Singh, I. S. Ahuja, C. L. Yadava, *Polyhedron*, 1 (1982) 327.
- [93] A. Usman, I. R. Razak, S. Chantrapromma, H. K. Fun, A. Sreekanth, S. Sivakumar, M. R. P. Kurup., *Acta Crystallogr. C Cryst. Struc. Commun.*, 58 (2002) m461.; R. P. John, A. Sreekanth, M. R. P. Kurup, S. M. Mobin, *Polyhedron*, 21 (2002) 2515.
- [94] K. Ortner, V. Abram, *Inorg. Chem. Commun.*, 1 (1998) 251.
- [95] M. A. Mansour, R. J. Lachicotte, H. J. Gysling, R. Eisenberg, *Inorg. Chem.*, 37 (1998) 4625.
- [96] J. Vicente, M. T. Chicote, M. D. Bermudez, M. Garcia-Garcia, *J. Organometallic Chem.*, 295 (1985) 125.
- [97] K. Nakomoto, P. J. McCarthy, B. Minitus, *Spectrochim. Acta*, 21 (1965) 379.
- [98] P. Braunstein, R. J. H. Clerk, *J. Chem. Soc., Dalton Transactions*, (1973) 1845.
- [99] V. Abram, K. Ortner, R. Gust, K. Sommer, *J. Chem. Soc., Dalton Transactions*, (2000) 735.
- [100] H. Sakurai, K. Fujii, H. Watanabe, H. Tamura, *Biochem. Biophys. Res. Commun.*, 214 (1995) 1095.
- [101] A. Pasini, M. Gullotti, *J. Coord. Chem.*, 3 (1974) 319.
- [102] C. J. Ballhausen, H. B. Gery, *Inorg. Chem.* 1 (1962) 111.
- [103] T. Ma, T. Kojima, Y. Matsuda, *Polyhedron*, 19 (2000) 1167.
- [104] J. M. Assour, J. Goldmacher, S. E. Harrison, *J. Chem. Phys.*, 43 (1965) 159.
- [105] D. Collison, B. Gahan, C. D. Garnen, F. E. Mabbs, *Inorg. Chem.*, 18 (1989) 902.
- [106] I. G. Asgedom, A. Sreedhara, J. Kivikoski, E. Kolehmainen, C. P. Rao, *J. Chem. Soc., Dalton Transactions*, (1996) 93.
- [107] F. A. Walker, R. L. Karlin, P. H. Reiger, *J. Chem. Phys.*, 45 (1966) 4181.
- [108] A. Sreekanth, S. Sivakumar, M. R. P. Kurup, *J. Mol. Struc.*, 655 (2003) 47.

Curriculum Vitae

SREEKANTH. A

Research Scholar
Dept. of Applied Chemistry
Cochin University of Science And Technology
Kochi, 682022, India
Phone : 91-484-2575804 (Dept), 91-484-2575944 (Hostel)
Mobile: 91-9846024431
E-mail : sreekanth@cusat.ac.in ; sreekanth_a@yahoo.com URL:www.cusat.ac.in/dac

Geethanjali
Parippu P. O
Kottayam
Kerala-686022
India

Career Objective:

Keenly interested in pursuing a career as a teacher without compromising my research objectives

Topics of interest:

Spectroscopic and Structural studies of Paramagnetic Complexes

Academic Curriculum:

Course	University/Board	% Marks	Year
M.Sc. Applied Chemistry	Department of Applied Chemistry CUSAT, Cochin.	74.5%	2000
B.Sc. Chemistry	C. M. S. College M. G. University, Kottayam	80%	1998

Computer awareness:

LATeX, Linux 8.0, ORTEP III, PLATON, Origin5.0, MS Office 2000

Other Activities

Member, Academic Council, CUSAT 2003-2004

Member, Library Advisory Committee, CUSAT 2002-2003

Secretary, Cochin University Research Scholars Association 2001-2003

Member, National Magnetic Resonance Society, India

Personal Details:

Age and Date of birth : 25 years, 28.05.1978
Sex : Male
Nationality : Indian
Marital status : Single

Publications in Refereed Journals

1. **A. Sreekanth**, M. R. Prathapachandra Kurup, H. K. Fun, Formation of a first gold(III) complex of 2-benzoylpyridine-*N*(4), *N*(4)-(butane-1,4-diyl) thiosemicarbazone: structure and Mössbauer spectrum, communicated
2. **A. Sreekanth**, M. R. P. Kurup, H. K. FUN, Bis[(2-benzoylpyridine- κN -*N*(4), *N*(4)-(butane-1,4-diyl) thiosemicarbazonato- $\kappa^2 N', S$) μ_2 -thio-copper(II)], communicated to Acta C
3. **A. Sreekanth**, M. R. P. Kurup, A. Kishore, S. M. Bhatt, M. Nethaji, Antimicrobial studies on copper(II) and iron(III) complexes of 2-benzoyl pyridine thiosemicarbazone and structure of a copper(II) complex: CuBpypTscCl, Communicated
4. **A. Sreekanth**, M. R. P. Kurup, H. Kun-Fun, Structural and spectral studies of Manganese(II) and vanadate(V) complexes of 2-benzoylpyridine *N*(4) substituted thiosemicarbazone, communicated
5. **A. Sreekanth**, M. R. P. Kurup, Synthesis, EPR and Mössbauer spectral studies of new iron(III) complexes with 2-benzoylpyridine-*N*(4), *N*(4)-(butane-1, 4-diyl) thiosemicarbazone (HBpypTsc): X-ray structure of [Fe(BpypTsc) $_2$]FeCl $_4$ ·2H $_2$ O and free ligand, Polyhedron, in press
6. **A. Sreekanth**, M. R. P Kurup, Structural and spectral studies on four coordinate copper(II) complexes of benzoyl-2-pyridine *N*(4), *N*(4)-(butane-1,4-diyl) thiosemicarbazone, Polyhedron, In press.
7. **A. Sreekanth**, U. L. Kala, C. R. Nayar, M. R. P. Kurup, Cobalt(III) ternary complexes of 2-hydroxyacetophenone *N*(4) phenyl semicarbazone containing heterocyclic coligands :syntheses, structure, and spectral studies, Polyhedron, in press.
8. **A. Sreekanth**, S. Sivakumar, M. R. Prathapachandra Kurup, Structural studies of six and four co-ordinate zinc(II), nickel(II) and dioxovanadium(V) complexes with thiosemicarbazones, *Journal of Molecular Structure*, 2003, 655/1 pp 47-58.
9. R. P. John, **A. Sreekanth**, M. R. P. Kurup, A. Usman, I. A. Razak and H. K. Fun., Spectral studies of a 2-hydroxyacetophenone 3-Hexamethyleneiminyl thiosemicarbazone(-2) copper(II) complex containing 1,10-phenanthroline., *Spectrochimica Acta Part A*. 2003, 59/6 pp. 1349-1358.
10. P. B. Sreeja, **A. Sreekanth**, C.R. Nayar, M. R. P. Kurup, A. Usman, I. A. Razak, S. Chantrapromma and H. K. Fun; Synthesis, spectral studies and structure of 2-hydroxyacetophenone nicotinic acid hydrazone, *Journal of Molecular Structure*, 645, pp 221 – 226, 2003.
11. R. P. John, **A. Sreekanth**, M. R. P. Kurup, S. M. Mobin, Synthesis, structural and spectroscopic studies of low spin Co(III) complexes of *N*(4) substituted thiosemicarbazones of 2-hydroxyacetophenone and heterocyclic bases, *Polyhedron*, 21, pp 2515-2521, 2002.
12. A. Usman, I. A. Razak, S. Chantrapromma, H. K. Fun, **A. Sreekanth**, S. Sivakumar, M. R. P. Kurup, Bis (1-pyridin-2-ylethanone- $\kappa N'$ -phenylthiosemicarbazonato- $\kappa N', S$)manganese(II), *Acta Crystallographica C Crystal Structure Communications*, C58, 2002, m461-m463.
13. A. Usman, I. A. Razak, S. Chantrapromma, H. K. Fun, V. Philip, **A. Sreekanth**, M. R. P. Kurup, Di-2-pyridyl ketone N' , N' -(butane-1,4-diyl)thiosemicarbazone, *Acta Crystallographica C: Crystal Structure Communications*, C58, 2002, o652-o654

Papers presented in Symposia

1. A. Sreekanth, Chandini. R. Nayar, U. L. Kala and M. R. Prathapachandra Kurup, "Conformational and structural studies on (1E)-1-(2-methylphenyl)ethan-1-one N-phenylsemicarbazone by 2D NMR spectroscopy"; Special Symposium on Recent Developments in NMR Methodology and National Symposium on Magnetic Resonance 3-6, February 2003, Bangalore, India.

2. A. Sreekanth, M. R. Prathapachandra Kurup, "EPR spectral studies on the bonding parameters and structure of copper(II) complexes of benzoyl-2-pyridine N⁴, N⁴-(butane-1, 4-diyl) thiosemicarbazone"; Special Symposium on Recent Developments in NMR Methodology and National Symposium on Magnetic Resonance 3-6, February 2003, Bangalore, India.

3. A. Sreekanth, R. P. John, M. R. P. Kurup, Novel Oxovanadium(IV) Complexes of N(4)-Disubstituted Thiosemicarbazones with Heterocyclic Bases : An EPR Study on the Unusual Solvent Coordination, XXXVth International Conference on Coordination Chemistry, P4.005, pp 543, July 21-26, 2002, Heidelberg, Germany.

4. B. S. Patro, A. Sreekanth., S. K. Dwivedi , S. Chatopadhyay, Brahma Singh and A. Banerji; "Anti-oxygenic Activity of Indian seabuckthron (*Hippophae Rhamnoids*)": National Symposium on Seabuckthron, at New Delhi in February 2001.

G 8634

